Spatially Distributed Molecular Communications via Diffusion: Second-Order Analysis

Spatially Distributed Molecular Communications Via Diffusion: Second Order Analysis

Flavio Zabini, *Member, IEEE*

***Abstract*—Unlike electromagnetic communications, where the noise is typically represented by a (Gaussian) independent source which is added to the useful signal (additive noise), molecular communications via diffusion are affected by a random disturbance which is intrinsically related to the random nature of emission, propagation (Brownian motion) and reception.**

In point-to-point molecular communications, the number of received molecules is generally a Poisson random variable. Thus, the evaluation of the signal-to-noise ratio (intended as the ratio between the squared mean value of the received molecules and its variance) is not a problem of interest, since its value simply equals the mean of such a random variable. However, in spatially distributed communications, where the point transmitters are randomly placed in the 3D space according to a point process, the number of received molecules derives from the contribution of a random sum of emissions, so that it is no more a Poisson random variable. Thus, the evaluation of the signal-to-noise ratio is not trivial. Here, we provide an analytical framework to evaluate the signal-to-noise ratio in spatially distributed molecular communications for both synchronous and asynchronous transmitters. The analysis is extended to the signal-to-interference-noise ratio when digital communications with intersymbol interference are considered.

***Index Terms*—Molecular communications, diffusion, point processes, asynchronous transmission, SNR and SINR evaluation**

I. Introduction

Molecular communications are one of the new paradigms which are rising to overcome constraints in the classic communication paradigms when moving to nano-scale (e.g., size constraints, energy problems, medium incompatibility) [1]–[3]. Differently than electromagnetic and acoustic communications (which are totally based on waves) and than optical and quantum communications (whose nature involves both waves and particles), molecular communications have a particle-based nature [4]–[9].

Important processes in Nature, such as cell development, cell coordination in tissues, and multi-cellular homeostasis, involve the processing, the transmission, the propagation, and the reception of molecules [10]–[12]. Molecular communications are a nano-scale paradigm: the size of molecules which propagate typically range from about one Angstrom to tens of nanometers, while emission/reception processes involve phenomena inside biological cells of about 100nm diameters [13]. This implies that human-made molecular communication systems (e.g., those based on nano-machines) access nano-scales properties of matter and fit in nano-scale spaces [14]–[16]. Application of nanomachines can be biomedical (e.g., bio-hybrid implants, monitoring glucose level, heart monitoring, cures against brain pathology, medication-carrying smart nanocapsules that detect and destroy tumors), military (e.g., nuclear, biological, and medical defense), industrial (e.g., food and water control, functionalized materials and fabric), and environmental (e.g., biodegradation, animals and biodiversity control, air pollution control) [17].

Molecular communications can be classified based on propagation: walkway-based (e.g., molecular motors [18]), advection-based (e.g., chemotaxis [19]–[21]), and diffusion based (i.e., diffusion through Brownian motion only [4], [5], [22], [23], or with flow [24]–[26]).

In this work, we focus on molecular communication via diffusion (MCvD) in the absence of flow. Differently than communications based on electromagnetic or acoustic waves, in this case it is not necessary to spend energy for the transmission, since information-carrying molecules are conveyed by the Brownian motion of the fluid. The negative aspect is represented by the random nature of such a kind of propagation. While in electromagnetic and acoustic communications the noise is usually represented by a source which is independent of the useful signal (e.g., additive white Gaussian noise (AWGN)), in such a way that it is sufficient to increase the signal power to increment the signal-to-noise ratio (SNR), in MCvD the signal itself is intrinsically affected by random disturbance.

More specifically, if the information is encoded in the local concentration of information-carrying molecules (i.e., in the number of molecules observed by a certain model of receiver in certain volume within a certain time), the signal results in a random process (or, equivalently, a random variable if a given time instant is considered). Such a stochastic characterization is analytically studied in the literature for both passive receiver model (the receiver counts the molecules inside a volume without interacting with them [27]) and fully absorbing receiver model (the receiver absorbs each molecule hitting its surface, thus removing it from the fluid [28]).

Due to chemical reasons [29], the number of emitted molecules can be modeled by a Poisson random variable. Moreover, it is shown in [4], [30] that also the number of received molecules after diffusion is a Poisson random variable (RV). Thus, in a point-to- point MCvD, the SNR, defined as the ratio between the square of the average number of received molecules and the corresponding variance, is equal to the average itself. As a consequence, the evaluation of the average number of received molecules (first order analysis) is sufficient to quantify the effectiveness of the communication in such scenario.

However, when a spatially distributed transmission is con-

This work has been carried out in the framework of the CNIT National Laboratory WiLab. F. Zabini is with DEI and WiLab, University of Bologna/CNIT, Italy, email: f.zabini@ieee.org.

sidered (e.g., when molecules are emitted by a swarm of point transmitters randomly placed in 3D), due to the superposition of effects, the overall number of received molecules results in a random sum of RVs with different random parameters (e.g., the distance from the receiver, the emission times, etc.) which is no more a Poisson RV even though each contribution, taken apart, is a Poisson RV. Thus, a second order stochastic characterization is needed to study spatially distributed MCvD in the terms of SNR.

Recent studies investigate such scenario in terms of bit error probability (in the case of on-off keying (OOK)) [7] and connectivity (each point transmitter is considered a node of a nano-network) [31]. In these works, a stochastic geometry approach is adopted and positions of point transmitter are modeled according to a homogeneous Poisson point process (HPPP) in 3D. However, their analytical frameworks assume that all point transmitters emit molecules at the same time instant (global-clock assumption). In many scenarios such a synchronous assumption may be not realistic: e.g., when emissions derive by chemical reactions that randomly happen in the fluid with a certain propensity function [32], or when point transmitters represent independent (not synchronized) nodes of a nano-network (in [31] such an asynchronous scenario is investigated via simulation).

The first attempt to analytically study asynchronous spatially distributed MCvD can be found in [8], where a first order analysis is presented involving methods from both point process theory and classic linear filtering theory [33], [34].

In the present work, such an approach is extended to a second order analysis, in order to evaluate the SNR in spatially distributed MCvD. It should be pointed out that a swarm of point transmitters, randomly placed according to a point process (PP), implies that the overall number of received molecules is given by a random sum of Poisson RVs with random parameters (which is no more a Poisson RV). Thus, unlike the case of point to point MCvD [31], in the large scale MCvD, the SNR is not equal to the mean value of received molecules and requires the evaluation of the variance of the received molecules themselves. The proposed framework puts in evidence that the spatially distributed case completely differs from the point-to-point case in terms of temporal evolution and asymptotic SNR analysis for infinite molecules emissions. Moreover, the stochastic geometry based approach is extended with respect to the case of the HPPP, usually adopted by the literature, by considering the effects of stochastic interactions (i.e., attraction and repulsion) among the scattered points. Besides, our framework includes also the SNR evaluation in case of multiple samples detector, as proposed by [35].

In order to make our study more comprehensive to the convolutional nature of the channel, we also derive analytical expressions for the mean and the variance of the inter-symbol interference (ISI) in case of digital transmission via OOK modulation, and compute the signal-to-interference-noise ratio (SINR). The bit error probability (BEP) is also analytically evaluated, by means of a Gaussian approximation, in order to verify how representative the SNR and the SINR are for a spatially distributed MCvD digital communication system.

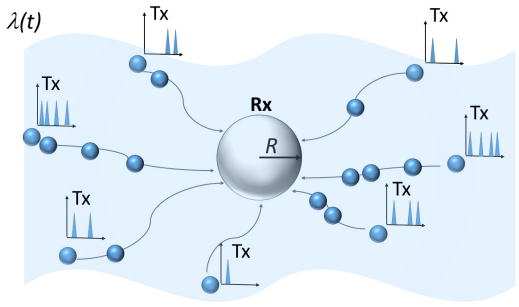

Fig. 1. A large scale MCvD system with a spherical receiver and a swarm of randomly placed point transmitters that randomly emit molecules according to independent time-domain PPs with the same intensity function $\lambda_{\mathrm{a}}(t)$.

Finally, numerical results obtained via Monte Carlo simulations are compared to those derived by the analysis to validate the proposed second order analysis of spatially distributed MCvD.

The paper is organized as follows. In Sec. II, the system model and notation are described. In Sec. III analytical expressions of the SNR are derived for both the concentration synchronous and timing asynchronous cases, also taking a general spatial distribution of point transmitters into account. In Sec. IV, analytical expressions of the SINR are obtained for spatially distributed digital MCvD affected by ISI, for concentration synchronous and timing asynchronous transmitters with a general spatial distribution. In Sec. V, for the sake of simplicity, a case study is presented based on a Poisson distribution of point transmitters. In Sec. VI numerical results are derived based on the closed forms previously derived for the cases considered. In Sec. VII conclusions are presented.

II. System Model

We consider a spatially distributed communication model where a swarm of point transmitters are randomly placed in a three dimensional space and the reception is performed by a receiver with dimension (e.g., spherical). For the emission, we consider all the three possible model adopted by the literature [36]: exact concentration, Poisson concentration and timing transmitters. All these cases have to be combined to the two possible scenarios which can arise when multiple transmitter are considered: all point transmitters emit molecules at the same time (global clock assumption, see [7]) or not (asynchronous case, see [8]). The diffusion process is assumed as without flow and without interaction between different information molecules, while the reception process is the full absorption. Here, we consider all the source of randomness, that have to be taken into account for the SNR evaluation, one by one.

A. Brownian motion and absorption process

The first source of randomness is the Brownian motion of molecules. Starting from Fick's law, it can be described stochastically. Here we define the function $F_{\mathrm{hit}}(r,t)$, which describes the fraction of molecules received (i.e., the probability that the emitted molecules is received) at distance r from the

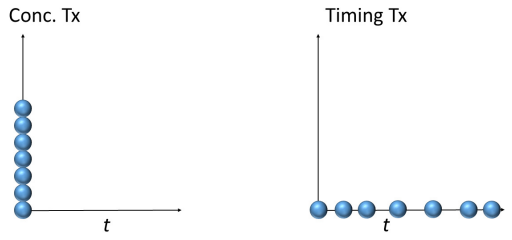

Fig. 2. Exact and Poisson concentration transmitters emit all molecules at $t = 0$. Timing transmitters emit molecules one-by-one at random instants.

point transmitter till time t , provided that the emission takes place at the time origin and $t \geqslant 0$. Such a function depends on the receiver model and on the way of considering finite molecule's lifetime.

According to [28], the fraction of molecules received by a spherical fully absorbing receiver (with radius R) at distance r from the point transmitter till time t is given by

$$F_{\text{hit}}(r,t) = \frac{R}{r}\text{erfc}\left(\frac{r-R}{\sqrt{4Dt}}\right) \tag{1}$$

where D is the diffusion coefficient (in m^2/s, see, e.g. [37]), provided that the emission happens at the time origin and $t \geqslant 0$.[1]

We assume that each information molecule subdues an independent diffusion and absorption process, such that the superposition of effects can be applied.

B. Transmitters models

When a deterministic number of molecules are emitted at a certain time (e.g., $t = 0$, without loss of generality) no randomness is obviously introduced (exact concentration model). However, it may happen both that the number of emitted molecules is a RV (e.g., Poisson concentration transmitter), or that the time instants at which each molecules is emitted are RVs (in timing transmitter models, the emission instants are controlled by the transmitter since they codify information: thus, they can be considered as random from an external perspective).

In order to develop a proper comparison among the three transmission models existing in the literature [36], we formalize such models by exploiting RVs stochastic description as follows.

1) Exact concentration transmitter model: When exactly N_{tx} are emitted at $t = 0$, we have to consider that each of the N_{tx} molecules has probability $F_{\text{hit}}(r,t)$ of being received at a distance r till time t. Thus, since the diffusion of each molecule is assumed as an independent process, the number $\mathsf{a}|_{r,t}$ of received molecules at distance r till time t due to such a transmission results in a binomial RV (as the sum of N_{tx} independent identically distributed (IID) Bernoulli RVs whose success probability corresponds to the successful reception of molecules):[2]

$$\mathsf{a}|_{r,t} \sim \mathcal{B}(N_{\text{tx}}, F_{\text{hit}}(r,t)) \,. \tag{2}$$

2) Poisson concentration transmitter model: In the Poisson concentration model, the number n_{tx} of emitted molecules at $t = 0$ is not deterministic, but it is modeled by a Poisson RV with mean N_{tx}.

Similarly to the previous case, each of the n_{tx} molecules has probability $F_{\text{hit}}(r,t)$ of being received at a distance r till time t. More formally, the diffusion process of the l-th molecule can be stochastically described (for given r and t) by the Bernoulli RV $\mathsf{b}_l|_{r,t}$

$$\mathsf{b}_l|_{r,t} \sim \mathcal{B}[F_{\text{hit}}(r,t)] \tag{3}$$

which takes value 1 if the l-th emitted molecule is received and 0 otherwise.

However, unlike the exact case, the number $\mathsf{a}|_{r,t}$ of received molecules at distance r till time t is no more a binomial RV, but it is given by the random sum of the aforementioned Bernoulli RVs

$$\mathsf{a}|_{r,t} = \sum_{l=1}^{\mathsf{n}_{\text{tx}}} \mathsf{b}_l|_{r,t} \tag{4}$$

where $\mathsf{b}_l|_{r,t}$ can be considered as IID due to the assumption of independent diffusion of each information molecule.

3) Timing transmitter model: According to the timing transmitter model, the transmitter releases individual molecules one by one, at specified time instances. If such instants are unknown a priori, they can be modeled by RVs. When emission times are independent of each other, they can be considered as instantiations of a temporal (generally, non-stationary) Poisson point process (PPP) Φ with intensity $\lambda(t)$.[3]

Formally, the l-th molecule is emitted at the random time $\tau_l \in \Phi$ and thus can be described (given r,t) by the Bernoulli RV

$$\mathsf{b}_l|_{r,t} \sim \mathcal{B}[F_{\text{hit}}(r,t-\tau_l)] \tag{5}$$

where $F_{\text{hit}}(r,t-\tau_l)$ (thanks to the time invariance of Fick's law) represents the probability of being received at distance r till time t.

As a consequence, the number of received molecules at distance r till time t is given by the random sum

$$\mathsf{a}|_{r,t} = \sum_{l \in \mathcal{I}\{\Phi\}} \mathsf{b}_l|_{r,t} \tag{6}$$

where $\mathcal{I}\{\Phi\}$ indicates the index set of Φ.

By comparing (6) to (4), it can be noticed that the Poisson concentration model can be derived as a special case of timing transmitter model where Φ is a PPP with $\varrho_{\Pi}^{(1)}(t) = N_{\text{tx}}\delta(t)$ in the sense of distributions.

[1] For $t < 0$ it is $F_{\text{hit}}(r,t) = 0$ since no molecule can be received before the emission.

[2] $\mathcal{B}(p)$ indicates the Bernoulli distribution with success probability p, while $\mathcal{B}(n,p)$ is the binomial distribution with n trials and success probability p for each trial.

[3] The intensity function $\rho(t)$ of a generic time domain PP in [8] is going to be identified with $\lambda(t)$ in this case, since here we deal with a time domain PPP.

C. Point transmitters positions and stochastic geometry

In spatially distributed molecular communications via diffusion, also the random positions of point transmitters represent a source of randomness that has to be taken into account for the SNR evaluation.

Let $\mathbf{\Psi}$ be a spatial isotropic PP in $\mathbb{R}^3$ with first and second order density functions given by:

$$\varrho^{(1)}_{\mathbf{\Psi}}(\boldsymbol{x}_1) = \lambda_{\mathbf{\Psi}} \tag{7}$$

$$\varrho^{(2)}_{\mathbf{\Psi}}(\boldsymbol{x}_1, \boldsymbol{x}_2) = \rho_{\mathbf{\Psi}}(\|\boldsymbol{x}_1 - \boldsymbol{x}_2\|) \tag{8}$$

for $\boldsymbol{x}_1, \boldsymbol{x}_2 \in \mathbb{R}^3$. We recall [38] that $\varrho^{(1)}_{\mathbf{\Psi}}(\boldsymbol{x}_1)d\boldsymbol{x}_1$ is the infinitesimal probability to have a point inside the infinitesimally small region around $\boldsymbol{x}_1$ with volume $|d\boldsymbol{x}_1|$,[4] while $\varrho^{(2)}_{\mathbf{\Psi}}(\boldsymbol{x}_1, \boldsymbol{x}_2)d\boldsymbol{x}_1 d\boldsymbol{x}_2$ is the *joint* probability to have a point inside the infinitesimally small region around $\boldsymbol{x}_1$ with volume $|d\boldsymbol{x}_1|$ *and* another point inside the infinitesimally small region around $\boldsymbol{x}_2$ with volume $|d\boldsymbol{x}_2|$. Thus, while the first order intensity function basically describe the density of the points, the second order intensity function is used to describe stochastic interactions between points. More precisely, we can have one of the following situation:

- if $\varrho^{(2)}_{\mathbf{\Psi}}(\boldsymbol{x}_1, \boldsymbol{x}_2) < \varrho^{(1)}_{\mathbf{\Psi}}(\boldsymbol{x}_1)\varrho^{(1)}_{\mathbf{\Psi}}(\boldsymbol{x}_2)$, that is, the joint probability of having a point in $\boldsymbol{x}_1$ and a point in $\boldsymbol{x}_2$ is lower than the product of the respective unconditional probabilities, then there is repulsion between points (it is the case, e.g., of the determinantal PPs, see [39]–[41]);
- if $\varrho^{(2)}_{\mathbf{\Psi}}(\boldsymbol{x}_1, \boldsymbol{x}_2) = \varrho^{(1)}_{\mathbf{\Psi}}(\boldsymbol{x}_1)\varrho^{(1)}_{\mathbf{\Psi}}(\boldsymbol{x}_2)$, that is, the joint probability of having a point in $\boldsymbol{x}_1$ and a point in $\boldsymbol{x}_2$ is equal to the product of the respective unconditional probabilities, than there is independence among points (it is the case of the PPP, see [42]).
- if $\varrho^{(2)}_{\mathbf{\Psi}}(\boldsymbol{x}_1, \boldsymbol{x}_2) > \varrho^{(1)}_{\mathbf{\Psi}}(\boldsymbol{x}_1)\varrho^{(1)}_{\mathbf{\Psi}}(\boldsymbol{x}_2)$, that is, the joint probability of having a point in $\boldsymbol{x}_1$ and a point in $\boldsymbol{x}_2$ is higher than the product of the respective unconditional probabilities, then there is attraction between points (it is usually the case of the clustering PPs such as Cox, see [43]–[46]).

We will investigate the impact of such stochastic interactions on the SNR when $\mathbf{\Psi}$ is the PP which models the positions of the point transmitters in spatially distributed molecular communications via diffusion.

D. Spatially distributed transmission models: superposition with generalization of Sec. II-B

Without loss of generality, the center of the spherical receiver is at the origin. The sphere of radius R representing its volume is denoted as $\mathbf{\Omega}_R$. Consider a swarm of point transmitters, whose random positions $\mathbf{x}_n \in \mathbb{R}^3$ are modeled as the outcomes of a spatial PP (not necessarily Poisson) $\mathbf{\Psi}$ in $\mathbb{R}^3 \backslash \mathbf{\Omega}_R$.[5] Thus, the distance between the n-th point transmitter and the receiver results in $\|\mathbf{x}_n\|$.

Due to the superposition of effects and the independence of the emissions from different point transmitters, the overall number of received molecules from all transmitters till time t results in

$$\mathsf{n}_{\mathrm{rx}}|_{\mathbf{\Psi}}(t) = \sum_{n \in \mathcal{I}\{\mathbf{\Psi}\}} \mathsf{a}_n|_{\mathbf{\Psi},t} \tag{9}$$

where, for different n, $\{\mathsf{a}_n|_{\mathbf{\Psi},t}\}$ are independent RVs modeling the contribution of the n-th transmitter placed at $\mathbf{x}_n \in \mathbf{\Psi}$. More precisely:[6]

Remark 1: Note that the stochastic properties of the n-th transmitter contribution in received molecules, $\mathsf{a}_n|_{\mathbf{\Psi},t}$, depends on the spatial PP $\mathbf{\Psi}$ (through the RVs $\{\mathbf{x}_n\}$) and on the transmitter model.

III. SNR Evaluation

To better understand all the problems involved by the SNR evaluation in MCvD with different transmitter models, we will focus, first, on the simple single transmitter case, then, we will apply the framework to the case of interest of spatially distributed transmission.

We define the SNR related to a received molecular signal as the ratio between the squared number of received molecules and the variance of received molecules themselves. However, such evaluation has to be adapted to the different scenarios considered: the received number of molecules depends on the distance from the transmitter in the point-to-point case, whereas it is a sum of contributions from the swarm of transmitters in the spatially distributed case.

A. SNR in point-to-point MCvD

The SNR at the distance r till time t is here defined as the ratio between the square of the mean of the number $\mathsf{a}|_{r,t}$ of received molecules, at distance r till time t, and the corresponding variance:

$$\mathrm{SNR}^{(0)}(r,t) \triangleq \frac{\left(\mathbb{E}\left\{\mathsf{a}|_{r,t}\right\}\right)^2}{\mathbb{V}\{\mathsf{a}|_{r,t}\}} \tag{11}$$

where the superscript "(0)" indicates the single transmitter case.

[4] $|\cdot|$ indicates the Lebesgue measure.

[5] and transmitters cannot be placed inside its volume $\mathbf{\Omega}_R$.

[6] Formally, $\mathsf{a}|_{r,t}$ is replaced by $\mathsf{a}_n|_{\mathbf{\Psi},t}$, since each contribution in (9) specifically refers to the n-th transmitter, and thus, is conditioned to its distance $\|\mathbf{x}_n\|$ from the receiver, where all $\{\mathbf{x}_n\}$ belong to the PP $\mathbf{\Psi}$.

$$\mathsf{a}_n|_{\mathbf{\Psi},t} = \sum_{l \in \mathcal{L}} \mathsf{b}_{n,l}|_{\mathbf{\Psi},t} \tag{10}$$

where

1) for exact concentration (synchronized) transmitters: $\mathcal{L} = \{1, 2, ..., N_{\mathrm{tx}}\}$ and $\mathsf{b}_{n,l}|_{\mathbf{\Psi},t} \sim \mathcal{B}[F_{\mathrm{hit}}(\|\mathbf{x}_n\|, t)]$ (all point transmitters are assumed to emit exactly N_{tx} molecules at $t = 0$);
2) for Poisson concentration (synchronized) transmitters: $\mathcal{L} = \{1, 2, ..., \mathsf{n}^{(n)}_{\mathrm{tx}}\}$ and $\mathsf{b}_{n,l}|_{\mathbf{\Psi},t} \sim \mathcal{B}[F_{\mathrm{hit}}(\|\mathbf{x}_n\|, t)]$, with $\{\mathsf{n}^{(n)}_{\mathrm{tx}}\}$ IID Poisson RVs with mean N_{tx} (each n-th point transmitter emits a random number $\mathsf{n}^{(n)}_{\mathrm{tx}}$ of molecules at $t = 0$);
3) for timing (asynchronous) transmitters: $\mathcal{L} = \mathcal{I}\{\mathbf{\Phi}^{(n)}\}$ and $\mathsf{b}_{n,l}|_{\mathbf{\Psi},t} \sim \mathcal{B}[F_{\mathrm{hit}}(\|\mathbf{x}_n\|, t - \boldsymbol{\tau}^{(n)}_l)]$, with $\mathbf{\Phi}^{(n)}$ time domain PPPs independent among n with intensity function $\lambda(t)$ whatever n, and $\boldsymbol{\tau}^{(n)}_l \in \mathbf{\Phi}^{(n)}$ (according to the asynchronous stochastic model proposed in [8], each point transmitter follows a timing transmitter model with random and independent emissions, and no synchronization is assumed: the l-th emission of the n-th transmitter is modeled by the RV $\boldsymbol{\tau}^{(n)}_l$ belonging to the time domain PP $\mathbf{\Phi}^{(n)}$).

1) SNR with exact concentration transmitter: By using (2) in the expressions for the mean and the variance of a binomial RV, we obtain the mean and variance of the received molecules in the case of exact concentration transmitter:

$$\mathbb{E}\left\{\mathsf{a}|_{r,t}\right\} = N_{\text{tx}}\, F_{\text{hit}}(r,t) \tag{12a}$$
$$\mathbb{V}\{\mathsf{a}|_{r,t}\} = N_{\text{tx}}\, F_{\text{hit}}(r,t)\left[1 - F_{\text{hit}}(r,t)\right]. \tag{12b}$$

Thus, from (11) it follows

$$\text{SNR}^{(0)}_{\text{Ex. conc.}}(r,t) = \frac{N_{\text{tx}}\, F_{\text{hit}}(r,t)}{1 - F_{\text{hit}}(r,t)}. \tag{13}$$

2) SNR with Poisson concentration transmitter: In Appendix A we show that, with Poisson concentration transmitter, the mean and the variance of the number of received molecules result in

$$\mathbb{E}\left\{\mathsf{a}|_{r,t}\right\} = \mathbb{V}\{\mathsf{a}|_{r,t}\} = N_{\text{tx}} F_{\text{hit}}(r,t). \tag{14}$$

Thus, (11) leads to

$$\text{SNR}^{(0)}_{\text{Po. conc.}}(r,t) = N_{\text{tx}} F_{\text{hit}}(r,t). \tag{15}$$

3) SNR with timing transmitter: In Appendix B we prove that, with timing transmitter, the mean and the variance of the number of received molecules result in

$$\mathbb{E}\left\{\mathsf{a}|_{r,t}\right\} = \mathbb{V}\{\mathsf{a}|_{r,t}\} = \int_{-\infty}^{+\infty} \lambda(\tau) F_{\text{hit}}(r, t-\tau) d\tau. \tag{16}$$

Thus, (11) leads to

$$\text{SNR}^{(0)}_{\text{Timing}}(r,t) = \int_{-\infty}^{+\infty} \lambda(\tau) F_{\text{hit}}(r, t-\tau) d\tau. \tag{17}$$

Remark 2: For Poisson concentration and timing transmitter models, the SNR equals the average number of received molecules. In our framework, this result follows from the Poisson assumption adopted in both these two models. In the previous literature for single transmitter MCvD, it is a known result derived by physical and chemical considerations [4].

B. SNR in spatially distributed MCvD

Definition 1 (SNR associated to received molecules from a swarm of point transmitters scattered according to a PP): We define the SNR due to the swarm of transmitters placed at positions $\{\mathbf{x}_n\} \in \mathbf{\Psi}$ as

$$\text{SNR}_{\mathbf{\Psi}}(t) \triangleq \frac{\left(\mathbb{E}\left\{\mathsf{n}_{\text{rx}}|_{\mathbf{\Psi}}(t)\right\}\right)^2}{\mathbb{V}\{\mathsf{n}_{\text{rx}}|_{\mathbf{\Psi}}(t)\}} = \frac{\left[\mathbb{E}\left\{\sum_{n\in\mathcal{I}\{\mathbf{\Psi}\}} \mathsf{a}_n|_{\mathbf{\Psi},t}\right\}\right]^2}{\mathbb{V}\left\{\sum_{n\in\mathcal{I}\{\mathbf{\Psi}\}} \mathsf{a}_n|_{\mathbf{\Psi},t}\right\}} \tag{18}$$

where $\mathsf{n}_{\text{rx}}|_{\mathbf{\Psi}}(t)$ is the RV describing the number of molecules received from all transmitters till time t and $\{\mathsf{a}_n|_{\mathbf{\Psi},t}\}$ are the RVs modeling the contribution of the n-th transmitter placed at $\mathbf{x}_n \in \mathbf{\Psi}$, given $\mathbf{\Psi}$.

In order to separate the effect of the transmitter model and that of multiple transmitters random displacement, we focus on the contribution of the generic transmitter; then, we consider the overall contribution of multiple transmitters by using the superposition of effects.

Theorem 1 (General expression of the SNR due to spatially-distributed transmission): The SNR due to multiple transmitters placed according to $\mathbf{\Psi} \in \mathbb{R}^3$ can be expressed as

$$\text{SNR}(t) = \frac{\left[\int_{\mathbb{R}^3\setminus\mathbf{\Omega}_R} \lambda_{\mathbf{\Psi}}\, \epsilon(\|\boldsymbol{x}\|,t) d\boldsymbol{x}\right]^2}{\int_{\mathbb{R}^3\setminus\mathbf{\Omega}_R} \lambda_{\mathbf{\Psi}}\, \xi(\|\boldsymbol{x}\|,t) d\boldsymbol{x} + \zeta_{\mathbf{\Psi}}(t)} \tag{19}$$

where

$$\zeta_{\mathbf{\Psi}}(t) \triangleq \int_{\mathbb{R}^3\setminus\mathbf{\Omega}_R}\int_{\mathbb{R}^3\setminus\mathbf{\Omega}_R} \left[\rho_{\mathbf{\Psi}}(\|\boldsymbol{x}_1 - \boldsymbol{x}_2\|) - \lambda_{\mathbf{\Psi}}^2\right] \times \epsilon(\|\boldsymbol{x}_1\|,t)\, \epsilon(\|\boldsymbol{x}_2\|,t)\, d\boldsymbol{x}_1 d\boldsymbol{x}_2 \tag{20}$$

and the functions $\epsilon(r,t)$ and $\xi(r,t)$ are defined such that

$$\epsilon(\|\mathbf{x}_n\|,t) = \mathbb{E}_{\mathsf{a}|\mathbf{\Psi}}\left\{\mathsf{a}_n|_{\mathbf{\Psi},t}\right\} \tag{21a}$$
$$\xi(\|\mathbf{x}_n\|,t) = \mathbb{E}_{\mathsf{a}|\mathbf{\Psi}}\left\{\mathsf{a}_n^2|_{\mathbf{\Psi},t}\right\} \tag{21b}$$

with $\mathbb{E}_{\mathsf{a}|\mathbf{\Psi}}\{\cdot\}$ indicating the averaging operator given the positions $\{\mathbf{x}_n\} \in \mathbf{\Psi}$ of the point transmitters.[7]

Proof: By using the superposition of effects stated in (9) in the definition of the SNR for multiple transmitters case (11), we obtain

$$\begin{aligned}
\mathbb{E}\left\{\mathsf{n}_{\text{rx}}|_{\mathbf{\Psi}}(t)\right\} =& \mathbb{E}\left\{\sum_{n\in\mathcal{I}\{\mathbf{\Psi}\}} \mathsf{a}_n|_{\mathbf{\Psi},t}\right\} \\
=& \mathbb{E}_{\mathbf{\Psi}}\left\{\sum_{n\in\mathcal{I}\{\mathbf{\Psi}\}} \mathbb{E}_{\mathsf{a}|\mathbf{\Psi}}\left\{\mathsf{a}_n|_{\mathbf{\Psi},t}\right\}\right\} \\
=& \mathbb{E}_{\mathbf{\Psi}}\left\{\sum_{\mathbf{x}_n\in\mathbf{\Psi}} \epsilon(\|\mathbf{x}_n\|,t)\right\}
\end{aligned} \tag{22a}$$

$$\begin{aligned}
\mathbb{E}\left\{\mathsf{n}_{\text{rx}}|_{\mathbf{\Psi}}^2(t)\right\} =& \mathbb{E}\left\{\left(\sum_{n\in\mathcal{I}\{\mathbf{\Psi}\}} \mathsf{a}_n|_{\mathbf{\Psi},t}\right)^2\right\} \\
=& \mathbb{E}_{\mathbf{\Psi}}\left\{\sum_{n\in\mathcal{I}\{\mathbf{\Psi}\}}\sum_{k\in\mathcal{I}\{\mathbf{\Psi}\}} \mathbb{E}_{\mathsf{a}|\mathbf{\Psi}}\left\{\mathsf{a}_n|_{\mathbf{\Psi},t}\mathsf{a}_m|_{\mathbf{\Psi}}(t)\right\}\right\} \\
=& \mathbb{E}_{\mathbf{\Psi}}\left\{\sum_{\mathbf{x}_n\in\mathbf{\Psi}} \xi(\|\mathbf{x}_n\|,t)\right\} \\
&+ \mathbb{E}_{\mathbf{\Psi}}\left\{\sum_{\mathbf{x}_n\in\mathbf{\Psi}}\sum_{\substack{\mathbf{x}_k\in\mathbf{\Psi}\\ \mathbf{x}_n\neq\mathbf{x}_k}} \epsilon(\|\mathbf{x}_n\|,t)\, \epsilon(\|\mathbf{x}_m\|,t)\right\}
\end{aligned} \tag{22b}$$

where by $\mathbb{E}_{\mathbf{\Psi}}\{\cdot\}$ we indicate the averaging over the transmitters positions $\{\mathbf{x}_n\} \in \mathbf{\Psi}$ and the last follows by observing that the contributions $\{\mathsf{a}_n|_{\mathbf{\Psi},t}\}$ are independent given $\mathbf{\Psi}$. By

[7] It can be readily noticed that, according to Sec. II-D, the RHS in (21) depend on $\mathbf{\Psi}$ through $\mathbf{x}_n \in \mathbf{\Psi}$ only.

applying the properties of first and second order product density function of a PP [38], [47], from (22) we obtain

$$\mathbb{E}\left\{\mathsf{n}_{\text{rx}}|_{\boldsymbol{\Psi}}(t)\right\} = \int_{\mathbb{R}^3\setminus\boldsymbol{\Omega}_R} \lambda_{\boldsymbol{\Psi}}\, \epsilon(\|\boldsymbol{x}\|,t)d\boldsymbol{x} \tag{23a}$$

$$\begin{aligned}\mathbb{E}\left\{\mathsf{n}_{\text{rx}}|^2_{\boldsymbol{\Psi}}(t)\right\} =& \int_{\mathbb{R}^3\setminus\boldsymbol{\Omega}_R} \lambda_{\boldsymbol{\Psi}}\, \xi(\|\boldsymbol{x}\|,t)d\boldsymbol{x} \\ &+ \int_{\mathbb{R}^3\setminus\boldsymbol{\Omega}_R}\int_{\mathbb{R}^3\setminus\boldsymbol{\Omega}_R} \rho_{\boldsymbol{\Psi}}(\|\boldsymbol{x}_1-\boldsymbol{x}_2\|) \\ &\times \epsilon(\|\boldsymbol{x}_1\|,t)\,\epsilon(\|\boldsymbol{x}_2\|,t)\,d\boldsymbol{x}_1 d\boldsymbol{x}_2\,.\end{aligned} \tag{23b}$$

From (23) it follows

$$\begin{aligned}\mathbb{V}\{\mathsf{n}_{\text{rx}}|_{\boldsymbol{\Psi}}(t)\} =& \mathbb{E}\left\{\mathsf{n}_{\text{rx}}|^2_{\boldsymbol{\Psi}}(t)\right\} - \left(\mathbb{E}\left\{\mathsf{n}_{\text{rx}}|_{\boldsymbol{\Psi}}(t)\right\}\right)^2 \\ =& \int_{\mathbb{R}^3\setminus\boldsymbol{\Omega}_R} \lambda_{\boldsymbol{\Psi}}\, \xi(\|\boldsymbol{x}\|,t)d\boldsymbol{x} \\ &+ \int_{\mathbb{R}^3\setminus\boldsymbol{\Omega}_R}\int_{\mathbb{R}^3\setminus\boldsymbol{\Omega}_R} \rho_{\boldsymbol{\Psi}}(\|\boldsymbol{x}_1-\boldsymbol{x}_2\|) \\ &\times \epsilon(\|\boldsymbol{x}_1\|,t)\,\epsilon(\|\boldsymbol{x}_2\|,t)\,d\boldsymbol{x}_1 d\boldsymbol{x}_2 \\ &- \int_{\mathbb{R}^3\setminus\boldsymbol{\Omega}_R}\int_{\mathbb{R}^3\setminus\boldsymbol{\Omega}_R} \lambda^2_{\boldsymbol{\Psi}}\, \epsilon(\|\boldsymbol{x}_1\|,t)\epsilon(\|\boldsymbol{x}_2\|,t)d\boldsymbol{x}_1 d\boldsymbol{x}_2 \\ =& \int_{\mathbb{R}^3\setminus\boldsymbol{\Omega}_R} \lambda_{\boldsymbol{\Psi}}\, \xi(\|\boldsymbol{x}\|,t)d\boldsymbol{x} + \zeta_{\boldsymbol{\Psi}}(t)\end{aligned} \tag{24}$$

which, jointly with (23a), leads to (19). □

Note that $\epsilon(\|\boldsymbol{x}\|,t)$ and $\xi(\|\boldsymbol{x}\|,t)$ depend on the transmission model. They will be given in the following for all the cases of spatially distributed transmission mentioned in II-D. First, the following definitions, related to the spatial distribution of the point transmitters (described by the PP $\boldsymbol{\Psi}$), are needed.

Definition 2 (First and second order MCvD channel characterization): We define the following functions, useful for the interpretation of the results:

$$H_{\text{all}}(t) \triangleq \lambda_{\boldsymbol{\Psi}} \int_{\mathbb{R}^3\setminus\boldsymbol{\Omega}_R} F_{\text{hit}}(\|\boldsymbol{x}\|,t)d\boldsymbol{x} \tag{25a}$$

$$H^{(2)}_{\text{all}}(t_1,t_2) \triangleq \lambda_{\boldsymbol{\Psi}} \int_{\mathbb{R}^3\setminus\boldsymbol{\Omega}_R} F_{\text{hit}}(\|\boldsymbol{x}\|,t_1)F_{\text{hit}}(\|\boldsymbol{x}\|,t_2)d\boldsymbol{x} \tag{25b}$$

$$\begin{aligned}G^{(2)}_{\text{all}}(t_1,t_2) \triangleq& \int_{\mathbb{R}^3\setminus\boldsymbol{\Omega}_R}\int_{\mathbb{R}^3\setminus\boldsymbol{\Omega}_R} \left[\rho_{\boldsymbol{\Psi}}(\|\boldsymbol{x}_1-\boldsymbol{x}_2\|) - \lambda^2_{\boldsymbol{\Psi}}\right] \\ &\times F_{\text{hit}}(\|\boldsymbol{x}_1\|,t_1)F_{\text{hit}}(\|\boldsymbol{x}_2\|,t_2)d\boldsymbol{x}_1 d\boldsymbol{x}_2\end{aligned} \tag{25c}$$

Note that (25a) is the so-called collective impulse response introduced by [7] and [8] for the first order analysis, while (25b) and (25c) are related to the second order characterization.

Remark 3: Differently than in point-to-point case, in the spatially distributed multiple transmitters case the variance of the number of received molecules is different than its mean: in fact, even in Poisson concentration and timing transmitter models,[8] the number of received molecules from all the randomly placed transmitters (according to a spatial PP) is not a Poisson RV. Thus, the proposed second-order evaluation is needed to correctly compute the SNR, since the quality of the reception cannot be evaluated through an averaging operation only, as done in previous works [7], [8], [31].

[8]Compare (22a) to (24), with $\epsilon(\mathbf{x}_n,t)$, $\xi(\mathbf{x}_n,t)$, and $\eta(\mathbf{x}_n,\mathbf{x}_m,t)$ provided by (27) and by Appendix C.

1) SNR with synchronous exact concentration transmitters: By using (10) in (21) with $\mathcal{L}=\{1,2,...,N_{\text{tx}}\}$ and $\mathsf{b}_{n,l}|_{\boldsymbol{\Psi},t} \sim \mathcal{B}[F_{\text{hit}}(\|\mathbf{x}_n\|,t)]$, it results

$$\begin{aligned}\epsilon(\mathbf{x}_n,t) &= N_{\text{tx}}F_{\text{hit}}(\|\mathbf{x}_n\|,t) \\ \xi(\mathbf{x}_n,t) &= N_{\text{tx}}F_{\text{hit}}(\|\mathbf{x}_n\|,t) + N_{\text{tx}}(N_{\text{tx}}-1)F^2_{\text{hit}}(\|\mathbf{x}_n\|,t)\,.\end{aligned}$$

Thus, by using (25) in (19) we obtain

$$\text{SNR}(t) = \frac{\left[H_{\text{all}}(t)\right]^2}{\frac{H_{\text{all}}(t)}{N_{\text{tx}}} + \left(1-\frac{1}{N_{\text{tx}}}\right)H^{(2)}_{\text{all}}(t,t) + G^{(2)}_{\text{all}}(t,t)}\,. \tag{26}$$

2) SNR with synchronous Poisson concentration transmitters: By using (10) in (21) with $\mathcal{L}=\{1,2,...,\mathsf{n}^{(n)}_{\text{tx}}\}$ and $\mathsf{b}_{n,l}|_{\boldsymbol{\Psi},t} \sim \mathcal{B}[F_{\text{hit}}(\|\mathbf{x}_n\|,t)]$, it results

$$\epsilon(\mathbf{x}_n,t) = N_{\text{tx}}\,F_{\text{hit}}(\mathbf{x}_n,t) \tag{27a}$$

$$\xi(\mathbf{x}_n,t) = N_{\text{tx}}F_{\text{hit}}(\mathbf{x}_n,t) + N^2_{\text{tx}}F^2_{\text{hit}}(\mathbf{x}_n,t)\,. \tag{27b}$$

Thus (19) and (25) lead to

$$\text{SNR}(t) = \frac{\left[H_{\text{all}}(t)\right]^2}{\frac{H_{\text{all}}(t)}{N_{\text{tx}}} + H^{(2)}_{\text{all}}(t,t) + G^{(2)}_{\text{all}}(t,t)}\,. \tag{28}$$

3) SNR with asynchronous timing transmitters: The following lemma is needed for the asynchronous case.

Lemma 1 (Mean and variance of the number of received molecules with asynchronous transmissions): If asynchronous timing transmitters, placed over $\mathbb{R}^3\setminus\boldsymbol{\Omega}_R$ according to the spatial PP $\boldsymbol{\Psi}$, emit molecules according to different and independent time domain PPs $\boldsymbol{\Phi}^{(n)}$ with first and second order product intensity functions $\rho(t)$ and $\rho^{(2)}(t,\tau)$, the mean and the variance of the number of received molecules result in:

$$\mathbb{E}\left\{\mathsf{n}_{\text{rx}}|_{\boldsymbol{\Psi}}(t)\right\} = \int_{-\infty}^{+\infty} \rho(\tau)H_{\text{all}}(t-\tau)d\tau \tag{29a}$$

$$\begin{aligned}\mathbb{V}\{\mathsf{n}_{\text{rx}}|_{\boldsymbol{\Psi}}(t)\} =& \int_{-\infty}^{+\infty} \rho(\tau)H_{\text{all}}(t-\tau)d\tau \\ &+ \int_{-\infty}^{+\infty}\int_{-\infty}^{+\infty} \rho^{(2)}(\tau,s)H^{(2)}_{\text{all}}(t-\tau,t-s)d\tau ds \\ &+ \int_{-\infty}^{+\infty}\int_{-\infty}^{+\infty} \rho(\tau)\rho(s)G^{(2)}_{\text{all}}(t-\tau,t-s)d\tau ds\,.\end{aligned} \tag{29b}$$

Proof: See Appendix C. □

If the time domain PPs are Poisson with intensity $\lambda(t)$, it is straightforward to obtain, from (18) and (29):[9]

$$\begin{aligned}\text{SNR}(t) =& \left[\int_{-\infty}^{+\infty} \lambda(\tau)H_{\text{all}}(t-\tau)d\tau\right]^2 \\ &\times \left[\int_{-\infty}^{+\infty} \lambda(\tau)\;H_{\text{all}}(t-\tau)d\tau\right. \\ &+ \int_{-\infty}^{+\infty}\int_{-\infty}^{+\infty} \lambda(\tau)\lambda(s)H^{(2)}_{\text{all}}(t-\tau,t-s)d\tau ds \\ &\left.+ \int_{-\infty}^{+\infty}\int_{-\infty}^{+\infty} \lambda(\tau)\lambda(s)G^{(2)}_{\text{all}}(t-\tau,t-s)d\tau ds\right]^{-1}.\end{aligned} \tag{30}$$

[9]Recall that, for a PPP, it is $\rho(t)=\lambda(t)$ and $\rho^{(2)}(t,\tau)=\lambda(t)\lambda(\tau)$ [42].

Remark 4: Note that in the SNR expressions (26), (28), and (30), the denominator is always composed by three components, corresponding to the three functions characterizing the MCvD channel according to (25):

- the mean (which depends on the first order characterization of the spatially distributed molecular channel $H_{\text{all}}(t)$, see also [8]);
- a component depending on the second order characterization of the spatially distributed molecular channel $H^{(2)}_{\text{all}}(t,\tau)$;
- a component depending on the stochastic characterization (attraction/repulsion) of the transmitters positions, $G^{(2)}_{\text{all}}(t,\tau)$, which, according to (25c), is negative for repulsive PP and positive for clustered PP.

C. Impact of stochastic interactions between transmitter positions on the SNR

The following theorem states that, in the multiple transmitters scenario, the SNR is increased by stochastic repulsion between transmitters and is decreased by stochastic attraction (clustering), with respect to the case of a Poisson distribution of the transmitters (stochastic independence) with the same intensity.

Theorem 2 (Effect of attraction/repulsion on the SNR): Let $\boldsymbol{\Psi}^{(\text{re})}$, $\boldsymbol{\Psi}^{(\text{Po})}$, and $\boldsymbol{\Psi}^{(\text{cl})}$ be, a repulsive, a Poisson and a clustered isotropic PP, respectively, with the same intensity $\lambda_{\boldsymbol{\Psi}}$. The following inequalities hold for the SNR due the swarm of transmitters placed according to $\boldsymbol{\Psi}^{(\text{cl})}$, $\boldsymbol{\Psi}^{(\text{Po})}$, and $\boldsymbol{\Psi}^{(\text{re})}$.

$$\text{SNR}^{(\text{cl})}(t) \leqslant \text{SNR}^{(\text{Po})}(t) \leqslant \text{SNR}^{(\text{re})}(t)\,. \tag{31}$$

Proof: By the definition of clustered and repulsive PPs, and comparing a clustered isotropic PP $\boldsymbol{\Psi}^{(\text{cl})}$ and a repulsive isotropic PP $\boldsymbol{\Psi}^{(\text{re})}$ with a homogeneous PPP $\boldsymbol{\Psi}^{(\text{Po})}$ with the same intensity $\lambda_{\boldsymbol{\Psi}}$, the following inequalities hold [38], [39], [43]:

$$\rho^{(\text{re})}_{\boldsymbol{\Psi}}(\|\boldsymbol{x}_1-\boldsymbol{x}_2\|) \leqslant \lambda^2_{\boldsymbol{\Psi}} \leqslant \rho^{(\text{cl})}_{\boldsymbol{\Psi}}(\|\boldsymbol{x}_1-\boldsymbol{x}_2\|) \tag{32}$$

for all $\boldsymbol{x}_1, \boldsymbol{x}_2 \in \mathbb{R}^3$. Thus, (23) leads to

$$\mathbb{E}\left\{\mathsf{n}_{\text{rx}}|^{(\text{re})}_{\boldsymbol{\Psi}}\right\} = \mathbb{E}\left\{\mathsf{n}_{\text{rx}}|^{(\text{Po})}_{\boldsymbol{\Psi}}\right\} = \mathbb{E}\left\{\mathsf{n}_{\text{rx}}|^{(\text{cl})}_{\boldsymbol{\Psi}}\right\} \tag{33a}$$

$$\mathbb{V}\left\{\mathsf{n}_{\text{rx}}|^{(\text{re})}_{\boldsymbol{\Psi}}\right\} \leqslant \mathbb{V}\left\{\mathsf{n}_{\text{rx}}|^{(\text{Po})}_{\boldsymbol{\Psi}}\right\} \leqslant \mathbb{V}\left\{\mathsf{n}_{\text{rx}}|^{(\text{cl})}_{\boldsymbol{\Psi}}\right\}\,. \tag{33b}$$

The theorem follows by using (32) and (33) in (18). □

Remark 5: Last result may appear as counter-intuitive, since one may argue that a cluster close to the receiver actually helps the communication. However, it has to be observed that PPs with stochastic interactions between points are considered here, which are however homogeneous (i.e., the density is independent of the position). Thus, for a clustered PP, the parent points (i.e., the centers of the clusters) are uniformly distributed over $\mathbb{R}^3$. A cluster close to the receiver helps the communication, but, in the same way, a cluster far from the receiver has opposite effect. Theorem 2 states that, in average, a clustered PP is not convenient. On the contrary, PPs with repulsion between points (e.g., determinantal PPs [47]) are. This is in accordance to the observation that stochastic repulsion lead to more regular point displacement [48].

D. Multiple-sample detection

The proposed "analog" approach can be extended to a "digital" scenario where the receiver counts the number of observed molecules several times within one symbol interval. Consider a multiple-samples detector as in [35]. Here, molecules are emitted and observed every Δt seconds within each symbol time T_{s}.[10] For both synchronous Poisson concentration and asynchronous timing transmitters, the following proposition can be derived using the results of Lemma 1.

Theorem 3 (SNR with multiple samples): Let K denote the number of samples. If the observation interval is Δt second long after each emission (thus, the whole observation interval is $[0, T_{\text{s}}]$), the SNR results in $\text{SNR}_{\text{mul}} = \frac{\mu^2_{\text{mul}}}{\sigma^2_{\text{mul}}}$, where

$$\mu_{\text{mul}} = N_{\text{tx}} \sum_{k=0}^{K-1} H_{\text{all}}(T_{\text{s}} - k\Delta t) \tag{34a}$$

$$\begin{aligned}\sigma^2_{\text{mul}} =& N_{\text{tx}} \sum_{k=0}^{K-1} H_{\text{all}}(T_{\text{s}} - k\Delta t) \\ &+ N^2_{\text{tx}} \sum_{k=0}^{K-1}\sum_{m=0}^{K-1} H^{(2)}_{\text{all}}(T_{\text{s}} - k\Delta t, T_{\text{s}} - m\Delta t) \\ &+ N^2_{\text{tx}} \sum_{k=0}^{K-1}\sum_{m=0}^{K-1} G^{(2)}_{\text{all}}(T_{\text{s}} - k\Delta t, T_{\text{s}} - m\Delta t)\end{aligned} \tag{34b}$$

for synchronous Poisson concentration transmitters, and

$$\mu_{\text{mul}} = \frac{N_{\text{tx}}}{T_{\text{a}}} \sum_{k=0}^{K-1} \int_{k\Delta t}^{k\Delta t + T_{\text{a}}} H_{\text{all}}(T_{\text{s}} - \tau) d\tau \tag{35a}$$

$$\begin{aligned}\sigma^2_{\text{mul}} =& \frac{N_{\text{tx}}}{T_{\text{a}}} \sum_{k=0}^{K-1} \int_{k\Delta t}^{k\Delta t + T_{\text{a}}} H_{\text{all}}(T_{\text{s}} - \tau) d\tau \\ &+ \frac{N^2_{\text{tx}}}{T^2_{\text{a}}} \sum_{k=0}^{K-1}\sum_{m=0}^{K-1} \int_{k\Delta t}^{k\Delta t + T_{\text{a}}} \int_{m\Delta t}^{m\Delta t + T_{\text{a}}} H^{(2)}_{\text{all}}(T_{\text{s}} - \tau, T_{\text{s}} - s) d\tau ds \\ &+ \frac{N^2_{\text{tx}}}{T^2_{\text{a}}} \sum_{k=0}^{K-1}\sum_{m=0}^{K-1} \int_{k\Delta t}^{k\Delta t + T_{\text{a}}} \int_{m\Delta t}^{m\Delta t + T_{\text{a}}} G^{(2)}_{\text{all}}(T_{\text{s}} - \tau, T_{\text{s}} - s) d\tau ds\end{aligned} \tag{35b}$$

for asynchronous timing transmitters with uniformly distributed emissions in $[0, T_{\text{a}}]$ with $T_{\text{a}} < \Delta t$.

Proof: First, observe that, for both Poisson concentration and timing transmitters, we can use the results obtained for timing transmitters with

$$\lambda(t) = \sum_{k=0}^{K} g(t - k\Delta t) \tag{36}$$

where $g(t) = N_{\text{tx}}\delta(t)$ for synchronous Poisson concentration transmitters and $g(t) = \frac{N_{\text{tx}}}{T_{\text{a}}}\text{rect}\left(\frac{t}{T_{\text{a}}}\right)$ for asynchronous timing

[10] In [35] passive receivers are considered and samples are instantaneous as a consequence. Here, with fully absorbing receivers, each sample has duration Δt.

transmitters. By using (36) in (29) with the properties of the time domain PPPs, we obtain

$$\begin{aligned}\mu_{\text{mul}} &= \sum_{k=0}^{K-1}\int_{-\infty}^{+\infty} g(\tau-k\Delta t)H_{\text{all}}(T_{\text{s}}-\tau)d\tau\\ \sigma^2_{\text{mul}} &= \sum_{k=0}^{K-1}\int_{-\infty}^{+\infty} g(\tau-k\Delta t)H_{\text{all}}(T_{\text{s}}-\tau)d\tau\\ &+\sum_{k=0}^{K-1}\sum_{m=0}^{K-1}\int_{-\infty}^{+\infty}\int_{-\infty}^{+\infty} g(\tau-k\Delta t)\\ &\times g(s-m\Delta t)H^{(2)}_{\text{all}}(T_{\text{s}}-\tau,T_{\text{s}}-s)d\tau ds\\ &+\sum_{k=0}^{K-1}\sum_{m=0}^{K-1}\int_{-\infty}^{+\infty}\int_{-\infty}^{+\infty} g(\tau-k\Delta t)\\ &\times g(s-m\Delta t)G^{(2)}_{\text{all}}(T_{\text{s}}-\tau,T_{\text{s}}-s)d\tau ds\end{aligned}$$

which result in (34) and (35). □

Note that the proposed evaluation do not require that samples are independent, which, generally, are not [37].

IV. Digital approach: ISI evaluation

SNR is key performance indicator when analog transmission is considered (e.g., for the MCvD case, when the information is encoded in the time continuous function $\lambda(t)$ and is revealed through the time continuous function $f(t)$). For digital transmission, the BEP has to be computed to evaluate the performance of MCvD. However, the framework developed for the SNR can be useful to such an evaluation. Indeed, in this section, first, we show that also signal-to-interference ratio (SIR) and the SINR due to the presence of ISI can be computed in a similar way. Then, by means of Gaussian approximation, we derive an expression for the BEP.

Since the BEP in case of exact concentration transmitters has been derived in [7], we focus on the Poisson concentration and the timing transmitters case. More specifically, we consider two different spatially distributed transmission scenarios:

- Poisson concentration synchronous transmitters representing nano-robots which emit all molecules at every time bit;
- timing asynchronous transmitters representing randomly generated molecules due to chemical reactions in the fluid, described by the propensity function (i.e., the intensity function $\lambda(t)$ in our model) [29], [32], [49], [50]. In such a case, digital communication is possible by controlling the propensity function in a proper way.

Note that the framework developed in Sec. III for asynchronous timing transmissions can capture both scenarios for proper $\lambda(t)$.[11]

A. Digital transmission via MCvD

Definition 3: We define a spatially distributed digital transmission via MCvD a scenario where all time domain PPs $\{\Phi^{(n)}\}$ (modeling the emissions of the n-th timing transmitter according to Sec. II-D) have an intensity function $\lambda(t)$ given by:[12]

$$\lambda(t) = \sum_{i=0}^{j} \mathsf{d}_i g(t - iT_{\text{b}}) \tag{37}$$

where T_{b} is the bit duration, d_i is the value of the i-th bit, j is the number bits transmitted before the j-th one,[13] and $g(t)$ can be considered as a sort of waveform such that

- for the synchronous Poisson transmissions, $g(t) = N_{\text{tx}}\delta(t)$;
- for the asynchronous timing transmissions, $g(t)$ is a function which is nonzero only inside the interval $[0, T_{\text{b}}]$: e.g., for uniformly distributed emissions in an activity interval of duration T_{a}, $g(t) = \frac{N_{\text{tx}}}{T_{\text{a}}}\text{rect}\left(\frac{t}{T_{\text{a}}}\right)$ (where the ratio $T_{\text{a}}/T_{\text{b}}$ can be considered as the duty cycle).

It follows that, by considering a digital transmission with bit duration T_{b}, the number of received molecules in the interval $[jT_{\text{b}}, (j+1)T_{\text{b}}]$ (i.e., the j-th time bit) due to the emissions of the n-th timing transmitter placed at $\mathbf{x}_n \in \boldsymbol{\Psi}$ results in

$$\mathsf{a}_n|_{\boldsymbol{\Psi},\boldsymbol{\lambda}}[j] = \sum_{l\in\mathcal{I}\{\boldsymbol{\Phi}^{(n)}\}} \mathsf{b}_{n,l}|_{\boldsymbol{\Psi},\boldsymbol{\lambda}}[j] \tag{38}$$

where $\mathsf{b}_{n,l}|_{\boldsymbol{\Psi},\boldsymbol{\lambda}}[j]$ is a Bernoulli random variable taking value 1 if the l-th molecule emitted by the n-th transmitter (given the intensity function $\lambda(t)$ of the time domain PP $\Phi^{(n)}$) is received in the interval $[jT_{\text{b}}, (j+1)T_{\text{b}}]$ and value 0 if not.

It is known [37] that $f_{\text{hit}}(r,t) \triangleq \frac{\partial F_{\text{hit}}(r,t)}{\partial t}$ represents the probability that a molecule emitted at the time origin at distance r is received at time t. Thus, the probability that a molecules emitted at $t=0$ is observed within the interval $[t_1, t_2]$ is given by $\int_{t_1}^{t_2} f_{\text{hit}}(r,t)dt = F_{\text{hit}}(r,t_2) - F_{\text{hit}}(r,t_1)$. Due to the linearity and the time invariance of the Fick's law of diffusion, if the emission happens at $t = t_0$, the probability that the molecules is received in the interval $[t_1, t_2]$ is $F_{\text{hit}}(r, t_2 - t_0) - F_{\text{hit}}(r, t_1 - t_0)$. It follows that the RV modeling the reception of the l-th molecule emitted at time $\boldsymbol{\tau}_l^{(n)}$ by the n-th transmitter placed at $\boldsymbol{x}_n$, during the interval $[jT_{\text{b}}, (j+1)T_{\text{b}}]$, is distributed as

$$\mathsf{b}_{n,l}|_{\boldsymbol{\Psi},\boldsymbol{\lambda}}[j] \sim \mathcal{B}[\overline{F}_{\text{hit}}(\|\mathbf{x}_n\|, jT_{\text{b}} - \boldsymbol{\tau}_l^{(n)})] \tag{39}$$

where

$$\overline{F}_{\text{hit}}(r,t) \triangleq F_{\text{hit}}(r, T_{\text{b}}+t) - F_{\text{hit}}(r,t)\,. \tag{40}$$

According to Sec. II-D, the total number of received molecules during the j-th time bit due to all transmitters (placed according to $\boldsymbol{\Psi}$) is

$$\mathsf{n}_{\text{rx}}|_{\boldsymbol{\Psi},\boldsymbol{\lambda}}[j] = \sum_{n\in\mathcal{I}\{\boldsymbol{\Psi}\}} \mathsf{a}_n|_{\boldsymbol{\Psi},\boldsymbol{\lambda}}[j]\,. \tag{41}$$

[11] According to Sec. II-B, the timing transmitter as here considered (which emit molecules one-by-one according to a non-stationary time domain PPP with intensity function $\lambda(t)$) reduces to a Poisson concentration transmitter for $\lambda(t) = N_{\text{tx}}\delta(t)$ (all emissions are concentrated at $t=0$ and the number of emitted molecules remains a Poisson RV n_{tx} with mean N_{tx}).

[12] Due to the random bit sequence $\{\mathsf{d}_i\}$, the intensity function $\boldsymbol{\lambda}(t)$ is now a random process.

[13] Without loss of generality, focusing on the j-th bit means taking into account the ISI due to the previous symbols and neglecting the influence of future symbols, according to the causality, as done by [7].

Thus, thanks to (38) and (41), we can write that the total number of molecules received in the j-th interval due to emissions with intensity function $\lambda(t)$ results in:

$$\mathsf{n}_{\rm rx}|_{\boldsymbol{\Psi},\boldsymbol{\lambda}}[j] = \sum_{n\in\mathcal{I}\{\boldsymbol{\Psi}\}} \sum_{l\in\mathcal{I}\{\boldsymbol{\Phi}^{(n)}\}} \mathsf{b}_{n,l}|_{\boldsymbol{\Psi},\boldsymbol{\lambda}}[j]\,. \tag{42}$$

Lemma 2: [Mean and variance of the number of molecules received during a bit interval] The number $\mathsf{n}_{\rm rx}|_{\boldsymbol{\Psi},\rho}[j]$ of molecules received during the interval $[jT_{\rm b},(j+1)T_{\rm b}]$, due to a swarm of timing transmitters, randomly placed according to the homogeneous spatial PP $\boldsymbol{\Psi}$ with intensity $\lambda_{\boldsymbol{\Psi}}$ and second order intensity function $\rho_{\boldsymbol{\Psi}}(\tau)$, and emitting molecules according to time-domain PPs $\{\Phi^{(n)}\}$ with first and second order intensity functions $\rho(t)$ and $\rho^{(2)}(t,\tau)$, respectively, has mean and variance as follows:

$$\mathbb{E}\left\{\mathsf{n}_{\rm rx}|_{\boldsymbol{\Psi},\rho}[j]\right\} = \int_{-\infty}^{+\infty} \rho(\tau+jT_{\rm b})\overline{H}_{\rm all}(-\tau)d\tau \tag{43a}$$

$$\begin{aligned}\mathbb{V}\{\mathsf{n}_{\rm rx}|_{\boldsymbol{\Psi},\rho}[j]\} &= \int_{-\infty}^{+\infty} \rho(\tau+jT_{\rm b})\overline{H}_{\rm all}(-\tau)d\tau \\ &+ \int_{-\infty}^{+\infty}\int_{-\infty}^{+\infty} \rho^{(2)}(\tau+jT_{\rm b},s+jT_{\rm b})\overline{H}^{(2)}_{\rm all}(-\tau,-s)d\tau ds \\ &+ \int_{-\infty}^{+\infty}\int_{-\infty}^{+\infty} \rho(\tau+jT_{\rm b})\rho(s+jT_{\rm b})\overline{G}^{(2)}_{\rm all}(-\tau,-s)d\tau ds\,.\end{aligned} \tag{43b}$$

where

$$\overline{H}_{\rm all}(t) \triangleq \lambda_{\boldsymbol{\Psi}} \int_{\mathbb{R}^3\setminus\boldsymbol{\Omega}_R} \overline{F}_{\rm hit}(\|\boldsymbol{x}\|,t)d\boldsymbol{x} \tag{44a}$$

$$\overline{H}^{(2)}_{\rm all}(t_1,t_2) \triangleq \lambda_{\boldsymbol{\Psi}} \int_{\mathbb{R}^3\setminus\boldsymbol{\Omega}_R} \overline{F}_{\rm hit}(\|\boldsymbol{x}\|,t_1)\overline{F}_{\rm hit}(\|\boldsymbol{x}\|,t_2)d\boldsymbol{x} \tag{44b}$$

$$\begin{aligned}\overline{G}^{(2)}_{\rm all}(t_1,t_2) \triangleq \int_{\mathbb{R}^3\setminus\boldsymbol{\Omega}_R}\int_{\mathbb{R}^3\setminus\boldsymbol{\Omega}_R} &\left[\rho_{\boldsymbol{\Psi}}(\|\boldsymbol{x}_1-\boldsymbol{x}_2\|)-\lambda^2_{\boldsymbol{\Psi}}\right] \\ &\times \overline{F}_{\rm hit}(\|\boldsymbol{x}_1\|,t_1)\overline{F}_{\rm hit}(\|\boldsymbol{x}_2\|,t_2)d\boldsymbol{x}_1 d\boldsymbol{x}_2\,.\end{aligned} \tag{44c}$$

Proof: First, we note that (42) is formally identical to (10) once that $\mathsf{b}_{n,l}|_{\boldsymbol{\Psi},t}$ is replaced by $\mathsf{b}_{n,l}|_{\boldsymbol{\Psi},\rho}[j]$ and $F_{\rm hit}(\|\mathsf{x}_n\|,t-\tau^{(n)}_l)$ is replaced by $\overline{F}_{\rm hit}(\|\mathsf{x}_n\|,jT_{\rm b}-\tau^{(n)}_l)$. Thus, by following step by step the proof in Appendix C with such replacements, it is straightforward to obtain

$$\mathbb{E}\left\{\mathsf{n}_{\rm rx}|_{\boldsymbol{\Psi},\rho}[j]\right\} = \int_{-\infty}^{+\infty} \rho(\tau)\overline{H}_{\rm all}(jT_{\rm b}-\tau)d\tau \tag{45a}$$

$$\begin{aligned}\mathbb{V}\{\mathsf{n}_{\rm rx}|_{\boldsymbol{\Psi},\rho}[j]\} &= \int_{-\infty}^{+\infty} \rho(\tau)\overline{H}_{\rm all}(jT_{\rm b}-\tau)d\tau \\ &+ \int_{-\infty}^{+\infty}\int_{-\infty}^{+\infty} \rho^{(2)}(\tau,s)\overline{H}^{(2)}_{\rm all}(jT_{\rm b}-\tau,jT_{\rm b}-s)d\tau ds \\ &+ \int_{-\infty}^{+\infty}\int_{-\infty}^{+\infty} \rho(\tau)\rho(s)\overline{G}^{(2)}_{\rm all}(jT_{\rm b}-\tau,jT_{\rm b}-s)d\tau ds\end{aligned} \tag{45b}$$

which is formally identical to (29) with $H_{\rm all}(t-\tau)$, $H^{(2)}_{\rm all}(t-\tau,t-s)$, and $G^{(2)}_{\rm all}(t-\tau,t-s)$ replaced by $\overline{H}_{\rm all}(jT_{\rm b}-\tau)$, $\overline{H}^{(2)}_{\rm all}(jT_{\rm b}-\tau,jT_{\rm b}-s)$, and $\overline{G}^{(2)}_{\rm all}(jT_{\rm b}-\tau,jT_{\rm b}-s)$, respectively. By applying the integration variable changes $\tau\to\tau+jT_{\rm b}$ and $s\to s+jT_{\rm b}$ we obtain (43). □

B. First and second order analysis

of spatially distributed digital MCvD It is now possible to use Lemma 2 for the first and second order analysis of both the useful and the ISI component of the received molecular signal. To this purpose, let's define:

$$\lambda_j(t) \triangleq \mathsf{d}_j g(t) \tag{46a}$$

$$\lambda_{\rm ISI}(t) \triangleq \sum_{i=0}^{j-1} \mathsf{d}_i g(t-iT_{\rm b})\,. \tag{46b}$$

It is immediate to note that $\lambda(t)=\lambda_j(t)+\lambda_{\rm ISI}(t)$ and that the supports of the two intensity functions do not overlap. Thus, given the data, each time domain PP $\Phi^{(n)}$ can be partitioned into: i) the PP $\Phi^{(n)}_j$ with intensity $\lambda_j(t)$; ii) the PP $\Phi^{(n)}_{\rm ISI}$ with intensity $\lambda_{\rm ISI}(t)$. Thus, we write

$$\mathsf{n}_{\rm rx}|_{\boldsymbol{\Psi},\boldsymbol{\lambda}}[j] = \mathsf{n}_{\rm rx}|_{\boldsymbol{\Psi},\mathsf{d}_j}[j] + \mathsf{n}_{\rm rx}|_{\boldsymbol{\Psi},\mathsf{d}_{1:j-1}}[j] \tag{47}$$

where:

$$\mathsf{n}_{\rm rx}|_{\boldsymbol{\Psi},\mathsf{d}_j}[j] \triangleq \sum_{n\in\mathcal{I}\{\boldsymbol{\Psi}\}} \sum_{l\in\mathcal{I}\{\boldsymbol{\Phi}^{(n)}_j\}} \mathsf{b}_{n,l}|_{\boldsymbol{\Psi},\boldsymbol{\lambda}_j}[j] \tag{48}$$

is the number of observed molecules due to the j-th transmitted bit;

$$\mathsf{n}_{\rm rx}|_{\boldsymbol{\Psi},\mathsf{d}_{1:j-1}}[j] \triangleq \sum_{n\in\mathcal{I}\{\boldsymbol{\Psi}\}} \sum_{l\in\mathcal{I}\{\boldsymbol{\Phi}^{(n)}_{\rm ISI}\}} \mathsf{b}_{n,l}|_{\boldsymbol{\Psi},\boldsymbol{\lambda}_{\rm ISI}}[j] \tag{49}$$

is the number of molecules observed in the same interval due to all the previous bits. Moreover, $\mathsf{b}_{n,l}|_{\boldsymbol{\Psi},\boldsymbol{\lambda}_j}[j]$ and $\mathsf{b}_{n,l}|_{\boldsymbol{\Psi},\boldsymbol{\lambda}_{\rm ISI}}[j]$ are independent (by neglecting collisions, different molecules have independent diffusion).

It is clear that, given $\mathsf{d}_j=0$, $\mathsf{n}_{\rm rx}|_{\boldsymbol{\Psi},\mathsf{d}_j=0}[j]=0$.[14]. The mean and the variance of the useful component given that $\mathsf{d}_j=1$, as well as those of the ISI component, are evaluated in the following corollaries, both derived from Lemma 2.

Corollary 1 (Mean and variance of the useful component): The number $\mathsf{n}_{\rm rx}|_{\boldsymbol{\Psi},\mathsf{d}_j=1}[j]$ of molecules received during the j time bit due to the emissions related to the j-th bit d_j (given that $\mathsf{d}_j=1$) has mean and variance as follows:

$$\mu_0 \triangleq \mathbb{E}\left\{\mathsf{n}_{\rm rx}|_{\boldsymbol{\Psi},\mathsf{d}_j=1}[j]\right\} = \int_{-\infty}^{+\infty} g(\tau)H_{\rm all}(T_{\rm b}-\tau)d\tau \tag{50a}$$

$$\begin{aligned}\sigma^2_0 \triangleq \mathbb{V}\left\{\mathsf{n}_{\rm rx}|_{\boldsymbol{\Psi},\mathsf{d}_j=1}[j]\right\} &= \int_{-\infty}^{+\infty} g(\tau)H_{\rm all}(T_{\rm b}-\tau)d\tau \\ &+ \int_{-\infty}^{+\infty}\int_{-\infty}^{+\infty} g(\tau)g(s)H^{(2)}_{\rm all}(T_{\rm b}-\tau,T_{\rm b}-s)d\tau ds \\ &+ \int_{-\infty}^{+\infty}\int_{-\infty}^{+\infty} g(\tau)g(s)G^{(2)}_{\rm all}(T_{\rm b}-\tau,T_{\rm b}-s)d\tau ds\,.\end{aligned} \tag{50b}$$

Proof: See Appendix D. □

Corollary 2 (Mean and Variance of the ISI component): The mean and the variance of the ISI component observed ad the

[14]It is an immediate consequence of (48) resulting in $\lambda_j(t)=0$.

j-th interval emitted in the previous intervals result as follows:

$$\begin{aligned}\mu_{\text{ISI}} \triangleq& \mathbb{E}\left\{\mathsf{n}_{\text{rx}}|_{\boldsymbol{\Psi},\mathsf{d}_{1:j-1}}[j]\right\}\\ =&p_1\sum_{i=0}^{j-1}\int_{-\infty}^{+\infty} g(\tau - iT_{\text{b}} + jT_{\text{b}})\overline{H}_{\text{all}}(-\tau)d\tau \qquad (51a)\\ \sigma^2_{\text{ISI}} \triangleq& \mathbb{V}\left\{\mathsf{n}_{\text{rx}}|_{\boldsymbol{\Psi},\mathsf{d}_{1:j-1}}[j]\right\}\\ =&p_1\sum_{i=0}^{j-1}\int_{-\infty}^{+\infty} g(\tau - iT_{\text{b}} + jT_{\text{b}})\overline{H}_{\text{all}}(-\tau)d\tau\\ &+ p_1^2\sum_{i=0}^{j-1}\int_{-\infty}^{+\infty}\int_{-\infty}^{+\infty} g(\tau - iT_{\text{b}} + jT_{\text{b}})\\ &\times g(s - iT_{\text{b}} + jT_{\text{b}})\overline{H}^{(2)}_{\text{all}}(-\tau,-s)d\tau ds\\ &+ p_1^2\sum_{i=0}^{j-1}\sum_{k=0}^{j-1}\int_{-\infty}^{+\infty}\int_{-\infty}^{+\infty} g(\tau - iT_{\text{b}} + jT_{\text{b}})\\ &\times g(s - kT_{\text{b}} + jT_{\text{b}})\overline{H}^{(2)}_{\text{all}}(-\tau,-s)d\tau ds\\ &+ p_1^2\sum_{i=0}^{j-1}\sum_{k=0}^{j-1}\int_{-\infty}^{+\infty}\int_{-\infty}^{+\infty} g(\tau - iT_{\text{b}} + jT_{\text{b}})\\ &\times g(s - kT_{\text{b}} + jT_{\text{b}})\overline{G}^{(2)}_{\text{all}}(-\tau,-s)d\tau ds \qquad (51b)\end{aligned}$$

where p_1 is the probability that $\mathsf{d}_j = 1$, while $\overline{H}_{\text{all}}(t)$, $\overline{H}^{(2)}_{\text{all}}(t_1,t_2)$, and $\overline{G}^{(2)}_{\text{all}}(t_1,t_2)$ can also be written as

$$\begin{aligned}\overline{H}_{\text{all}}(t) =& H_{\text{all}}(T_{\text{b}}+t) - H_{\text{all}}(t) \qquad (52a)\\ \overline{H}^{(2)}_{\text{all}}(t_1,t_2) =& H^{(2)}_{\text{all}}(T_{\text{b}}+t_1,T_{\text{b}}+t_2) - H^{(2)}_{\text{all}}(t_1,T_{\text{b}}+t_2)\\ &- H^{(2)}_{\text{all}}(T_{\text{b}}+t_1,t_2) + H^{(2)}_{\text{all}}(t_1,t_2) \qquad (52b)\\ \overline{G}^{(2)}_{\text{all}}(t_1,t_2) =& G^{(2)}_{\text{all}}(T_{\text{b}}+t_1,T_{\text{b}}+t_2) - G^{(2)}_{\text{all}}(t_1,T_{\text{b}}+t_2)\\ &- G^{(2)}_{\text{all}}(T_{\text{b}}+t_1,t_2) + G^{(2)}_{\text{all}}(t_1,t_2)\,. \qquad (52c)\end{aligned}$$

Proof: See Appendix E □

Now, it is finally possible to compute the SIR and SINR due to ISI as follows.

Definition 4 (SIR and SINR due to ISI): The SIR and the SINR in the presence of ISI are defined as:

$$\text{SIR} \triangleq \frac{\mu_0^2}{\sigma^2_{\text{ISI}}} \qquad (53a)$$

$$\text{SINR} \triangleq \frac{\mu_0^2}{\sigma_0^2 + \sigma^2_{\text{ISI}}}\,. \qquad (53b)$$

C. Impact of stochastic interaction on the ISI component

As well as for the SNR, also for the SIR and the SINR it is possible to study the impact of stochastic interactions between the points of the spatial PP modeling transmitters positions.

Theorem 4 (Effect of attraction/repulsion on the ISI component): Let $\boldsymbol{\Psi}^{(\text{re})}$, $\boldsymbol{\Psi}^{(\text{Po})}$, and $\boldsymbol{\Psi}^{(\text{cl})}$ be, a repulsive, a Poisson and a clustered isotropic PP, respectively, with the same intensity $\lambda_{\boldsymbol{\Psi}}$. The mean and the variance of the ISI component are such that:

$$\text{SIR}^{(\text{cl})} \leqslant \text{SIR}^{(\text{Po})} \leqslant \text{SIR}^{(\text{re})} \qquad (54a)$$

$$\text{SINR}^{(\text{cl})} \leqslant \text{SINR}^{(\text{Po})} \leqslant \text{SINR}^{(\text{re})}\,. \qquad (54b)$$

Proof: By observing that (50a) do not depend on the second order product density function of $\boldsymbol{\Psi}$, we have

$$\mu_0^{(\text{re})} = \mu_0^{(\text{Po})} = \mu_0^{(\text{cl})}\,. \qquad (55)$$

Moreover, note that, from (40), $\overline{F}_{\text{hit}}(r,t) \geqslant 0\ \forall t$. Thus, from (44a) and (44b), it follows, respectively, that $\overline{H}_{\text{all}}(t) \geqslant 0$ and $\overline{H}^{(2)}_{\text{all}}(t,\tau) \geqslant 0\ \forall t,\tau$. By using inequalities (32) in (51b), it is immediate to obtain

$$\sigma^{2\ (\text{re})}_{\text{ISI}} \leqslant \sigma^{2\ (\text{Po})}_{\text{ISI}} \leqslant \sigma^{2\ (\text{cl})}_{\text{ISI}}\,. \qquad (56)$$

By substituting (55) and (56) in (53) we obtain (54). □

The following corollary can also be obtained, which is useful to establish whether the variance of ISI diverges for infinite number j of transmitted symbols, by evaluating the mean only.

Corollary 3 (ISI variance for non-repulsive spatial PPPs): If the PP Φ modeling the transmitters positions is non-repulsive, then the variance of the ISI is greater or equal to the mean, i.e.:

$$\begin{aligned}\sigma^{2\ (\text{Po})}_{\text{ISI}} &\geqslant \mu^{(\text{Po})}_{\text{ISI}}\\ \sigma^{2\ (\text{cl})}_{\text{ISI}} &\geqslant \mu^{(\text{cl})}_{\text{ISI}}\,.\end{aligned}$$

Proof: For a non-repulsive PP, $\rho_{\boldsymbol{\Psi}}(\|\boldsymbol{x}_1 - \boldsymbol{x}_2\|) \geqslant \lambda^2_{\boldsymbol{\Psi}}$, where the equality holds for the PPP. Thus, from (44c), it is $\overline{G}_{\text{all}}(t,\tau) \geqslant 0$ for all t,τ. The thesis follows by comparing (51b) to (51a). □

An immediate consequence is that, if μ_{ISI} approaches the infinity for infinite number of transmitted symbol j, then both the SIR and the SINR tends to zero.

D. BEP evaluation (with the Gaussian approximation)

In the OOK modulation, the number of molecules received during the j-th time bit, i.e., $\mathsf{n}_{\text{rx}}|_{\boldsymbol{\Psi},\boldsymbol{\lambda}}[j]$ in (47), is compared to a certain threshold N_{th} and, if $\mathsf{n}_{\text{rx}}|_{\boldsymbol{\Psi},\boldsymbol{\lambda}}[j] > N_{\text{th}}$, $\hat{d_0} = 1$ is decided, while $d_0 \hat{=} 0$ is decided if, instead, $\mathsf{n}_{\text{rx}}|_{\boldsymbol{\Psi},\boldsymbol{\lambda}}[j] < N_{\text{th}}$. In case of single sample, the bit error probability can be computed through the Bayes rule as follows:

$$P_{\text{e}} = p_1 P_{\text{e}}|_{\mathsf{d}_j=1} + p_0 P_{\text{e}}|_{\mathsf{d}_j=0} \qquad (57)$$

where p_1 and p_0 are, respectively, the probability that a bit is 1 or 0, and

$$P_{\text{e}}|_{\mathsf{d}_0=1} = \text{Prob}\{\mathsf{n}_{\text{rx}}|_{\boldsymbol{\Psi},\boldsymbol{\lambda}}[j] < N_{\text{th}}\} \qquad (58a)$$

$$P_{\text{e}}|_{\mathsf{d}_0=0} = \text{Prob}\{\mathsf{n}_{\text{rx}}|_{\boldsymbol{\Psi},\boldsymbol{\lambda}}[j] > N_{\text{th}}\}\,. \qquad (58b)$$

The cases of single bit transmission (no ISI) and that of multiple bit transmission (with ISI) have to be distinguished.

1) Single bit transmission (no ISI): If $\mathsf{d}_i = 0$ for all $i < j$, no ISI occurs ($\mathsf{n}_{\text{rx}}|_{\boldsymbol{\Psi},\mathsf{d}_{1:j-1}}[j]$ in (47) is zero), and all received molecules are due to the transmissions within the j-th interval. Indeed, (47) becomes simply $\mathsf{n}_{\text{rx}}|_{\boldsymbol{\Psi},\boldsymbol{\lambda}}[j] = \mathsf{n}_{\text{rx}}|_{\boldsymbol{\Psi},\mathsf{d}_j}[j]$. Thus, by recalling that $\mathsf{n}_{\text{rx}}|_{\boldsymbol{\Psi},\mathsf{d}_j=0} = 0$ with probability 1, we have

$$\begin{aligned}P_{\text{e}} &= p_1 P_{\text{e}}|_{\mathsf{d}_j=1} + p_0 P_{\text{e}}|_{\mathsf{d}_j=0}\\ &= p_1\text{Prob}\{\mathsf{n}_{\text{rx}}|_{\boldsymbol{\Psi},\mathsf{d}_j=1} < N_{\text{th}}\} + p_0\text{Prob}\{\mathsf{n}_{\text{rx}}|_{\boldsymbol{\Psi},\mathsf{d}_j=0} > N_{\text{th}}\}\\ &= p_1\text{Prob}\{\mathsf{n}_{\text{rx}}|_{\boldsymbol{\Psi},\mathsf{d}_j=1} < N_{\text{th}}\}\,. \qquad (59)\end{aligned}$$

By approximating $\mathsf{n}_{\text{rx}}|_{\boldsymbol{\Psi},\mathsf{d}_j=1}[j]$ with a Gaussian RV,[15] with mean μ_0 and variance σ_0^2 evaluated by (50), we easily get

$$P_{\text{e}} \approx p_1 \int_{-\infty}^{N_{\text{th}}} \frac{1}{\sqrt{2\pi\sigma_0^2}} e^{-\frac{(\mu_0-x)^2}{2\sigma_0^2}} dx = \frac{p_1}{2}\text{erfc}\left(\frac{\mu_0 - N_{\text{th}}}{\sqrt{2}\sigma_0}\right). \tag{60}$$

If we choose $N_{\text{tx}} = \mu_0/2$,[16] it results

$$P_{\text{e}} \approx \frac{p_1}{2}\text{erfc}\left[\sqrt{\frac{\gamma(T_{\text{b}})}{8}}\right]. \tag{61}$$

To refine the Gaussian approximation, [51] shows that a generalized Gaussian distribution can be adopted, with probability density function (PDF)

$$p(x) = \frac{\beta}{2\alpha\Gamma\left(\frac{1}{\beta}\right)} \exp^{-\left(\frac{x-\mu}{\alpha}\right)^{\beta}} \tag{62}$$

where $\Gamma(\cdot)$ is the gamma function, μ is the mean, β is a shaping parameter, and α is a scale parameter such that the variance results in $\alpha^2\frac{\Gamma(3/\beta)}{\Gamma(1/\beta)}$. It can be readily noticed that, for $\beta = 2$, (62) results in the well-known normal distribution. Thus, we can consider the PDF of $\mathsf{n}_{\text{rx}}|_{\boldsymbol{\Psi},\mathsf{d}_j=1}$ given by (62) with $\mu = \mu_0$ and $\alpha^2\frac{\Gamma(3/\beta)}{\Gamma(1/\beta)} = \sigma_0^2$. The approximation (60) is thus refined as

$$P_{\text{e}} \approx p_1 \int_{-\infty}^{N_{\text{th}}} p_{\mathsf{n}_{\text{rx}}|_{\boldsymbol{\Psi},\mathsf{d}_j=1}}(x)dx = \frac{p_1}{2}\left\{1 - \frac{\gamma\left[\frac{1}{\beta}, \left(\frac{\mu_0 - N_{\text{th}}}{\alpha}\right)^{\beta}\right]}{\Gamma\left(\frac{1}{\beta}\right)}\right\} \tag{63}$$

where $\gamma(s,x) \triangleq \int_0^x t^{s-1}e^{-t}dt$ denotes the lower incomplete gamma function. Again, if $N_{\text{th}} = \mu_0/2$, (63) reduces to a function of the SNR:

$$P_{\text{e}} \approx \frac{p_1}{2}\left\{1 - \frac{\gamma\left[\frac{1}{\beta}, \left(\frac{\Gamma(3/\beta)}{4\Gamma(1/\beta)}\text{SNR}\right)^{\beta/2}\right]}{\Gamma\left(\frac{1}{\beta}\right)}\right\}. \tag{64}$$

2) Multiple bit transmission (with ISI): Note that, in both components of (47), the sum over n has an infinite number of elements (due to the infinite cardinality of the PP Φ). Thus, we approximate also the ISI component $\mathsf{n}_{\text{rx}}|_{\boldsymbol{\Psi},\mathsf{d}_{1:j-1}}[j]$ as a Gaussian RV, with mean μ_{ISI} and variance σ_{ISI}^2 evaluated by (51). It follows that the BEP results in (57) with

$$\begin{aligned} P_{\text{e}}|_{\mathsf{d}_j=1} &= \text{Prob}\{\mathsf{n}_{\text{rx}}|_{\boldsymbol{\Psi},\mathsf{d}_j=1} + \mathsf{n}_{\text{rx}}|_{\boldsymbol{\Psi},\mathsf{d}_{1:j-1}}[j] < N_{\text{th}}\} \\ &\approx \int_{-\infty}^{N_{\text{th}}} \frac{1}{\sqrt{2\pi(\sigma_0^2+\sigma_{\text{ISI}}^2)}} e^{-\frac{(\mu_0-\mu_{\text{ISI}}-x)^2}{2(\sigma_0^2+\sigma_{\text{ISI}}^2)}} dx \\ &= \frac{1}{2}\text{erfc}\left(\frac{\mu_0 + \mu_{\text{ISI}} - N_{\text{th}}}{\sqrt{2(\sigma_0^2+\sigma_{\text{ISI}}^2)}}\right) \end{aligned} \tag{65}$$

and

$$\begin{aligned} P_{\text{e}}|_{d_0=0} &= \text{Prob}\{\mathsf{n}_{\text{rx}}|_{\boldsymbol{\Psi},\mathsf{d}_{1:j-1}}[j] > N_{\text{th}}\} \\ &\approx \int_{N_{\text{th}}}^{+\infty} \frac{1}{\sqrt{2\pi\sigma_{\text{ISI}}^2}} e^{-\frac{(\mu_{\text{ISI}}-x)^2}{2\sigma_{\text{ISI}}^2}} dx \\ &= \frac{1}{2}\text{erfc}\left(\frac{N_{\text{th}} - \mu_{\text{ISI}}}{\sqrt{2\sigma_{\text{ISI}}^2}}\right). \end{aligned} \tag{66}$$

By choosing $N_{\text{th}} = \mu_{\text{ISI}} + \frac{\mu_0}{2}$ we obtain

$$P_{\text{e}} \approx \frac{p_1}{2}\text{erfc}\left(\sqrt{\frac{\text{SINR}}{8}}\right) + \frac{p_0}{2}\text{erfc}\left(\sqrt{\frac{\text{SIR}}{8}}\right). \tag{67}$$

By using the generalized Gaussian distribution, we obtain

$$\begin{aligned} P_{\text{e}}|_{\mathsf{d}_j=1} &\approx \int_{-\infty}^{N_{\text{th}}} \frac{\beta_1}{2\alpha_1\Gamma\left(\frac{1}{\beta_1}\right)} \exp^{-\left(\frac{x-\mu_0-\mu_{\text{ISI}}}{\alpha_1}\right)^{\beta_1}} dx \\ &= \frac{1}{2}\left\{1 - \frac{\gamma\left[\frac{1}{\beta_1}, \left(\frac{\mu_0+\mu_{\text{ISI}}-N_{\text{th}}}{\alpha_1}\right)^{\beta_1}\right]}{\Gamma\left(\frac{1}{\beta_1}\right)}\right\} \end{aligned} \tag{68}$$

and

$$\begin{aligned} P_{\text{e}}|_{d_0=0} &\approx \int_{-\infty}^{N_{\text{th}}} \frac{\beta_0}{2\alpha_0\Gamma\left(\frac{1}{\beta_0}\right)} \exp^{-\left(\frac{x-\mu_{\text{ISI}}}{\alpha_0}\right)^{\beta_0}} dx \\ &= \frac{1}{2}\left\{1 - \frac{\gamma\left[\frac{1}{\beta_0}, \left(\frac{\mu_{\text{ISI}}-N_{\text{th}}}{\alpha_0}\right)^{\beta_0}\right]}{\Gamma\left(\frac{1}{\beta_0}\right)}\right\} \end{aligned} \tag{69}$$

where the variance in case of $\mathsf{d}_j = 1$ and $\mathsf{d}_j = 0$ results, respectively, in

$$\alpha_1^2\frac{\Gamma(3/\beta_1)}{\Gamma(1/\beta_1)} = \sigma_0^2 + \sigma_{\text{ISI}}^2 \tag{70a}$$

$$\alpha_0^2\frac{\Gamma(3/\beta_0)}{\Gamma(1/\beta_0)} = \sigma_{\text{ISI}}^2 \tag{70b}$$

while β_1 and β_0 are the shaping parameters to be tuned.

By choosing $N_{\text{th}} = \mu_{\text{ISI}} + \frac{\mu_0}{2}$, (70) leads to

$$\begin{aligned} P_{\text{e}} \approx &\frac{p_1}{2}\left\{1 - \frac{\gamma\left[\frac{1}{\beta_1}, \left(\frac{\Gamma(3/\beta_1)}{4\Gamma(1/\beta_1)}\text{SINR}\right)^{\beta_1/2}\right]}{\Gamma\left(\frac{1}{\beta_1}\right)}\right\} \\ &+ \frac{p_0}{2}\left\{1 - \frac{\gamma\left[\frac{1}{\beta_0}, \left(\frac{\Gamma(3/\beta_0)}{4\Gamma(1/\beta_0)}\text{SIR}\right)^{\beta_0/2}\right]}{\Gamma\left(\frac{1}{\beta_0}\right)}\right\}. \end{aligned} \tag{71}$$

V. Case Study: Closed forms for SNR and ISI with Poisson distributed transmitters

The method proposed here is very general and can be easily extended to cases with different type of receivers (e.g., passive) with or without molecules decay, once that (1) is replaced by a different expression for the probability that a molecule is received within the time t. For the sake of simplicity, in this section we propose closed form results for Poisson distributed transmitters in case of active receiver without molecules decay.

[15]Note that, according to (48), the large number of transmitters modeled by the PP Φ, i.e., the number of addenda in the sum in $n \in \mathcal{I}\{\Phi\}$, makes the Gaussian approximation more accurate than in the single transmitter case

[16]Note that, if no interferer molecules are considered, this is not the optimal choice, which would be, instead, $N_{\text{th}} = 1$, as shown in [7] in case of exact concentration transmitters and as evident from (60) for Poisson concentration and timing transmitter cases

A. Closed forms for SNR

1) Spatially distributed case: Consider a fully absorbing spherical receiver with radius R and a swarm of point transmitters placed in the whole $\mathbb{R}^3$ according to a homogeneous PPP with intensity $\lambda_{\mathbf{\Psi}}$ in an environment with diffusivity D [m^2/s].

Proposition 1 (SNR for transmitters positions modeled by homogeneous Poisson point process): If the point transmitters are distributed according a homogeneous PPP with intensity $\lambda_{\mathbf{\Psi}}$ on the whole $\mathbb{R}^3$, the SNR results as follows

- exact concentration (synchronous) transmitters:

$$\mathrm{SNR}^{(\mathrm{sync})}_{\text{Ex. conc.}}(t) = \frac{\left[N_{\mathrm{tx}} H_{\mathrm{all}}(t)\right]^2}{N_{\mathrm{tx}} H_{\mathrm{all}}(t) + N_{\mathrm{tx}}(N_{\mathrm{tx}}-1) H^{(2)}_{\mathrm{all}}(t,t)}; \tag{72}$$

- Poisson concentration (synchronous) transmitters:

$$\mathrm{SNR}^{(\mathrm{sync})}_{\text{Po. conc.}}(t) = \frac{\left[N_{\mathrm{tx}} H_{\mathrm{all}}(t)\right]^2}{N_{\mathrm{tx}} H_{\mathrm{all}}(t) + N^2_{\mathrm{tx}} H^{(2)}_{\mathrm{all}}(t,t)} \tag{73}$$

- timing (asynchronous) transmitters with emissions modeled by a time domain PPP with intensity $\lambda(t)$:

$$\begin{aligned}\mathrm{SNR}^{(\mathrm{async})}_{\text{Timing}}(t) = &\left[\int_{-\infty}^{+\infty} \lambda(\tau) H_{\mathrm{all}}(t-\tau) d\tau\right]^2 \\ &\times \left[\int_{-\infty}^{+\infty} \lambda(\tau) H_{\mathrm{all}}(t-\tau) d\tau \right. \\ &\left. + \int_{-\infty}^{+\infty}\int_{-\infty}^{+\infty} \lambda(\tau)\lambda(s) H^{(2)}_{\mathrm{all}}(t-\tau, t-s) d\tau ds\right]^{-1}\end{aligned} \tag{74}$$

where, for all aforementioned cases,

$$H_{\mathrm{all}}(t) = 4\lambda_{\mathbf{\Psi}} R\sqrt{\pi D t}\left(2R + \sqrt{\pi D t}\right) \tag{75a}$$

$$H^{(2)}_{\mathrm{all}}(t,\tau) = 8R^2\lambda_{\mathbf{\Psi}}\sqrt{\pi D}\left(\sqrt{\tau} + \sqrt{t} - \sqrt{\tau + t}\right) \tag{75b}$$

provided that $t, \tau \geqslant 0$.[17]

Proof: See Appendix F □

Remark 6: Equation (75a) corresponds to the results in [7], [8], while (75b) is a novel result which extends the analysis to the second order. Both expressions have been derived here in parallel to make this work self contained.

Now, to better analyze and find close forms for (74), we choose the intensity function for timing transmitters as constant in a finite activity interval $[0, T_{\mathrm{a}}]$.

Corollary 4 (Uniform distribution of emission times into a definite activity interval): In the settings of Proposition 1, if the intensity function of the time domain PPP modeling timing transmitters is $\lambda(t) = \frac{N_{\mathrm{tx}}}{T_{\mathrm{a}}}\mathrm{rect}\left(\frac{t}{T_{\mathrm{a}}}\right)$,[18] the SNR can be expressed in closed form as follows

$$\mathrm{SNR}^{(\mathrm{async})}_{\text{Timing}}(t) = \frac{8\lambda_{\mathbf{\Psi}} R^2\sqrt{\pi D}\frac{N_{\mathrm{tx}}}{T_{\mathrm{a}}}\ \psi^2\left(t, T_{\mathrm{a}}, \frac{\sqrt{\pi D}}{R}\right)}{\psi\left(t, T_{\mathrm{a}}, \frac{\sqrt{\pi D}}{R}\right) + \frac{N_{\mathrm{tx}}}{T_{\mathrm{a}}}\theta(t, T_{\mathrm{a}})} \tag{76}$$

[17]For $t, \tau < 0$, both functions are zero.

[18]We define the function $\mathrm{rect}(t)$ such that it is equal to 1 for $0 \leqslant t \leqslant 1$ and equal to 0 elsewhere.

for $t \geqslant 0$, where

$$\psi(t,T,x) \triangleq \begin{cases} \frac{2\sqrt{t^3}}{3} + \frac{t^2 x}{4}, & \text{for } t \leqslant T \\ \frac{2}{3}\left(\sqrt{t^3} - t\sqrt{t-T} + T\sqrt{t-T}\right) & \\ \quad + \frac{Tx}{2}\left(t - \frac{T}{2}\right) & \text{for } t > T \end{cases}$$

and

$$\theta(t,T) \triangleq \begin{cases} \left(\frac{4}{15}(7-4\sqrt{2})\sqrt{t^5}\right), & \text{for } t \leqslant T \\ \frac{4T}{3}\left(\sqrt{t^3} - t\sqrt{t-T} + T\sqrt{t-T}\right) & \\ -\frac{4}{15}\left[\sqrt{(2t)^5} - 2\sqrt{(2t-T)^5}\right. & \\ \left. + \sqrt{32(t-T)^5}\right], & \text{for } t > T \end{cases}.$$

Proof: See Appendix G □

2) Comparison to the point-to-point case: The analytical procedure developed in Sec. III can be applied to the simpler point-to-point case. If an absorbing receiver is considered in point-to-point transmission, the SNR can be evaluated by using (1) in (13), (15), and (17). In particular, for exact and Poisson concentration (with an average value of N_{tx} emitted molecules), and timing (with an uniform emission intensity equal to λ_{a} in $[0, T_{\mathrm{a}}]$ and zero elsewhere), we obtain, respectively

$$\mathrm{SNR}^{(0)}_{\text{Ex. conc.}}(r,t) = \frac{N_{\mathrm{tx}}\, R\ \mathrm{erfc}\left(\frac{r-R}{\sqrt{4Dt}}\right)}{r - R\ \mathrm{erfc}\left(\frac{r-R}{\sqrt{4Dt}}\right)} \tag{77a}$$

$$\mathrm{SNR}^{(0)}_{\text{Po. conc.}}(r,t) = N_{\mathrm{tx}}\frac{R}{r}\mathrm{erfc}\left(\frac{r-R}{\sqrt{4Dt}}\right) \tag{77b}$$

$$\mathrm{SNR}^{(0)}_{\text{Timing}}(r,t) = \frac{R\ \lambda_{\mathrm{a}}}{r}\begin{cases} \zeta\left(\frac{r-R}{\sqrt{4D}}, t\right), & \text{for } t \leqslant T_{\mathrm{a}} \\ \zeta\left(\frac{r-R}{\sqrt{4D}}, t\right) & \\ -\zeta\left(\frac{r-R}{\sqrt{4D}}, t - T_{\mathrm{a}}\right), & \text{for } t > T_{\mathrm{a}} \end{cases} \tag{77c}$$

where $\zeta(x,t) \triangleq (2x^2 + t)\mathrm{erfc}\left(\frac{x}{\sqrt{t}}\right) - 2x\sqrt{\frac{t}{\pi}}\, e^{-\frac{x^2}{t}}$.

Now, to further investigate MCvD properties, we consider asymptotic scenarios ($t \to +\infty$ and infinite emissions).

3) Asymptotic analysis with respect to time: Spatially distributed and point to point MCvD substantially differ for infinite time.

For point-to-point MCvD, from (77) we obtain:

$$\lim_{t\to+\infty} \mathrm{SNR}^{(0)}_{\text{Ex. conc.}}(r,t) = \frac{N_{\mathrm{tx}}\ R}{r - R} \tag{78a}$$

$$\lim_{t\to+\infty} \mathrm{SNR}^{(0)}_{\text{Po. conc.}}(r,t) = \frac{N_{\mathrm{tx}}\ R}{r} \tag{78b}$$

$$\lim_{t\to+\infty} \mathrm{SNR}^{(0)}_{\text{Timing}}(r,t) = \frac{\lambda_{\mathrm{a}} T_{\mathrm{a}}\ R}{r} \tag{78c}$$

Note that a saturation effect arises with an asymptote which is higher for exact concentration model. Poisson concentration and timing transmitters attain the same asymptote if the average number of emitted molecules are the same (i.e., if $N_{\mathrm{tx}} = \lambda_{\mathrm{a}} T_{\mathrm{a}}$).

For spatially distributed MCvD, from (72), (73), and (76), we obtain, respectively

$$\lim_{t\to+\infty} \mathrm{SNR}^{(\mathrm{sync})}_{\text{Ex. conc.}}(t) = \lim_{t\to+\infty} \mathsf{n}_{\mathrm{tx}} 4\lambda_{\boldsymbol{\Psi}} R\pi D\; t = +\infty \quad (79a)$$

$$\lim_{t\to+\infty} \mathrm{SNR}^{(\mathrm{sync})}_{\text{Po. conc.}}(t) = \lim_{t\to+\infty} \mathsf{n}_{\mathrm{tx}} 4\lambda_{\boldsymbol{\Psi}} R\pi D\; t = +\infty \quad (79b)$$

$$\lim_{t\to+\infty} \mathrm{SNR}^{(\mathrm{async})}_{\text{Timing}}(t) = \lim_{t\to+\infty} \lambda_{\mathrm{a}} T_{\mathrm{a}}\; 4\lambda_{\boldsymbol{\Psi}} R\pi D\; t = +\infty\,. \quad (79c)$$

Note that, for all concentration transmitters cases, the SNR indefinitely increases with a slope of $\mathsf{n}_{\mathrm{tx}} 4\lambda_{\boldsymbol{\Psi}} R\pi D$. For the asynchronous timing transmitter case the slope results to be $\lambda_{\mathrm{a}} T_{\mathrm{a}} 4\lambda_{\boldsymbol{\Psi}} R\pi D$. Thus, there are no saturation effects with respect to time in spatially-distributed MCvD, and the slope of the asymptote is proportional to the transmitters density, the diffusion coefficient and the receiver radius.

4) Asymptotic analysis with respect emissions: Spatially distributed and point to point MCvD also differ for infinite emissions (infinite number of emitted molecules for concentration transmitters and infinite emission intensity for timing transmitters).

For point-to-point MCvD, from (77) we obtain

$$\lim_{\mathsf{n}_{\mathrm{tx}}\to\infty} \mathrm{SNR}^{(0)}_{\text{Ex. conc.}}(r,t) = +\infty$$

$$\lim_{\mathsf{n}_{\mathrm{tx}}\to\infty} \mathrm{SNR}^{(0)}_{\text{Po. conc.}}(r,t) = +\infty$$

$$\lim_{\lambda_{\mathrm{a}}\to\infty} \mathrm{SNR}^{(0)}_{\text{Timing}}(r,t) = +\infty\,.$$

For spatially distributed MCvD, (72), (73), and (76) lead to

$$\lim_{\mathsf{n}_{\mathrm{tx}}\to\infty} \mathrm{SNR}^{(\mathrm{sync})}_{\text{Ex. conc.}}(t) = \frac{\lambda_{\boldsymbol{\Psi}}\sqrt{2\pi D t}\;(2R+\sqrt{\pi D t})^2}{\left(\sqrt{2}-1\right)} \quad (80a)$$

$$\lim_{\mathsf{n}_{\mathrm{tx}}\to\infty} \mathrm{SNR}^{(\mathrm{sync})}_{\text{Po. conc.}}(t) = \frac{\lambda_{\boldsymbol{\Psi}}\sqrt{2\pi D t}\;(2R+\sqrt{\pi D t})^2}{\left(\sqrt{2}-1\right)} \quad (80b)$$

$$\lim_{\lambda_{\mathrm{a}}\to\infty} \mathrm{SNR}^{(\mathrm{async})}_{\text{Timing}}(t) = \frac{8\lambda_{\boldsymbol{\Psi}} R^2\sqrt{\pi D}\;\psi^2\left(t, T_{\mathrm{a}}, \frac{\sqrt{\pi D}}{R}\right)}{\theta(t, T_{\mathrm{a}})}\,. \quad (80c)$$

It has to be noticed that in any case the SNR for spatially distributed MCvD shows a saturation effect with respect to the number of emitted molecules (or the emission intensity) which has no counterpart in point-to-point MCvD. It means that, if one wants to increase the SNR in spatially distributed MCvD, it is useless to further increase the number of emitted molecules (or the emission intensity), since the SNR saturation level depends on the transmitters density. This conclusion could be useful to interpret the error probability evaluated in [7], in the same scenario. On the other hand, if one wants to interpret the cells behavior in Biology under the MCvD perspective, it is possible to infer that the communication is more effective with many cells (e.g., the cells of a whole tissue) transmitting relatively few molecules, rather than with few cells transmitting a massive number of molecules.

B. Closed forms for SIR and SINR due to ISI

Proposition 2 (ISI for transmitters positions modeled by homogeneous Poisson point process): If the point transmitters are distributed according a homogeneous PPP with intensity $\lambda_{\boldsymbol{\Psi}}$ on the whole $\mathbb{R}^3$, and $p_0 = p_1 = 1/2$, the mean and the variance of the ISI component due to the previous j symbols result as follows

- Poisson concentration (synchronous) transmitters:

$$\mu_{\mathrm{ISI}} = \frac{N_{\mathrm{tx}}}{2}[H_{\mathrm{all}}(j+1)T_{\mathrm{b}}] - H_{\mathrm{all}}(T_{\mathrm{b}})] \quad (81a)$$

$$\begin{aligned}\sigma^2_{\mathrm{ISI}} = {} & \frac{N_{\mathrm{tx}}}{2}[H_{\mathrm{all}}[(j+1)T_{\mathrm{b}}] - H_{\mathrm{all}}(T_{\mathrm{b}})] \\ & + \frac{N^2_{\mathrm{tx}}}{4}\sum_{k=1}^{j}\{H^{(2)}_{\mathrm{all}}[(k+1)T_{\mathrm{b}}, (k+1)T_{\mathrm{b}}] \\ & - H^{(2)}_{\mathrm{all}}[kT_{\mathrm{b}}, (k+1)T_{\mathrm{b}}]\} \\ & + \frac{N^2_{\mathrm{tx}}}{4}\sum_{k=1}^{j}\{H^{(2)}_{\mathrm{all}}(kT_{\mathrm{b}}, kT_{\mathrm{b}}) - H^{(2)}_{\mathrm{all}}[(k+1)T_{\mathrm{b}}, kT_{\mathrm{b}}]\} \\ & + \frac{N^2_{\mathrm{tx}}}{4}\sum_{k=1}^{j}\{H^{(2)}_{\mathrm{all}}[(k+1)T_{\mathrm{b}}, (j+1)T_{\mathrm{b}}] \\ & - H^{(2)}_{\mathrm{all}}[(k+1)T_{\mathrm{b}}, T_{\mathrm{b}}]\} \\ & + \frac{N^2_{\mathrm{tx}}}{4}\sum_{k=1}^{j}\{H^{(2)}_{\mathrm{all}}[kT_{\mathrm{b}}, T_{\mathrm{b}}] - H^{(2)}_{\mathrm{all}}[kT_{\mathrm{b}}, (j+1)T_{\mathrm{b}}]\}\end{aligned} \quad (81b)$$

  where $H_{\mathrm{all}}(t)$ and $H^{(2)}_{\mathrm{all}}(t_1, t_2)$ are evaluated, respectively, in (75a) and (75b).
- Timing (asynchronous) transmitters with uniformly distributed emissions in an activity interval T_{a}:

$$\mu_{\mathrm{ISI}} = \frac{N_{\mathrm{tx}}}{2T_{\mathrm{a}}}(h_{j+1} - h_1) \quad (82a)$$

$$\begin{aligned}\sigma^2_{\mathrm{ISI}} = {} & \frac{N_{\mathrm{tx}}}{2T_{\mathrm{a}}}(h_{j+1} - h_1) \\ & + \frac{N^2_{\mathrm{tx}}}{4T^2_{\mathrm{a}}}\sum_{k=1}^{j}(g_{k+1,k+1} - g_{k,k+1} + g_{k,k} - g_{k+1,k}) \\ & + \frac{N^2_{\mathrm{tx}}}{4T^2_{\mathrm{a}}}\sum_{k=1}^{j}(g_{j+1,k+1} - g_{1,k+1} + g_{1,k} - g_{j+1,k})\end{aligned} \quad (82b)$$

where

$$h_k = 8\lambda_{\boldsymbol{\Psi}} R^2\sqrt{\pi D}\;\psi\left(kT_{\mathrm{b}}, T_{\mathrm{a}}, \frac{\sqrt{\pi D}}{R}\right) \quad (83a)$$

$$g_{k,m} = 8\lambda_{\boldsymbol{\Psi}} R^2\sqrt{\pi D}\;\eta(kT_{\mathrm{b}}, mT_{\mathrm{b}}, T_{\mathrm{a}}) \quad (83b)$$

with $\psi(t, T, x)$ defined in Corollary 4 and

$$\begin{aligned}\eta(t_1, t_2, T) \triangleq {} & \frac{2T}{3}\left[\sqrt{t_1^3} - \sqrt{(t_1 - T)^3}\right. \\ & \left. + \sqrt{t_2^3} - \sqrt{(t_2 - T)^3}\right] - \frac{4}{15}\left[\sqrt{(t_1+t_2)^5}\right. \\ & \left. - 2\sqrt{(t_1+t_2-T)^5} + \sqrt{(t_1+t_2-2T)^5}\right]\,.\end{aligned}$$

Proof: See Appendix H. □

Proposition 3 (SIR and SINR for transmitters positions modeled by homogeneous Poisson point process): If the point

transmitters are distributed according a homogeneous PPP with intensity $\lambda_{\boldsymbol{\Psi}}$ on the whole $\mathbb{R}^3$, and $p_0 = p_1 = 1/2$, the SIR and the SINR in the presence of j interferer symbols result in (53) where

- for Poisson concentration (synchronous) transmitters:

$$\text{SIR} = \frac{N_{\text{tx}}^2 [H_{\text{all}}(T_{\text{b}})]^2}{\sigma_{\text{ISI}}^2} \tag{84a}$$

$$\text{SINR} = \frac{N_{\text{tx}}^2 [H_{\text{all}}(T_{\text{b}})]^2}{N_{\text{tx}} H_{\text{all}}(T_{\text{b}}) + N_{\text{tx}}^2 H_{\text{all}}^{(2)}(T_{\text{b}}, T_{\text{b}}) + \sigma_{\text{ISI}}^2} \tag{84b}$$

  where σ_{ISI}^2 is given by (81b), while $H_{\text{all}}(t)$ and $H_{\text{all}}^{(2)}(t_1, t_2)$ are evaluated, respectively, in (75a) and (75b).
- for timing (asynchronous) transmitters with uniformly distributed emissions in an activity interval T_{a}:

$$\text{SIR} = [8\lambda_{\boldsymbol{\Psi}} R^2 \sqrt{\pi D}]^2 \, \frac{N_{\text{tx}}^2}{T_{\text{a}}^2} \, \frac{\psi^2\left(T_{\text{b}}, T_{\text{a}}, \frac{\sqrt{\pi D}}{R}\right)}{\sigma_{\text{ISI}}^2} \tag{85a}$$

$$\text{SINR} = \frac{8\lambda_{\boldsymbol{\Psi}} R^2 \sqrt{\pi D} \frac{N_{\text{tx}}^2}{T_{\text{a}}^2} \, \psi^2\left(T_{\text{b}}, T_{\text{a}}, \frac{\sqrt{\pi D}}{R}\right)}{\frac{N_{\text{tx}} \psi\left(T_{\text{b}}, T_{\text{a}}, \frac{\sqrt{\pi D}}{R}\right)}{T_{\text{a}}} + \frac{N_{\text{tx}}^2}{T_{\text{a}}^2} \theta(T_{\text{b}}, T_{\text{a}}) + \frac{\sigma_{\text{ISI}}^2}{8\lambda_{\boldsymbol{\Psi}} R^2 \sqrt{\pi D}}} \tag{85b}$$

  where σ_{ISI}^2 is given by (82b), while $\theta(t, T)$ and $\psi(t, T, x)$ are defined in Corollary 4.

Proof: From (50) with $G_{\text{all}}^{(2)}(t, \tau) = 0$ and $g(t) = N_{\text{tx}} \delta(t)$ we obtain

$$\mu_0 = N_{\text{tx}} H_{\text{all}}(T_{\text{b}})$$
$$\sigma_0^2 = N_{\text{tx}} H_{\text{all}}(T_{\text{b}}) + N_{\text{tx}}^2 H_{\text{all}}^{(2)}(T_{\text{b}}, T_{\text{b}})$$

which, substituted in (53), lead to (84). From (50) with $G_{\text{all}}^{(2)}(t, \tau) = 0$ and $g(t) = \frac{N_{\text{tx}}}{T_{\text{a}}} \text{rect}\left(\frac{t}{T_{\text{a}}}\right)$ we obtain

$$\mu_0 = 8\lambda_{\boldsymbol{\Psi}} R^2 \sqrt{\pi D} \, \frac{N_{\text{tx}}}{T_{\text{a}}} \, \psi\left(T_{\text{b}}, T_{\text{a}}, \frac{\sqrt{\pi D}}{R}\right)$$

$$\sigma_0^2 = 8\lambda_{\boldsymbol{\Psi}} R^2 \sqrt{\pi D} \, \frac{N_{\text{tx}}}{T_{\text{a}}} \, \psi\left(T_{\text{b}}, T_{\text{a}}, \frac{\sqrt{\pi D}}{R}\right) + 8\lambda_{\boldsymbol{\Psi}} R^2 \sqrt{\pi D} \, \frac{N_{\text{tx}}^2}{T_{\text{a}}^2} \, \theta(T_{\text{b}}, T_{\text{a}})$$

which, substituted in (53), provide (85). □

Now, it is interesting to verify the behavior of SIR and SINR when the average number of transmitted symbols and the transmitters density approach infinity.

1) Asymptotic analysis with respect emissions: Define the quantity

$$\Theta_j \triangleq \sum_{k=1}^{j} (f_{k+1,k+1} - f_{k,k+1} + f_{k,k} - f_{k+1,k}) + \sum_{k=1}^{j} (f_{j+1,k+1} - f_{1,k+1} + f_{1,k} - f_{j+1,k})$$

with $f_{k,m} = \sqrt{kT_{\text{b}}} + \sqrt{mT_{\text{b}}} - \sqrt{kT_{\text{b}} + mT_{\text{b}}}$ for Poisson concentration (synchronous) transmitters and $f_{k,m} = \eta(kT_{\text{b}}, mT_{\text{b}}, T_{\text{a}})$ for timing (asynchronous) transmitters. From Proposition 3 it is easy to derive the following limits

- Poisson concentration (synchronous) transmitters:

$$\lim_{N_{\text{tx}} \to +\infty} \text{SIR} = \frac{2\lambda_{\boldsymbol{\Psi}} \sqrt{\pi D} T_{\text{b}} \, (2R + \sqrt{\pi D T_{\text{b}}})^2}{\frac{1}{4}\Theta_j} \tag{86a}$$

$$\lim_{N_{\text{tx}} \to +\infty} \text{SINR} = \frac{2\lambda_{\boldsymbol{\Psi}} \sqrt{\pi D} T_{\text{b}} \, (2R + \sqrt{\pi D T_{\text{b}}})^2}{(\sqrt{2} - 1)\sqrt{T_{\text{b}}} + \frac{1}{4}\Theta_j} \tag{86b}$$

- Timing (asynchronous) transmitters with uniformly distributed emissions within an activity interval T_{a}:

$$\lim_{N_{\text{tx}} \to +\infty} \text{SIR} = \frac{8\lambda_{\boldsymbol{\Psi}} \sqrt{\pi D} \, \psi^2\left(T_{\text{b}}, T_{\text{a}}, \frac{\sqrt{\pi D}}{R}\right)}{\frac{1}{4}\Theta_j} \tag{87a}$$

$$\lim_{N_{\text{tx}} \to +\infty} \text{SINR} = \frac{8\lambda_{\boldsymbol{\Psi}} \sqrt{\pi D} \, \psi^2\left(T_{\text{b}}, T_{\text{a}}, \frac{\sqrt{\pi D}}{R}\right)}{\theta(T_{\text{b}}, T_{\text{a}}) + \frac{1}{4}\Theta_j} \, . \tag{87b}$$

2) Asymptotic analysis with respect transmitters density: From Proposition 3 it is also straightforward to derive, that, if the number of interferer symbols j is finite, it results, for both synchronous and asynchronous cases:

$$\lim_{\lambda_{\boldsymbol{\Psi}} \to \infty} \text{SIR} = \lim_{\lambda_{\boldsymbol{\Psi}} \to \infty} \text{SINR} = +\infty \, . \tag{88}$$

This confirms that the best strategy, in a spatially distributed molecular communication system, is to increase the transmitters density rather than the number of molecules emitted by each transmitter.

VI. Numerical Results

In this section, we present numerical results derived by the proposed analytical framework and verified by simulations.

A. Model validation via simulation

The stochastic description of Brownian motion is well-established [52]. In particular, Fick's law of diffusion which leads to equation (1) for spherical absorbing receiver has been extensively verified in literature, e.g. in [28] and [7] via particle-based simulation. Here, we focus on the validation of the proposed spatio-temporal model for molecules transmission. As in [8] we assume that (1) holds and we generate Bernoulli random variables with parameter $F_{\text{hit}}(\|\boldsymbol{x}_n\|, t - \boldsymbol{\tau}_l^{(n)})$ to simulate the reception process of each emitted molecule at a certain time instant $\boldsymbol{\tau}_l^{(n)}$ at a certain position $\boldsymbol{x}_n$ (which is, indeed, received with probability $F_{\text{hit}}(\|\boldsymbol{x}_n\|, t - \boldsymbol{\tau}_l^{(n)})$). By exploiting the superposition of effects (implicit in the linearity of diffusion equations), we compute the total number of received molecules as the sum of all contributions. By using Monte Carlo method, we evaluate the mean and the variance by averaging over thousands of realizations of the point processes modeling the transmitters positions and the emission times. The same is done for the ISI component. To compute the bit error rate (BER),[19] the number of received molecules obtained as described is compared to the threshold according to OOK modulation as described in Sec. IV-D.

[19]We use the term "rate" when we refer to simulations, while for the analysis it is preferred the term "probability".

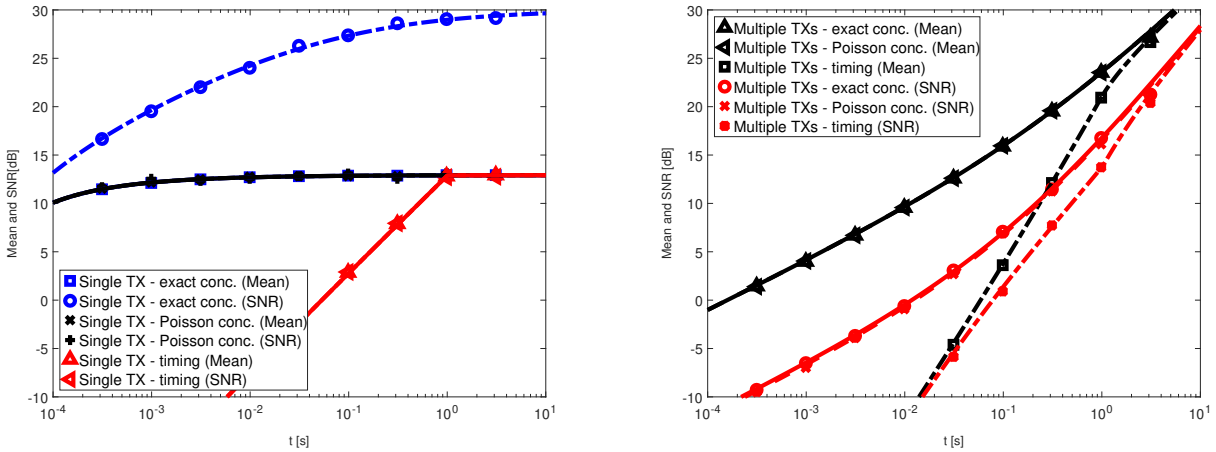

(a) Single Transmitter (Tx-RX distance $r = 5.1\mu$m)

(b) Swarm of Transmitters (transmitters density $\lambda_{\mathbf{\Psi}} = 10^{15} m^{-3}$)

Fig. 3. SNR as a function of time ($N_{\text{tx}} = 20$), and timing transmitters (for a fair comparison, we consider $\lambda_{\text{a}} T_{\text{a}} = N_{\text{tx}}$). Lines represents analytical results, while marked points are from simulation.

B. Analog scenario

We refer to the case study in Sec. V-A. In the following, unless stated otherwise, an unbounded space is considered, the diffusion coefficient is[20] $D = 120 \cdot 10^{-12}\text{m}^2/\text{s}$, the transmitters density is $\lambda_{\mathbf{\Psi}} = 10^{15}\text{m}^{-3}$, the radius of the spherical fully absorbing receiver is $r = 5\mu$m, the number of emitted molecules by concentration transmitters are $N_{\text{tx}} = 20$, and the activity interval of timing transmitters is $T_{\text{a}} = 1$s. Such numerical values are consistent with [7], [9].

1) Comparison between point to point and spatially distributed MCvD: For a fair comparison, the single transmitter is considered at distance $r = 5.1\mu$m from the receiver, which is equal to the average distance between the nearest points belonging to an homogeneous PPP with intensity $10^{15} m^{-3}$ (i.e., the intensity considered for the multiple transmitters case).

2) Temporal Evolution of the first and second order statistics: In Fig. 3(a) and 3(b), the mean number of received molecules and the SNR as defined by (11) and (18) are shown as functions of time for the point-to-point and the spatially distributed cases, respectively. Poisson concentration, and timing (with activity interval $T_{\text{a}} = 1$s) transmitters are considered. For a fair comparison between different transmitter models, the average number of emitted molecules for timing transmitters during the activity interval ($\lambda_{\text{a}} T_{\text{a}}$) is assumed to be equal to the average number of molecules emitted by concentration transmitters (N_{tx}).

In a single-transmitter system case as shown in Fig. 3(a), the SNR is strictly related to the average number of received molecules. More specifically, for Poisson concentration and timing transmitter (with molecules emitted one-by-one according to a time domain PPP: see Sec. II-B3) the SNR results equal to the mean number of received molecules (see Remark 2), while for the exact concentration case it results higher, due to the deterministic emission (which reduces the variance for the same average). The mean number of received molecules, instead, is the same for both exact and Poisson concentration cases. Before the end of the activity interval (1s in the example), the timing transmitter leads to lower values of mean and SNR compared to both concentration models. This is due to the delayed emission of molecules (in the timing model) with respect to the instant $t = 0$ at which all molecules are emitted by concentration models. After the end of the activity interval, the timing transmitter tends to attain the same mean and SNR as the Poisson concentration transmitters, since for both the number of emitted molecules are Poisson RV having the same parameter after T_{a}. For all the models a saturation effect occurs in the upper range of the t values; the asymptotes are found in exact coincidence with formulas (78).

In a spatially distributed system case as shown in Fig. 3(b), the SNR significantly diverges from the average number of received molecules (according to the remark 3) for all cases. First, note that for all cases of multiple transmitters, the SNR does not saturate as with a single transmitter, but continuously increases as t increases. Second, unlike in the single-transmitter case, exact and Poisson concentration models are almost indistinguishable (in terms of both mean and SNR) just for $\mathsf{n}_{\text{tx}} = 20$.[21] Finally, the timing transmitter leads to lower values of mean and SNR compared to both concentration models for $t < T_{\text{a}} = 1$s. After the end of the activity, interval, both mean and SNR tend to the same values as for Poisson concentration. It can be explained as for the corresponding single transmitters cases. It should be remarked that after 1s (in the scenario considered) a significant value of SNR is obtained for all the models.

For all cases, simulation results (marked points) are in almost perfect agreement with the analysis (lines).

3) Saturation effects: In Fig. 4(b) and 4(a) the SNR is depicted as a function of the time t after the beginning of the emissions and of the average number N_{tx} of emitted

[20] See also [53], [54], [8], and [9] for typical values in similar scenarios.

[21] For such a reason, in the following figures, exact and Poisson concentration transmitter model will be considered together under the name of "concentration transmitter".

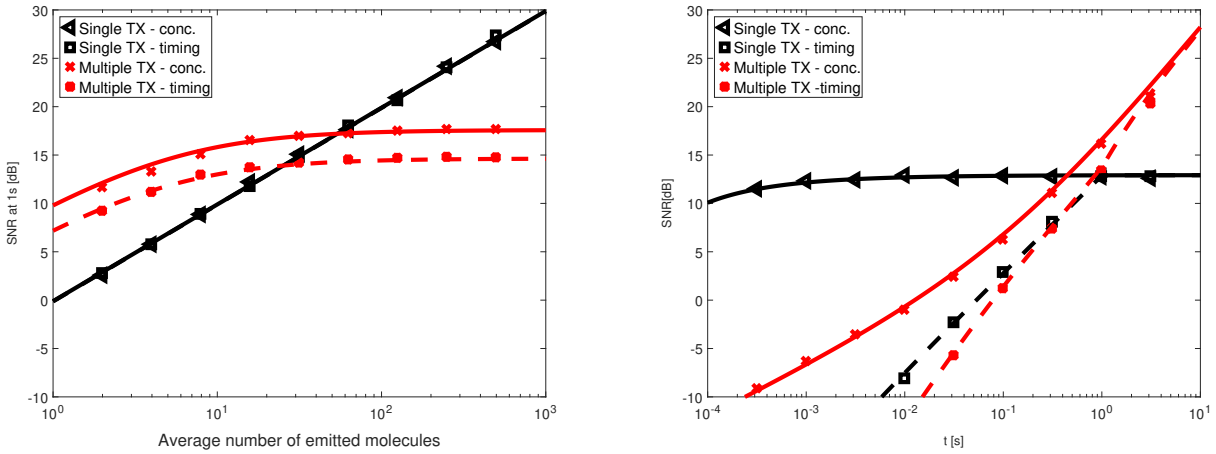

(a) SNR as a function of time for single and multiple transmitters scenarios. Concentration and timing transmitters (with $\lambda_a T_a = N_{tx}$) are compared.

(b) SNR at $t = 1$s as a function of emitted molecules for single and multiple transmitters scenarios. Concentration and timing transmitters (with $\lambda_a T_a = N_{tx} = 20$) are compared.

Fig. 4. Different (dual) saturation effects for single and multiple transmitters scenarios. Lines represents analytical results, while marked points are from simulation.

molecules, respectively. Single and multiple transmitters cases are compared in the same plots. Both concentration[22] and timing transmitters (with $T_a = 1$s) are considered.

Fig. 4(a) shows that, for high N_{tx}, the SNR (evaluated 1 second after the emission) linearly increases as the number of emitted molecules increases for the single transmitter case, while a saturation effect arises for the multiple transmitters case. This can be explained as follows:

- In the single transmitter scenario, for both Poisson concentration and timing transmitter models, the number of received molecules is a Poisson RV and thus the SNR equals the mean which continues to increase;
- In a spatially distributed scenario, the number of received molecules cannot be modeled as a Poisson RV,[23] due to the random number and the random positions of the transmitters. In fact, in the scenario considered, the average value of the molecules received increases linearly as N_{tx} increases (according to the literature [7], [8]), while the variance is shown to have a higher increasing with N_{tx} compared to the mean (due to the aforementioned spatial randomness). Thus, the ratio (18) saturates.

Fig. 4(b) shows that, as the time increases, the SNR continues to increase for the multiple transmitters case, while a saturation effect arises for the single transmitter case. This can be explained as follows:

- In the single transmitter scenario, the probability that a molecule is received at time t, i.e., the hitting rate (the derivative of (1)), decreases as $t^{-3/2}$ (see also [28], [55], and [37]). Thus, the number of received molecules does not significantly increase after a time much longer than the average time of arrival of the molecule;

[22]We mean Poisson concentration, since exact concentration has been previously shown to be similar in the spatially distributed transmitters case.

[23]Only its density function conditioned to the transmitters positions and to the emission times can be considered as a Poisson distribution.

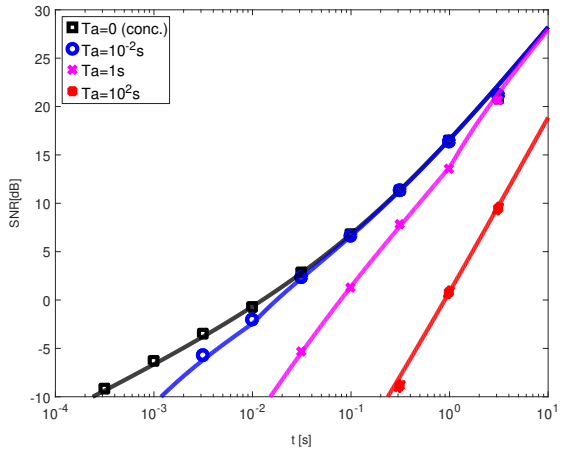

Fig. 5. Spatially distributed emissions: SNR as a function of time for timing (asynchronous) transmitters with different durations of the activity interval. The case of Poisson concentration (synchronous) transmitter is reported as reference. Lines represents analytical results, while marked points are from simulation.

- In the multiple transmitters scenario, if the space of the PP modeling the transmitters positions is unbounded and no molecules decay is considered, the aforementioned effect is counteracted by the large number of contributions from transmitters placed very far from the receiver (whose molecules arrive long time after the emission).[24]

Observe that, for all cases, simulation results (marked points) are in good agreement with analytical results (lines).

4) Activation Time: In Fig. 5 the SNR is depicted as a function of time for spatially distributed timing (asynchronous) transmitters with an activity interval $[0 - T_a]$. SNR values corresponding to $T_a = 10^2,\ 1,\ 10^{-2}$ are compared to the

[24]According to Proposition 1, both the mean and the variance of the received molecules in a spatially distributed transmitters scenario linearly increase for large t, (see (75a)) such that the ratio (18) increases too.

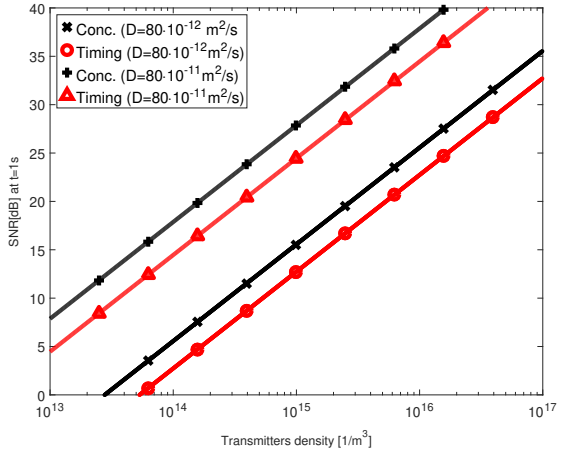

(a) SNR at $t = 1$s as a function of transmitters density for concentration (synchronous) and timing (asynchronous) transmitters. Two different values for the diffusion coefficients are considered.

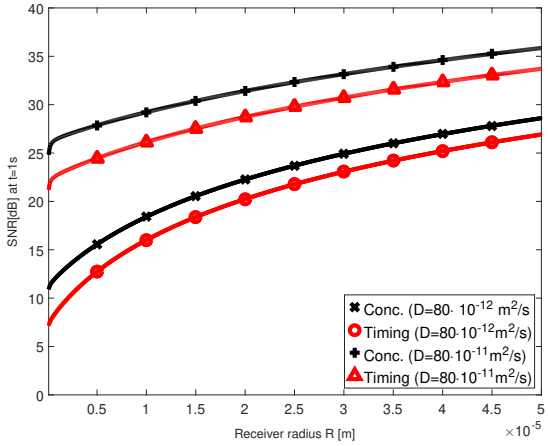

(b) SNR at $t = 1$s as a function of the receiver radius for concentration (synchronous) and timing (asynchronous) transmitters. Two different values for the diffusion coefficients are considered.

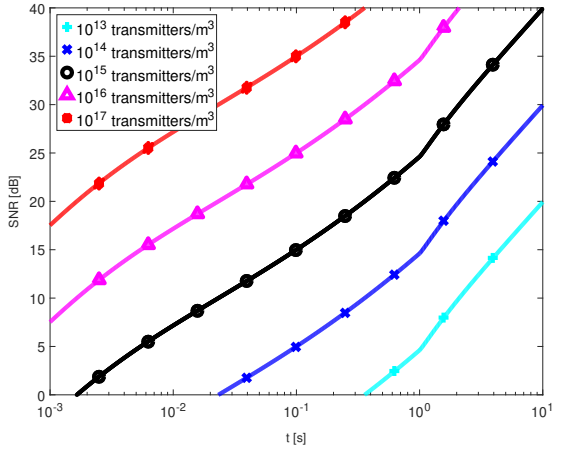

(c) SNR as a function of time for timing (asynchronous) transmitters with different values for the receiver radius

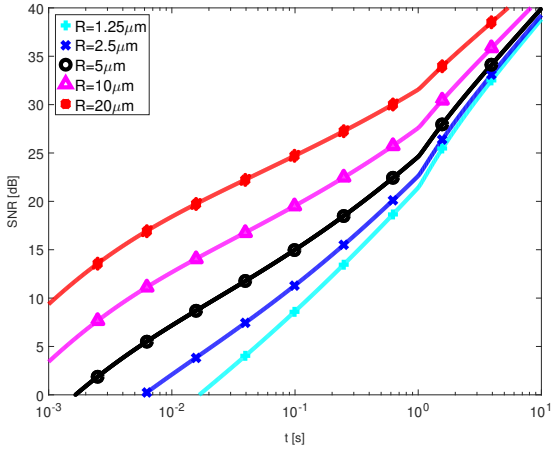

(d) SNR as a function of time for timing (asynchronous) transmitters with different values of the transmitters density.

Fig. 6. SNR as a function of spatial parameters

case $T_a \to 0$, which corresponds to the Poisson concentration (synchronous) transmitters case. For fair comparison, the same average number of emitted molecules $N_{tx} = 20$ is considered for all cases (i.e., the emission intensity λ_a is chosen such that, for each case, $\lambda_a T_a = N_{tx}$). It has to be noticed that the duration of the activity interval can have a strong impact on the SNR. On one hand, it can be observed that, with an activity interval of duration 10^2s, only a fraction of N_{tx} is emitted within 1s after the start. This produces the lower SNR for cases where $T_a < 1$s. On the other hand, with an activity interval of duration 10^{-2} and 1s, the gap in terms of SNR with respect to the case of concentration transmitter (all molecules emitted at $t = 0$) vanishes for $t > 10^{-2}$s and $t > 1$s, respectively. In fact, after T_a, all the molecules are emitted with probability 1. The comparison between simulation (marked points) and analysis (lines) validates the proposed spatio-temporal model also for the second order statistics. Thus, the following figures of this subsection will report analytical results only.

5) Spatial distribution parameters: In Fig. 6(c) and 6(d) the SNR at $t = 1$s for both concentration and timing (with $T_a = 10^{-2}$s) transmitters is shown as a function of the transmitters density λ_Ψ and of the receiver radius R, respectively. Two different values for the diffusion coefficient D are considered in both cases. One can notice that the SNR linearly increases as λ_Ψ increase, while it shows lower increase with respect to linearity, as the receiver radius increases. This represents another difference with respect to electromagnetic waves communications, where usually (e.g., in the case of parabolic antennas and AWGN channel) the gain of the receiving antenna (and, thus, the SNR) increases as the square of its radius.

In Fig. 6(a) and 6(b) the SNR for the case of spatially distributed (asynchronous) timing transmitters is represented as a function of time for different values of the transmitters density and of the receiver radius, respectively.

First, it can be noticed that the gap between SNR values corresponding to different transmitters density is almost constant among time. This is a consequence of the linear dependence between the SNR and the transmitters density. This means that, in a spatially distributed emissions scenario, the density

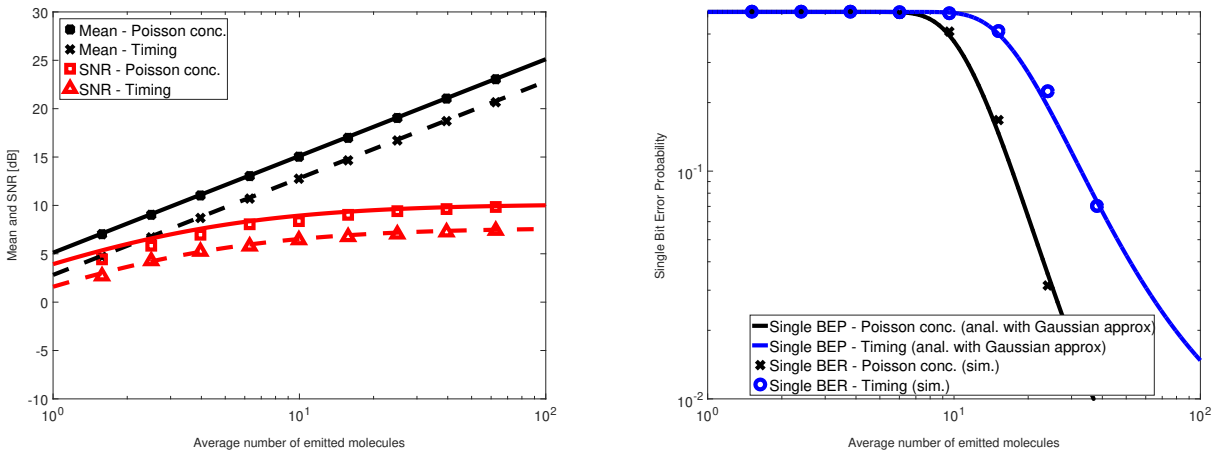

(a) SNR as a function of the average number of emitted molecules. Concentration and timing transmitters (with $T_a = T_b$) are compared.

(b) Single BEP as a function of the average number emitted molecules. Concentration and timing transmitters (with $T_a = T_b$) are compared.

Fig. 7. Performance vs Emitted molecules (without ISI). Lines represents analytical results, while marked points are from simulations.

of the transmitters is the key parameter for the communication efficiency.

Second, the gap between SNR values corresponding to different receiver radius values is reduced as the time increases. It means that, in the molecular communication scenario considered, the benefit of a higher radius receiver is "time-varying" and more relevant in the earlier instants. This differs from the classical electromagnetic wave communications, where, e.g., the benefit of an higher gain antenna is, in general, not time varying for a fixed scenario.

C. Digital scenario

Unless otherwise stated, for digital molecular communications via diffusion, we consider on-off keying with a bit time $T_b = 0.2$s and a threshold $N_{th} = 40$. All the other parameters are set as for the analog scenario.

1) Performance vs Emitted molecules without ISI: Fig 7(a) and 7(b) show, respectively the SNR and the single BEP as functions of the average number of transmitted molecules. Both Poisson concentration (synchronous) and timing (asynchronous) transmitters are considered. In the latter case, the activation time T_a is set equal to the bit time T_b.[25] It can be noticed that, as expected, without ISI, for increasing average number of emitted molecules, an increasing SNR corresponds to a decreasing BEP. Note the results for the BEP, obtained through the Gaussian approximation (60), show an acceptable agreement with the simulation results.

2) Performance vs Bit rate without ISI: Fig 8(a) and 8(b) show, respectively the SNR and the single BEP as functions of the bit rate $1/T_b$. As before, both Poisson concentration (synchronous) and timing (asynchronous) transmitters are considered and, in the latter case, the activation time T_a is set equal to the bit time T_b. It can be noticed that, in the absence of ISI, as the bit rate decreases (i.e., the bit time increases), the SNR increases (according to what shown for the analog case) and the BEP decreases indefinitely.

[25]This represents the worst case, i.e., without any guard time.

3) Performance in the presence ISI: In Fig. 11(a) and 10 the impact of ISI on the performance of the considered spatially distributed molecular communication scenario is studied via both analysis and simulations. In Fig. 11(a) the SIR and the SINR are shown as functions of the average number of emitted molecules. Analytical results from (84) and (85), with $j = 1$ (ISI with one interferer symbol) are compared to simulations. Both ratios, as expected, increases as N_{tx} increases. According to Corollary 3, the growing of the variance is faster than that of the mean, so that the SIR and the SINR saturate. The matching between analytical and simulation results validate the proposed stochastic model even in the presence of ISI. In Fig. 10 the Gaussian approximation used in (65) and (66) is applied to evaluate the bit error probability in the presence of ISI for both Poisson concentration (synchronous) and timing (asynchronous) transmitters. Due to the ISI component, the choice of the threshold is critical (according to what shown in [7] for exact concentration transmitters). The optimal threshold, for which the BEP is minimized, results to be $N_{th} = 40$, for the considered values of $N_{tx} = 20$ and $\lambda_{\Psi} = 10^{15} m^{-3}$. Note that such a higher value (due to the presence of ISI component) makes the Gaussian approximation tighter with respect the case of no ISI (for which the optimal threshold is $N_{th} = 1$.).

Once validated the analytical model, we can use (84) and (85) to investigate the asymptotic behavior of both SINR and BEP with respect the average number of transmitted molecules and the density of transmitters. In Fig. 11(a) and 11(b), respectively, the SINR and the BEP are shown as functions of the average number of emitted molecules. As expected, the SINR saturates for high values for N_{tx} and the BEP presents a floor as consequence. It is in accordance to results known for the single transmitter case [35]. The impact of the length of the ISI sequence ($j = 1,\ 4,\ 16,\ 64$) can also be appreciated (e.g., about 5dB loss between 1 and 64 interferer symbols). Moreover, it has to be noticed that asynchronous transmissions (dashed lines) imply a loss of about 4dB (with respect the synchronous transmissions) for all cases.

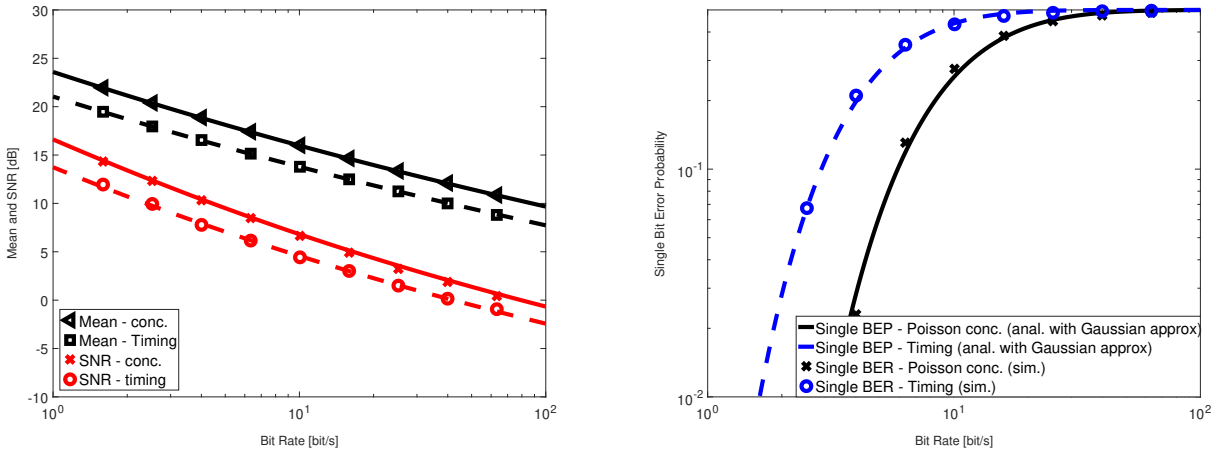

(a) SNR as a function of the average number of emitted molecules. Concentration and timing transmitters (with $T_{\mathrm{a}} = T_{\mathrm{b}}$) are compared.

(b) Single BEP as a function of the average number emitted molecules. Concentration and timing transmitters (with $T_{\mathrm{a}} = T_{\mathrm{b}}$) are compared.

Fig. 8. Performance vs Emitted molecules (without ISI). Lines represents analytical results, while marked points are from simulations.

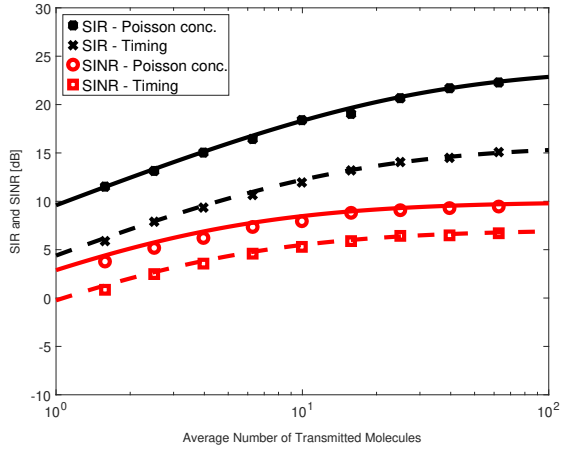

Fig. 9. SIR and SINR with $j = 1$ symbol. Lines represents analytical results, while marked points are from simulations.

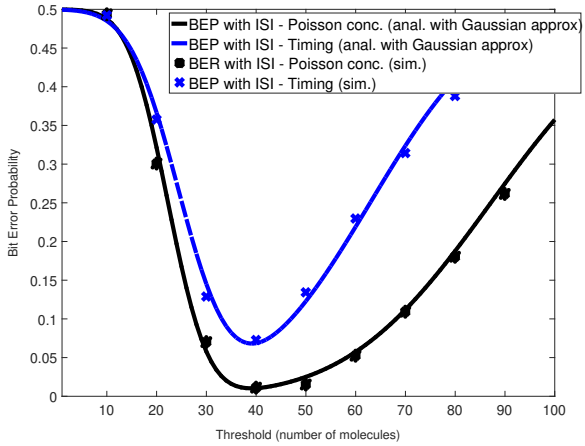

Fig. 10. BEP as a function of the threshold in the presence of ISI (1 interferer symbol). Lines represents analytical results, while marked points are from simulations.

Fig. 11(c) and 11(d) present the SINR and the BEP as functions of the transmitters density λ_{Ψ}. Here, a characteristic effect of the spatially distributed transmission arises. Both SIR and SINR linearly increase with λ_{Ψ} without any saturation. The BEP decreases accordingly without any floor. Long (but finite) ISI sequences (e.g., $i = 10,\ 100$) introduce gaps in both figures, without modifying the asymptotic behavior, which is in accordance to (88). Such an apparently counter-intuitive effect[26] strictly depends on the stochastic geometry and can be explained as follows. ISI arises due to molecules which arrive delayed (with respect to the emission interval). Thus, most of the molecules emitted by transmitters far from the receiver contribute to the ISI component, while most of the molecules transmitted by points very close to the receiver contribute to the useful signal. However, for transmitters randomly placed according to a homogeneous PPP, the number of received molecules is dominated by contributions of transmitters very close to the receiver when the PPP density is high (see also [8]). The impact of ISI for high transmitters density is proportionally reduced as a consequence.

It is shown in [51] that, for a high number of interferer symbols, the generalized Gaussian approximation (62) with $\beta > 2$ seems to be more accurate than the standard Gaussian, achieving a very good fitting by tuning the shape parameter. However, in Fig. 12, we show that, for β ranging between 2 and 8 (for the sake of simplicity, in (68) and (69) we considered $\beta_1 = \beta_0 = \beta$),[27], the impact on the BEP is negligible in the values of interest for the transmitters density. More precisely, the generalized Gaussian approximation is slightly more pessimistic (with respect the Gaussian approximation, i.e., $\beta = 2$) for low values of the transmitters density while it is more optimistic (lower values of the BEP) for high densities. This implies that positive effect of an high transmitters density (which counteracts ISI in MCvD as previously explained)

[26] In classical communications, the ISI detrimental effect is not counteracted by simply increasing the number of transmitters

[27] Note that such an interval includes all values proposed by [51]

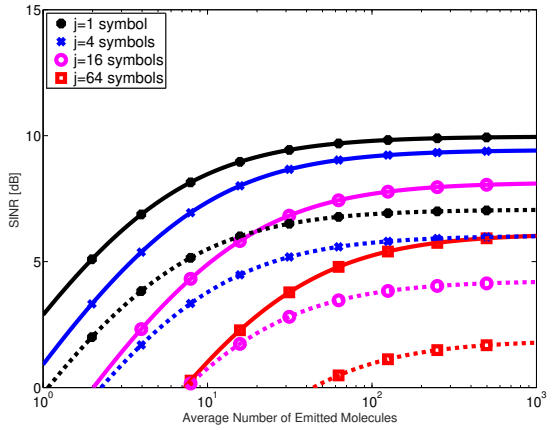

(a) SINR as function of average number of transmitted molecules N_{tx} for concentration (synchronous) and timing (asynchronous) transmitters. Different lenghts of the ISI sequence are considered

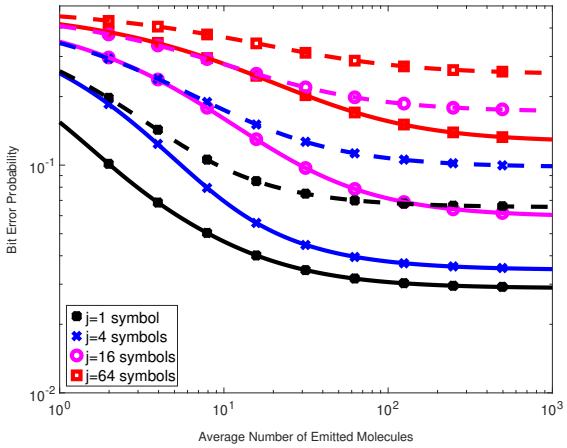

(b) BEP as a function of the average number of transmitted molecules N_{tx} for concentration (synchronous) and timing (asynchronous) transmitters. Different lengths of the ISI sequence are considered.

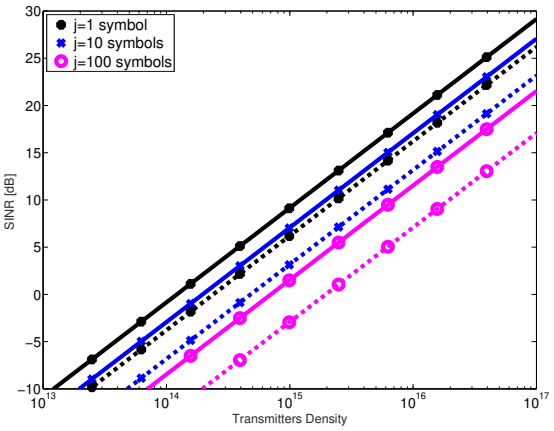

(c) SINR as function of the transmitters density λ_{Ψ} for concentration (synchronous) and timing (asynchronous) transmitters. Different lenghts of the ISI sequence are considered. Units in abscissa are m^{-3}.

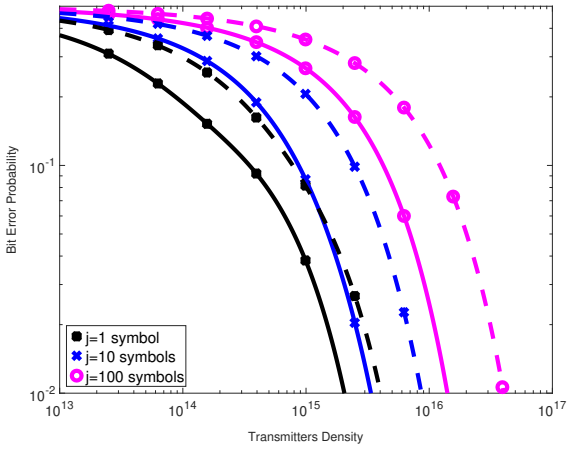

(d) BEP as a function of the transmitters density λ_{Ψ} for concentration (synchronous) and timing (asynchronous) transmitters with different values of the transmitters density. Units in abscissa are m^{-3}.

Fig. 11. Analytical results for SIR, SINR and BEP in spatially distributed molecular communications. ISI is considered with different number of interferer symbols. Continuous lines represent the synchronous case, dashed lines the asynchronous.

is not affected by the Gaussian approximation. Finally, note that the gap in terms of BEP between the synchronous and asynchronous case is always appreciable.

VII. Conclusion and Future Works

In this work, a scenario with a swarm of point transmitters randomly placed in $\mathbb{R}^3$ and a spherical fully absorbing receiver is considered as case study, according to the recent literature on spatially distributed MCvD. However, for the first time, not only the average number of received molecules is evaluated here, but also its variance. This allows the evaluation of the SNR for the received molecular signal, defined as the ratio between the squared average number of received molecules and the corresponding variance.

Making use of the stochastic geometry and the point processes theory, analytical expressions for the SNR in spatially distributed MCvD are derived for synchronous concentration and asynchronous timing transmitters. It is shown that, in spatially distributed MCvD, the SNR indefinitely increases as the time increases, unlike in point-to-point MCvD, for which saturation effects arise with respect to time. On the contrary, the SNR in spatially distributed MCvD shows a saturation effect with respect to the number of emitted molecules (for concentration transmitter models) and to the emission intensity (for the timing transmitter model). Such an effect derives from the random position of transmitters in the considered spatially distributed scenario and has no counterpart in point-to-point MCvD. These results suggest that spatially distributed MCvD is more effective than point-to-point MCvD for long observation times (where high SNRs can be obtained even with few emitted molecules per transmitter), while it tends to be less effective in scenarios where high SNRs have to be obtained through an high number of emitted molecules per transmitter.

Besides, the proposed second order analysis clarifies the role of the spatial distribution of the point transmitters. It is

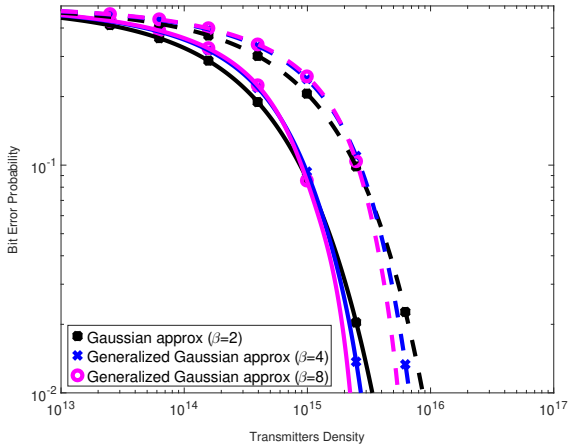

Fig. 12. BEP as a function of the transmitters density in the presence of ISI (10 interferer symbols). Generalized Gaussian approximation with different values of β. Continuous lines represent the synchronous case, dashed lines the asynchronous.

shown that, when the point process modeling the transmitters positions involves stochastic repulsion among points, the SNR is increased with respect to the case of independently scattered points (PPP). On the contrary, clustering effects leads to a reduced SNR with respect to the reference case of the PPP. This results suggests that the typical cells displacement in organic tissues (a middle way between fully random and regular displacements) might also have beneficial effects if such cells play the role of transmitters in MCvD.

In addition, the extensive analysis put also in evidence some general aspects of MCvD which may be considered counter-intuitive, if compared to the classical electromagnetic wave communications: e.g, the SNR increases sublinearly as a function of the receiver radius, and the benefit of a larger radius is reduced by time.

The analysis is completed by the evaluation of the SINR when digital communications affected by ISI are considered. The BEP in case of OOK modulation is obtained via Gaussian approximation.

Numerical results obtained via Monte Carlo simulations show a perfect agreement with the analytical results for the SNR and the ISI (thus validating the proposed second order spatiotemporal stochastic model) and a good agreement (in the range of interest) with the BEP expression derived by the Gaussian approximation (thus confirming that such an approximation is acceptable with a large number of transmitters).

The analysis shows that both SINR saturation and BEP error floor, which arise for increasing number of emitted molecules, do not arise for increasing transmitters density. Such an effect is due to the homogeneous Poisson distribution of the point transmitter and allows spatially distributed molecular communication to counteract the detrimental effect of ISI.

Finally, the cases of multiple samples detector and of spatial PPs with stochastic interactions (attraction/repulsion) between points representing transmitters positions have been considered here for the first time in a spatially distributed MCvD scenario. Deeper investigations about these two topics could represent future lines of research.

Appendix A
Mean and Variance of the Number of Received Molecules with a Poisson Concentration Tx

In case of Poisson concentration transmitter, the contribution of the l-th emitted molecules (3) has a Bernoulli distribution with success probability $F_{\text{hit}}(r,t)$. Thus, using (4) we get

$$\begin{aligned}\mathbb{E}\left\{\mathsf{a}|_{r,t}\right\} &= \mathbb{E}\left\{\sum_{l=1}^{\mathsf{n}_{\text{tx}}} \mathsf{b}_l(r,t)\right\} = \mathbb{E}\left\{\sum_{l=1}^{\mathsf{n}_{\text{tx}}} F_{\text{hit}}(r,t)\right\} \\ &= \mathbb{E}\left\{\mathsf{n}_{\text{tx}}\right\} F_{\text{hit}}(r,t) = N_{\text{tx}}\, F_{\text{hit}}(r,t) \end{aligned} \tag{89}$$

and

$$\begin{aligned}\mathbb{E}\left\{\mathsf{a}^2(r,t)\right\} &= \mathbb{E}\left\{\left(\sum_{l=1}^{\mathsf{n}_{\text{tx}}} \mathsf{b}_l(r,t)\right)^2\right\} \\ &= \mathbb{E}\left\{\sum_{l=1}^{\mathsf{n}_{\text{tx}}} \mathsf{b}_l^2(r,t)\right\} + \mathbb{E}\left\{\sum_{l=1}^{\mathsf{n}_{\text{tx}}}\sum_{\substack{m=1\\m\neq l}}^{\mathsf{n}_{\text{tx}}} \mathsf{b}_l(r,t)\mathsf{b}_m(r,t)\right\} \\ &= \mathbb{E}\left\{\sum_{l=1}^{\mathsf{n}_{\text{tx}}} F_{\text{hit}}(r,t)\right\} + \mathbb{E}\left\{\sum_{l=1}^{\mathsf{n}_{\text{tx}}}\sum_{\substack{m=1\\m\neq l}}^{\mathsf{n}_{\text{tx}}} F_{\text{hit}}^2(r,t)\right\} \\ &= \mathbb{E}\left\{\mathsf{n}_{\text{tx}}\right\} F_{\text{hit}}(r,t) + \mathbb{E}\left\{\mathsf{n}_{\text{tx}}(\mathsf{n}_{\text{tx}}-1)\right\} F_{\text{hit}}^2(r,t) \\ &= N_{\text{tx}}F_{\text{hit}}(r,t) + (N_{\text{tx}} + N_{\text{tx}}^2 - N_{\text{tx}})F_{\text{hit}}^2(r,t) \\ &= N_{\text{tx}}F_{\text{hit}}(r,t) + N_{\text{tx}}^2 F_{\text{hit}}^2(r,t) \end{aligned} \tag{90}$$

from which it follows

$$\mathbb{V}\{\mathsf{a}|_{r,t}\} = N_{\text{tx}}F_{\text{hit}}(r,t)\,. \tag{91}$$

Appendix B
Mean and Variance of the Number of Received Molecules with a Timing Transmitter

From (6), using the properties of a Bernoulli RV and applying the Campbell theorem to the time domain PPP Φ, we obtain

$$\begin{aligned}\mathbb{E}\left\{\mathsf{a}|_{r,t}\right\} &= \mathbb{E}\left\{\sum_{\boldsymbol{\tau}_l\in\boldsymbol{\Phi}} \mathsf{b}(r,t-\boldsymbol{\tau}_l)\right\} \\ &= \mathbb{E}_{\boldsymbol{\Phi}}\left\{\sum_{\boldsymbol{\tau}_l\in\boldsymbol{\Phi}} F_{\text{hit}}(r,t-\boldsymbol{\tau}_l)\right\} \\ &= \int_{-\infty}^{+\infty} \lambda(\tau) F_{\text{hit}}(r,t-\tau)d\tau\,. \end{aligned} \tag{92}$$

and

$$\begin{aligned}\mathbb{E}\left\{\left[\mathsf{a}|_{r,t}\right]^2\right\} =& \mathbb{E}\left\{\left[\sum_{\boldsymbol{\tau}_l\in\boldsymbol{\Phi}}\mathsf{b}(r,t-\boldsymbol{\tau}_l)\right]^2\right\}\\ =& \mathbb{E}\left\{\sum_{\boldsymbol{\tau}_l\in\boldsymbol{\Phi}}\mathsf{b}^2(r,t-\boldsymbol{\tau}_l)\right\}\\ &+\mathbb{E}\left\{\sum_{\boldsymbol{\tau}_l\in\boldsymbol{\Phi}}\sum_{\substack{\boldsymbol{\tau}_k\in\boldsymbol{\Phi}\\ \boldsymbol{\tau}_k\neq\boldsymbol{\tau}_l}}\mathsf{b}(r,t-\boldsymbol{\tau}_l)\mathsf{b}(r,t-\boldsymbol{\tau}_k)\right\}\\ =&\mathbb{E}_{\boldsymbol{\Phi}}\left\{\sum_{\boldsymbol{\tau}_l\in\boldsymbol{\Phi}}\mathbb{E}_{\mathsf{b}|\boldsymbol{\Psi}}\left\{\mathsf{b}^2(r,t-\boldsymbol{\tau}_l)\right\}\right\}\\ &+\mathbb{E}_{\boldsymbol{\Phi}}\left\{\sum_{\boldsymbol{\tau}_l\in\boldsymbol{\Phi}}\sum_{\substack{\boldsymbol{\tau}_k\in\boldsymbol{\Phi}\\ \boldsymbol{\tau}_k\neq\boldsymbol{\tau}_l}}\mathbb{E}_{\mathsf{b}|\boldsymbol{\Psi}}\left\{\mathsf{b}(r,t-\boldsymbol{\tau}_l)\mathsf{b}(r,t-\boldsymbol{\tau}_k)\right\}\right\}\\ =&\mathbb{E}_{\boldsymbol{\Phi}}\left\{\sum_{\boldsymbol{\tau}_l\in\boldsymbol{\Phi}}F_{\text{hit}}(r,t-\boldsymbol{\tau}_l)\right\}\\ &+\mathbb{E}_{\boldsymbol{\Phi}}\left\{\sum_{\boldsymbol{\tau}_l\in\boldsymbol{\Phi}}\sum_{\substack{\boldsymbol{\tau}_k\in\boldsymbol{\Phi}\\ \boldsymbol{\tau}_k\neq\boldsymbol{\tau}_l}}F_{\text{hit}}(r,t-\boldsymbol{\tau}_l)F_{\text{hit}}(r,t-\boldsymbol{\tau}_k)\right\}\\ =&\int_{-\infty}^{+\infty}\lambda(\tau)F_{\text{hit}}(r,t-\tau)d\tau\\ &+\int_{-\infty}^{+\infty}\int_{-\infty}^{+\infty}\lambda(\tau)\lambda(s)F_{\text{hit}}(r,t-\tau)\\ &\times F_{\text{hit}}(r,t-s)d\tau ds\\ =&\int_{-\infty}^{+\infty}\lambda(\tau)F_{\text{hit}}(r,t-\tau)d\tau\\ &+\left[\int_{-\infty}^{+\infty}\lambda(\tau)F_{\text{hit}}(r,t-\tau)d\tau\right]^2. \end{aligned}\tag{93}$$

Thus

$$\mathbb{V}\{\mathsf{a}|_{r,t}\}=\int_{-\infty}^{+\infty}\int_{-\infty}^{+\infty}\lambda(\tau)\lambda(s)F_{\text{hit}}(r,t-\tau)F_{\text{hit}}(r,t-s)d\tau ds\,.\tag{94}$$

Appendix C
Mean and variance of the number of received molecules for spatially distributed asynchronous timing transmission

Proof: By using (10) with $\mathcal{L}=\mathcal{I}\{\boldsymbol{\Phi}^{(n)}\}$ and $\mathsf{b}_{n,l}|_{\boldsymbol{\Psi},t}\sim\mathcal{B}[F_{\text{hit}}(\|\mathbf{x}_n\|,t-\boldsymbol{\tau}_l^{(n)})]$, (21) leads to

$$\begin{aligned}\epsilon(\mathbf{x}_n,t)=&\mathbb{E}_{\boldsymbol{\Phi},\mathsf{b}|\boldsymbol{\Psi}}\left\{\sum_{l\in\mathcal{I}\{\boldsymbol{\Phi}^{(n)}\}}\mathsf{b}_{n,l}|_{\boldsymbol{\Psi},t}\right\}\\ =&\mathbb{E}_{\boldsymbol{\Phi}}\left\{\sum_{\boldsymbol{\tau}_l^{(n)}\in\boldsymbol{\Phi}^{(n)}}F_{\text{hit}}(\|\mathbf{x}_n\|,t-\boldsymbol{\tau}_l^{(n)})\right\}\\ =&\int_{-\infty}^{+\infty}\rho(\tau)F_{\text{hit}}(\|\mathbf{x}_n\|,t-\tau)d\tau\end{aligned}\tag{95}$$

and

$$\begin{aligned}\xi(\mathbf{x}_n,t)=&\mathbb{E}_{\boldsymbol{\Phi},\mathsf{b}|\boldsymbol{\Psi}}\left\{\left[\sum_{l\in\mathcal{I}\{\boldsymbol{\Phi}^{(n)}\}}\mathsf{b}_{n,l}|(t)\right]^2\right\}\\ =&\mathbb{E}_{\boldsymbol{\Phi},\mathsf{b}|\boldsymbol{\Psi}}\left\{\sum_{l\in\mathcal{I}\{\boldsymbol{\Phi}^{(n)}\}}\mathsf{b}_{n,l}^2(t)\right\}\\ &+\mathbb{E}_{\boldsymbol{\Phi},\mathsf{b}|\boldsymbol{\Psi}}\left\{\sum_{l\in\mathcal{I}\{\boldsymbol{\Phi}^{(n)}\}}\sum_{\substack{k\in\mathcal{I}\{\boldsymbol{\Phi}^{(n)}\}\\ k\neq l}}\mathsf{b}_{n,l}(t)\mathsf{b}_{n,k}(t)\right\}\\ =&\mathbb{E}_{\boldsymbol{\Phi}}\left\{\sum_{\boldsymbol{\tau}_l\in\boldsymbol{\Phi}^{(n)}}\mathbb{E}_{\mathsf{b}|\boldsymbol{\Phi},\boldsymbol{\Psi}}\left\{\mathsf{b}_{n,l}^2(t)\right\}\right\}\\ &+\mathbb{E}_{\boldsymbol{\Phi}}\left\{\sum_{l\in\mathcal{I}\{\boldsymbol{\Phi}^{(n)}\}}\sum_{\substack{k\in\mathcal{I}\{\boldsymbol{\Phi}^{(n)}\}\\ k\neq l}}\mathbb{E}_{\mathsf{b}|\boldsymbol{\Phi},\boldsymbol{\Psi}}\left\{\mathsf{b}_{n,l}(t)\mathsf{b}_{n,k}(t)\right\}\right\}\\ =&\mathbb{E}_{\boldsymbol{\Phi}}\left\{\sum_{\boldsymbol{\tau}_l^{(n)}\in\boldsymbol{\Phi}^{(n)}}F_{\text{hit}}(\|\mathbf{x}_n\|,t-\boldsymbol{\tau}_l^{(n)})\right\}\\ &+\mathbb{E}_{\boldsymbol{\Phi}}\Bigg\{\sum_{\boldsymbol{\tau}_l^{(n)}\in\boldsymbol{\Phi}^{(n)}}\sum_{\substack{\boldsymbol{\tau}_k^{(n)}\in\boldsymbol{\Phi}^{(n)}\\ \boldsymbol{\tau}_k^{(n)}\neq\boldsymbol{\tau}_l^{(n)}}}F_{\text{hit}}(\|\mathbf{x}_n\|,t-\boldsymbol{\tau}_l^{(n)})\\ &\times F_{\text{hit}}(\|\mathbf{x}_n\|,t-\boldsymbol{\tau}_k^{(n)})\Bigg\}\\ =&\int_{-\infty}^{+\infty}\rho(\tau)F_{\text{hit}}(\|\mathbf{x}_n\|,t-\tau)d\tau\\ &+\int_{-\infty}^{+\infty}\int_{-\infty}^{+\infty}\rho^{(2)}(\tau,s)F_{\text{hit}}(\|\mathbf{x}_n\|,t-\tau)\\ &\times F_{\text{hit}}(\|\mathbf{x}_n\|,t-s)d\tau ds\end{aligned}\tag{96}$$

where in the last step we applied the Campbell's theorem for the second order product density function to the time domain PP $\Phi^{(n)}$. By using (95) and (96) in (23a), (24), and (20), we obtain

$$\begin{aligned}\mathbb{E}\left\{\mathsf{n}_{\text{rx}}|_{\boldsymbol{\Psi}}(t)\right\}=&\int_{\mathbb{R}^3\setminus\boldsymbol{\Omega}_R}\lambda_{\boldsymbol{\Psi}}\int_{-\infty}^{+\infty}\rho(\tau)F_{\text{hit}}(\|\boldsymbol{x}\|,t-\tau)d\tau d\boldsymbol{x}\\ =&\int_{-\infty}^{+\infty}\rho(\tau)\int_{\mathbb{R}^3\setminus\boldsymbol{\Omega}_R}\lambda_{\boldsymbol{\Psi}}F_{\text{hit}}(\|\boldsymbol{x}\|,t-\tau)d\boldsymbol{x}d\tau\end{aligned}\tag{97}$$

and

$$\begin{aligned}\mathbb{V}\{\mathsf{n}_{\text{rx}}|_{\boldsymbol{\Psi}}(t)\} =& \int_{\mathbb{R}^3\setminus\boldsymbol{\Omega}_R} \lambda_{\boldsymbol{\Psi}} \int_{-\infty}^{+\infty} \rho(\tau) F_{\text{hit}}(\|\boldsymbol{x}\|, t-\tau) d\tau d\boldsymbol{x} \\ &+ \int_{\mathbb{R}^3\setminus\boldsymbol{\Omega}_R} \lambda_{\boldsymbol{\Psi}} \int_{-\infty}^{+\infty} \int_{-\infty}^{+\infty} \rho^{(2)}(\tau, s) F_{\text{hit}}(\|\boldsymbol{x}\|, t-\tau) \\ &\times F_{\text{hit}}(\|\boldsymbol{x}\|, t-s) d\tau \; d\boldsymbol{x} + \zeta_{\boldsymbol{\Psi}}(t) \\ =& \int_{-\infty}^{+\infty} \rho(\tau) \int_{\mathbb{R}^3\setminus\boldsymbol{\Omega}_R} \lambda_{\boldsymbol{\Psi}} F_{\text{hit}}(\|\boldsymbol{x}\|, t-\tau) d\boldsymbol{x} d\tau \\ &+ \int_{-\infty}^{+\infty} \int_{-\infty}^{+\infty} \rho^{(2)}(\tau, s) \int_{\mathbb{R}^3\setminus\boldsymbol{\Omega}_R} \lambda_{\boldsymbol{\Psi}} F_{\text{hit}}(\|\boldsymbol{x}\|, t-\tau) \\ &\times F_{\text{hit}}(\|\boldsymbol{x}\|, t-s) d\boldsymbol{x} \; d\tau ds + \zeta_{\boldsymbol{\Psi}}(t) \end{aligned} \tag{98}$$

with

$$\begin{aligned}\zeta_{\boldsymbol{\Psi}}(t) =& \int_{\mathbb{R}^3\setminus\boldsymbol{\Omega}_R} \int_{\mathbb{R}^3\setminus\boldsymbol{\Omega}_R} \left[\rho_{\boldsymbol{\Psi}}(\|\boldsymbol{x}_1 - \boldsymbol{x}_2\|) - \lambda_{\boldsymbol{\Psi}}^2\right] \\ &\times \int_{-\infty}^{+\infty} \rho(\tau) F_{\text{hit}}(\|\boldsymbol{x}_1\|, t-\tau) d\tau \int_{-\infty}^{+\infty} \rho(s) \\ &\times F_{\text{hit}}(\|\boldsymbol{x}_2\|, t-s) ds \; d\boldsymbol{x}_1 d\boldsymbol{x}_2 \\ =& \int_{-\infty}^{+\infty} \int_{-\infty}^{+\infty} \rho(\tau)\rho(s) \int_{\mathbb{R}^3\setminus\boldsymbol{\Omega}_R} \int_{\mathbb{R}^3\setminus\boldsymbol{\Omega}_R} \left[\rho_{\boldsymbol{\Psi}}(\|\boldsymbol{x}_1 - \boldsymbol{x}_2\|) - \lambda_{\boldsymbol{\Psi}}^2\right] \\ &\times F_{\text{hit}}(\|\boldsymbol{x}_1\|, t-\tau) F_{\text{hit}}(\|\boldsymbol{x}_2\|, t-s) d\boldsymbol{x}_1 d\boldsymbol{x}_2 \; d\tau ds \end{aligned} \tag{99}$$

where we remark that, in both cases, the possibility to exchange the order of integrals is insured by Fubini's theorem (note that the integrand functions are positive and the integrals converge). By using (25) in (97), (98), and (99), we obtain (29). □

Appendix D
Proof of Corollary 1

Proof: By applying Lemma 2 with $\rho(t) = \lambda_j(t) = g(t - jT_{\text{b}})$ and $\rho^{(2)}(t,\tau) = \lambda_j(t)\lambda_j(\tau) = g(t - jT_{\text{b}})g(\tau - jT_{\text{b}})$ we get

$$\mathbb{E}\left\{\mathsf{n}_{\text{rx}}|_{\boldsymbol{\Psi},\mathsf{d}_j=1}[j]\right\} = \int_{-\infty}^{+\infty} g(\tau)\overline{H}_{\text{all}}(-\tau)d\tau \tag{100a}$$

$$\begin{aligned}\mathbb{V}\left\{\mathsf{n}_{\text{rx}}|_{\boldsymbol{\Psi},\mathsf{d}_j=1}[j]\right\} =& \int_{-\infty}^{+\infty} g(\tau)\overline{H}_{\text{all}}(-\tau)d\tau \\ &+ \int_{-\infty}^{+\infty} \int_{-\infty}^{+\infty} g(\tau)g(s)\overline{H}_{\text{all}}^{(2)}(-\tau,-s)d\tau ds \\ &+ \int_{-\infty}^{+\infty} \int_{-\infty}^{+\infty} g(\tau)g(s)\overline{G}_{\text{all}}^{(2)}(-\tau,-s)d\tau ds\,. \end{aligned} \tag{100b}$$

Note that $g(t)$ is zero for $t < 0$. Thus, the contribution of the integrals is non-zero only when the integration variables (τ ans s) are non-negative. For $\tau \geqslant 0$, $\overline{F}_{\text{hit}}(r,-\tau) = F_{\text{hit}}(r, T_{\text{b}} - \tau) - F_{\text{hit}}(r,-\tau) = F_{\text{hit}}(r, T_{\text{b}} - \tau)$. Thus, according to (44) and (25), (100) results in (29) with $t = T_{\text{b}}$, $\rho(t) = g(t)$, and $\rho^{(2)}(t,\tau) = g(t)g(\tau)$. □

Appendix E
Proof of Corollary 2

Proof: First, note that, if previous bits $(\mathsf{d}_0, \mathsf{d}_1, ...\mathsf{d}_{j-1})$ are RVs, $\mathsf{\lambda}_{\text{ISI}}(t) = \sum_{i=0}^{j-1} \mathsf{d}_i g(t - iT_{\text{b}})$ is a random process and $\{\Phi_{\text{ISI}}^{(n)}\}$ result in Cox PPs with first and second order intensity functions given by:

$$\begin{aligned}\rho(t) =& \mathbb{E}\left\{\mathsf{\lambda}_{\text{ISI}}(t)\right\} = \mathbb{E}\left\{\sum_{i=0}^{j-1} \mathsf{d}_i g(t - iT_{\text{b}})\right\} \\ =& p_1 \sum_{i=0}^{j-1} g(t - iT_{\text{b}}) \end{aligned} \tag{101}$$

and

$$\begin{aligned}\rho^{(2)}(t,\tau) =& \mathbb{E}\left\{\mathsf{\lambda}_{\text{ISI}}(t)\mathsf{\lambda}_{\text{ISI}}(\tau)\right\} \\ =& \mathbb{E}\left\{\sum_{i=0}^{j-1} \mathsf{d}_i g(t - iT_{\text{b}}) \sum_{k=0}^{j-1} \mathsf{d}_k g(\tau - kT_{\text{b}})\right\} \\ =& \sum_{i=0}^{j-1} \mathbb{E}\left\{\mathsf{d}_i^2\right\} g(t - iT_{\text{b}})g(\tau - iT_{\text{b}}) \\ &+ \sum_{i=0}^{j-1} \sum_{\substack{k=0 \\ k\neq i}}^{j-1} \mathbb{E}\left\{\mathsf{d}_i\right\}\mathbb{E}\left\{\mathsf{d}_k\right\} g(t - iT_{\text{b}})g(\tau - kT_{\text{b}}) \\ =& p_1 \sum_{i=0}^{j-1} g(t - iT_{\text{b}})g(\tau - iT_{\text{b}}) \\ &+ p_1^2 \sum_{i=0}^{j-1} \sum_{\substack{k=0 \\ k\neq i}}^{j-1} g(t - iT_{\text{b}})g(\tau - kT_{\text{b}}) \\ =& p_1^2 \sum_{i=0}^{j-1} g(t - iT_{\text{b}})g(\tau - iT_{\text{b}}) \\ &+ p_1^2 \sum_{i=0}^{j-1} \sum_{k=0}^{j-1} g(t - iT_{\text{b}})g(\tau - kT_{\text{b}}) \end{aligned} \tag{102}$$

respectively. By applying Lemma 2 with $\rho(t)$ and $\rho^{(2)}(t,\tau)$ as in (101) and (102), we obtain (51). Second, note that from (44) and (40) we have

$$\begin{aligned}\overline{H}_{\text{all}}(t) =& \lambda_{\boldsymbol{\Psi}} \int_{\mathbb{R}^3\setminus\boldsymbol{\Omega}_R} \left[F_{\text{hit}}(\|\boldsymbol{x}\|, T_{\text{b}} + t) - F_{\text{hit}}(\|\boldsymbol{x}\|, t)\right] d\boldsymbol{x} \\ \overline{H}_{\text{all}}^{(2)}(t_1,t_2) =& \lambda_{\boldsymbol{\Psi}} \int_{\mathbb{R}^3\setminus\boldsymbol{\Omega}_R} \left[F_{\text{hit}}(\|\boldsymbol{x}\|, T_{\text{b}} + t_1) - F_{\text{hit}}(\|\boldsymbol{x}\|, t_1)\right] \\ &\times \left[F_{\text{hit}}(\|\boldsymbol{x}\|, T_{\text{b}} + t_2) - F_{\text{hit}}(\|\boldsymbol{x}\|, t_2)\right] d\boldsymbol{x} \\ \overline{G}_{\text{all}}^{(2)}(t_1,t_2) =& \int_{\mathbb{R}^3\setminus\boldsymbol{\Omega}_R} \int_{\mathbb{R}^3\setminus\boldsymbol{\Omega}_R} \left[\rho_{\boldsymbol{\Psi}}(\|\boldsymbol{x}_1 - \boldsymbol{x}_2\|) - \lambda_{\boldsymbol{\Psi}}^2\right] \\ &\times \left[F_{\text{hit}}(\|\boldsymbol{x}_1\|, T_{\text{b}} + t_1) - F_{\text{hit}}(\|\boldsymbol{x}_1\|, t_1)\right] \\ &\times \left[F_{\text{hit}}(\|\boldsymbol{x}_2\|, T_{\text{b}} + t_2) - F_{\text{hit}}(\|\boldsymbol{x}_2\|, t_2)\right] d\boldsymbol{x}_1 d\boldsymbol{x}_2 \end{aligned} \tag{103a}$$

which result in (52). □

Appendix F
Proof of Proposition 1

Proof: First, for an homogeneous PPP it is $\rho_{\boldsymbol{\Psi}}(\|\boldsymbol{x}_1 - \boldsymbol{x}_2\|) = \lambda_{\boldsymbol{\Psi}}^2$ and (25) lead to

$$G_{\text{all}}^{(2)}(t,\tau) = 0 \tag{104}$$

Thus, (26), (28), and (30) reduce to (72), (73), and (74), respectively. Second, by substituting (1) in (25a), we obtain

$$\begin{aligned} H_{\text{all}}(t) &= \lambda_{\boldsymbol{\psi}} \int_{\mathbb{R}^3 \setminus \mathcal{A}} F_{\text{hit}}(\boldsymbol{x}, t) d\boldsymbol{x} \\ &= \lambda_{\boldsymbol{\psi}} \int_R^{+\infty} 4\pi r^2 F_{\text{hit}}(r, t) dr \\ &= 4\pi \lambda_{\boldsymbol{\psi}} R \int_R^{+\infty} r \operatorname{erfc}\left(\frac{r-R}{\sqrt{4Dt}}\right) dr \end{aligned}$$

that results in (75a). Finally, from (1) and (25c) it follows

$$\begin{aligned} H^{(2)}_{\text{all}}(t,\tau) =& \lambda_{\boldsymbol{\psi}} \int_{\mathbb{R}^3 \setminus \boldsymbol{\Omega}_R} F_{\text{hit}}(\boldsymbol{x}, t) F_{\text{hit}}(\boldsymbol{x}, \tau) d\boldsymbol{x} \\ =& \int_{\mathbb{R}^3 \setminus \boldsymbol{\Omega}_R} \lambda_{\boldsymbol{\psi}} \frac{R^2}{\|\boldsymbol{x}\|^2} \operatorname{erfc}\left(\frac{\|\boldsymbol{x}\|-R}{\sqrt{4Dt}}\right) \operatorname{erfc}\left(\frac{\|\boldsymbol{x}\|-R}{\sqrt{4D\tau}}\right) d\boldsymbol{x} \\ =& \lambda_{\boldsymbol{\psi}} 4\pi \int_R^{+\infty} R^2 \operatorname{erfc}\left(\frac{r-R}{\sqrt{4Dt}}\right) \operatorname{erfc}\left(\frac{r-R}{\sqrt{4D\tau}}\right) dr \\ =& 4\pi \lambda_{\boldsymbol{\psi}} \sqrt{4D} \int_0^{+\infty} R^2 \operatorname{erfc}\left(\frac{r'}{\sqrt{t}}\right) \operatorname{erfc}\left(\frac{r'}{\sqrt{\tau}}\right) dr' \\ =& 8\pi R^2 \lambda_{\boldsymbol{\psi}} \sqrt{\frac{Dt\tau}{\pi}} \left(\frac{1}{\sqrt{t}} + \frac{1}{\sqrt{\tau}} - \sqrt{\frac{1}{t}+\frac{1}{\tau}}\right) \end{aligned} \tag{105}$$

which results in (75b). □

Appendix G
Proof of Corollary 4

Proof: For a function $\lambda(t)$ which is $N_{\text{tx}}/T_{\text{a}}$ in $[0, T_{\text{a}}]$ and 0 elsewhere, it is

$$\begin{aligned} &\int_{-\infty}^{+\infty} \lambda(\tau) H_{\text{all}}(t-\tau) d\tau = \frac{N_{\text{tx}}}{T_{\text{a}}} \int_0^{\min\{t, T_{\text{a}}\}} H_{\text{all}}(t-\tau) d\tau \\ =& \frac{N_{\text{tx}}}{T_{\text{a}}} \int_0^{\min\{t, T_{\text{a}}\}} 4\lambda_{\boldsymbol{\psi}} R \sqrt{\pi D(t-\tau)} \left\{2R + \sqrt{\pi D(t-\tau)}\right\} d\tau \\ =& \frac{8 N_{\text{tx}} \lambda_{\boldsymbol{\psi}} R^2 \sqrt{\pi D}}{T_{\text{a}}} \int_0^{\min\{t, T_{\text{a}}\}} \sqrt{t-\tau} d\tau \\ &+ \frac{4 N_{\text{tx}} \lambda_{\boldsymbol{\psi}} R \pi D}{T_{\text{a}}} \int_0^{\min\{t, T_{\text{a}}\}} (t-\tau) d\tau \\ =& \begin{cases} \frac{16 N_{\text{tx}} \lambda_{\boldsymbol{\psi}} R^2 \sqrt{\pi D t^3}}{3 T_{\text{e}}} + \frac{2 N_{\text{tx}} \lambda_{\boldsymbol{\psi}} R \pi D t^2}{T_{\text{a}}}, & \text{for } t \leqslant T_{\text{a}} \\ \frac{16 N_{\text{tx}} \lambda_{\boldsymbol{\psi}} R^2 \sqrt{\pi D}}{3 T_{\text{a}}} \left(\sqrt{t^3} - t\sqrt{t-T_{\text{a}}}\right. & \\ \left. + T_{\text{a}} \sqrt{t-T_{\text{a}}}\right) + \frac{4 N_{\text{tx}} \lambda_{\boldsymbol{\psi}} R \pi D}{T_{\text{a}}} \left(t T_{\text{a}} - \frac{T_{\text{a}}^2}{2}\right) & \text{for } t > T_{\text{a}} \end{cases} \end{aligned} \tag{106}$$

and

$$\begin{aligned} &\int_{-\infty}^{+\infty} \int_{-\infty}^{+\infty} \lambda(\tau)\lambda(s) H^{(2)}_{\text{all}}(t-\tau, t-s) d\tau ds \\ =& \frac{N_{\text{tx}}^2}{T_{\text{a}}^2} \int_0^{T_{\text{a}}} \int_0^{T_{\text{a}}} H^{(2)}_{\text{all}}(t-\tau, t-s) d\tau ds \\ =& \frac{8 N_{\text{tx}}^2 R^2 \lambda_{\boldsymbol{\psi}} \sqrt{\pi D}}{T_{\text{a}}^2} \int_0^{\min\{t, T_{\text{a}}\}} \int_0^{\min\{t, T_{\text{a}}\}} (\sqrt{t-\tau} + \sqrt{t-s} \\ & - \sqrt{2t-\tau-s}) d\tau ds \\ =& \frac{8 N_{\text{tx}}^2 R^2 \lambda_{\boldsymbol{\psi}} \sqrt{\pi D}}{T_{\text{a}}^2} \begin{cases} \left(\frac{4}{15}(7-4\sqrt{2})\sqrt{t^5}\right), & \text{for } t \leqslant T_{\text{a}} \\ \frac{4T_{\text{a}}}{3}\left(\sqrt{t^3} - t\sqrt{t-T_{\text{a}}}\right. & \\ \left. + T_{\text{a}}\sqrt{t-T_{\text{a}}}\right) & \\ - \int_0^{T_{\text{a}}} \frac{2}{3}\left[\sqrt{(2t-s)^3}\right. & \\ \left. - \sqrt{(2t-s-T_{\text{a}})^3}\right] ds, & \text{for } t > T_{\text{a}} \end{cases} \\ =& \frac{8 N_{\text{tx}}^2 R^2 \lambda_{\boldsymbol{\psi}} \sqrt{\pi D}}{T_{\text{a}}^2} \begin{cases} \left(\frac{4}{15}(7-4\sqrt{2})\sqrt{t^5}\right), & \text{for } t \leqslant T_{\text{a}} \\ \frac{4T_{\text{a}}}{3}\left(\sqrt{t^3} - t\sqrt{t-T_{\text{a}}}\right. & \\ \left. + T_{\text{a}}\sqrt{t-T_{\text{a}}}\right) & \\ - \frac{4}{15}\left[\sqrt{(2t)^5}\right. & \\ - 2\sqrt{(2t-T_{\text{a}})^5} & \\ \left. + \sqrt{(2t-2T_{\text{a}})^5}\right], & \text{for } t > T_{\text{a}} \end{cases} \end{aligned} \tag{107}$$

which, substituted in (74), provide (76). □

Appendix H
Proof of Proposition 2

Proof: First, note that, in both cases, if Φ is a PPP, then $\rho_{\boldsymbol{\psi}}(\|\boldsymbol{x}_1 - \boldsymbol{x}_2\|) = \lambda_{\boldsymbol{\psi}}^2$ and thus, from (44c), it is $\overline{G}_{\text{all}}(t,\tau) = 0$. For Poisson concentration transmitters, $g(t) = N_{\text{tx}}\delta(t)$, and thus (51) leads to

$$\begin{aligned} \mu_{\text{ISI}} =& \frac{N_{\text{tx}}}{2} \sum_{i=0}^{j-1} \int_{-\infty}^{+\infty} \delta(\tau - iT_{\text{b}} + jT_{\text{b}}) \overline{H}_{\text{all}}(-\tau) d\tau \\ =& \frac{N_{\text{tx}}}{2} \sum_{i=0}^{j-1} \overline{H}_{\text{all}}[(j-i)T_{\text{b}}] = \frac{N_{\text{tx}}}{2} \sum_{k=1}^{j} \overline{H}_{\text{all}}(kT_{\text{b}}) \end{aligned} \tag{108}$$

and

$$\begin{aligned}\sigma^2_{\text{ISI}} =&\frac{N_{\text{tx}}}{2}\sum_{i=0}^{j-1}\int_{-\infty}^{+\infty}\delta(\tau - iT_{\text{b}} + jT_{\text{b}})\overline{H}_{\text{all}}(-\tau)d\tau\\ &+\frac{N_{\text{tx}}^2}{4}\sum_{i=0}^{j-1}\int_{-\infty}^{+\infty}\int_{-\infty}^{+\infty}\delta(\tau - iT_{\text{b}} + jT_{\text{b}})\\ &\times\delta(s - iT_{\text{b}} + jT_{\text{b}})\overline{H}^{(2)}_{\text{all}}(-\tau,-s)d\tau ds\\ &+\frac{N_{\text{tx}}^2}{4}\sum_{i=0}^{j-1}\sum_{l=0}^{j-1}\int_{-\infty}^{+\infty}\int_{-\infty}^{+\infty}\delta(\tau - iT_{\text{b}} + jT_{\text{b}})\\ &\times\delta(s - lT_{\text{b}} + jT_{\text{b}})\overline{H}^{(2)}_{\text{all}}(-\tau,-s)d\tau ds\\ =&\frac{N_{\text{tx}}}{2}\sum_{i=0}^{j-1}\overline{H}_{\text{all}}[(j-i)T_{\text{b}}]\\ &+\frac{N_{\text{tx}}^2}{4}\sum_{i=0}^{j-1}\overline{H}^{(2)}_{\text{all}}[(j-i)T_{\text{b}},(j-i)T_{\text{b}}]\\ &+\frac{N_{\text{tx}}^2}{4}\sum_{i=0}^{j-1}\sum_{l=0}^{j-1}\overline{H}^{(2)}_{\text{all}}[(j-i)T_{\text{b}},(j-l)T_{\text{b}}]\\ =&\frac{N_{\text{tx}}}{2}\sum_{k=1}^{j}\overline{H}_{\text{all}}(kT_{\text{b}}) + \frac{N_{\text{tx}}^2}{4}\sum_{k=1}^{j}\overline{H}^{(2)}_{\text{all}}(kT_{\text{b}},kT_{\text{b}})\\ &+\frac{N_{\text{tx}}^2}{4}\sum_{k=1}^{j}\sum_{m=1}^{j}\overline{H}^{(2)}_{\text{all}}(kT_{\text{b}},mT_{\text{b}}) \qquad (109)\end{aligned}$$

where in the last step we introduces the index $k \triangleq j - i$ and $m \triangleq j - l$. By using (52), (108) and (109) become

$$\mu_{\text{ISI}} = \frac{N_{\text{tx}}}{2}\sum_{k=1}^{j}\{H_{\text{all}}[(k+1)T_{\text{b}}] - H_{\text{all}}(kT_{\text{b}})\} \qquad (110a)$$

$$\begin{aligned}\sigma^2_{\text{ISI}} =&\frac{N_{\text{tx}}}{2}\sum_{k=1}^{j}\{H_{\text{all}}[(k+1)T_{\text{b}}] - H_{\text{all}}(kT_{\text{b}})\}\\ &+\frac{N_{\text{tx}}^2}{4}\sum_{k=1}^{j}\{H^{(2)}_{\text{all}}[(k+1)T_{\text{b}},(k+1)T_{\text{b}}]\\ &-H^{(2)}_{\text{all}}[kT_{\text{b}},(k+1)T_{\text{b}}]\}\\ &+\frac{N_{\text{tx}}^2}{4}\sum_{k=1}^{j}\{H^{(2)}_{\text{all}}(kT_{\text{b}},kT_{\text{b}})\\ &-H^{(2)}_{\text{all}}[(k+1)T_{\text{b}},kT_{\text{b}}]\}\\ &+\frac{N_{\text{tx}}^2}{4}\sum_{k=1}^{j}\sum_{m=1}^{j}\{H^{(2)}_{\text{all}}[(k+1)T_{\text{b}},(m+1)T_{\text{b}}]\\ &-H^{(2)}_{\text{all}}[kT_{\text{b}},(m+1)T_{\text{b}}]\}\\ &+\frac{N_{\text{tx}}^2}{4}\sum_{k=1}^{j}\sum_{m=1}^{j}\{H^{(2)}_{\text{all}}(kT_{\text{b}},mT_{\text{b}})\\ &-H^{(2)}_{\text{all}}[(k+1)T_{\text{b}},mT_{\text{b}}]\} \qquad (110b)\end{aligned}$$

which result in (81) by noticing that, in the sums over the index k, the positive part k-th element is deleted by the negative part of the $k+1$-th element.

For timing transmitters with uniformly distributed emissions in an activity interval, $g(t) = \frac{N_{\text{tx}}}{T_{\text{a}}}\text{rect}\frac{t}{T_{\text{a}}}$, and thus (51) leads to

$$\begin{aligned}\mu_{\text{ISI}} =&\frac{N_{\text{tx}}}{2T_{\text{a}}}\sum_{i=0}^{j-1}\int_{(i-j)T_{\text{b}}}^{(i-j)T_{\text{b}}+T_{\text{a}}}\overline{H}_{\text{all}}(-\tau)d\tau\\ =&\frac{N_{\text{tx}}}{2T_{\text{a}}}\sum_{i=0}^{j-1}\int_{0}^{T_{\text{a}}}\overline{H}_{\text{all}}[(j-i)T_{\text{b}}-u]du \qquad (111)\end{aligned}$$

and

$$\begin{aligned}\sigma^2_{\text{ISI}} =&\frac{N_{\text{tx}}}{2T_{\text{a}}}\sum_{i=0}^{j-1}\int_{(i-j)T_{\text{b}}}^{(i-j)T_{\text{b}}+T_{\text{a}}}\overline{H}_{\text{all}}(-\tau)d\tau\\ &+\frac{N_{\text{tx}}^2}{4T_{\text{a}}^2}\sum_{i=0}^{j-1}\int_{(i-j)T_{\text{b}}}^{(i-j)T_{\text{b}}+T_{\text{a}}}\int_{(i-j)T_{\text{b}}}^{(i-j)T_{\text{b}}+T_{\text{a}}}\overline{H}^{(2)}_{\text{all}}(-\tau,-s)d\tau ds\\ &+\frac{N_{\text{tx}}^2}{4T_{\text{a}}^2}\sum_{i=0}^{j-1}\sum_{l=0}^{j-1}\int_{(i-j)T_{\text{b}}}^{(i-j)T_{\text{b}}+T_{\text{a}}}\int_{(l-j)T_{\text{b}}}^{(l-j)T_{\text{b}}+T_{\text{a}}}\overline{H}^{(2)}_{\text{all}}(-\tau,-s)d\tau ds\\ =&\frac{N_{\text{tx}}}{2T_{\text{a}}}\sum_{i=0}^{j-1}\int_{0}^{T_{\text{a}}}\overline{H}_{\text{all}}[(j-i)T_{\text{b}}-u]du\\ &+\frac{N_{\text{tx}}^2}{4T_{\text{a}}^2}\sum_{i=0}^{j-1}\int_{0}^{T_{\text{a}}}\int_{0}^{T_{\text{a}}}\overline{H}^{(2)}_{\text{all}}[(j-i)T_{\text{b}}-u,(j-i)T_{\text{b}}-v]dudv\\ &+\frac{N_{\text{tx}}^2}{4T_{\text{a}}^2}\sum_{i=0}^{j-1}\sum_{l=0}^{j-1}\int_{0}^{T_{\text{a}}}\int_{0}^{T_{\text{a}}}\overline{H}^{(2)}_{\text{all}}[(j-i)T_{\text{b}}-u,(j-l)T_{\text{b}}-v]dudv \qquad (112)\end{aligned}$$

where $u = \tau + (j-i)T_{\text{b}}$ and $v = s + (j-l)$. By using the index $k = j - i$ and $m = j - l$ and by recalling (52), we get

$$\mu_{\text{ISI}} = \frac{N_{\text{tx}}}{2T_{\text{a}}}\sum_{k=1}^{j}(h_{k+1} - h_k) \qquad (113)$$

$$\begin{aligned}\sigma^2_{\text{ISI}} =&\frac{N_{\text{tx}}}{2T_{\text{a}}}\sum_{k=1}^{j}(h_{k+1} - h_k)\\ &+\frac{N_{\text{tx}}^2}{4T_{\text{a}}^2}\sum_{k=1}^{j}(g_{k+1,k+1} - g_{k,k+1} + g_{k,k} - g_{k+1,k})\\ &+\frac{N_{\text{tx}}^2}{4T_{\text{a}}^2}\sum_{k=1}^{j}\sum_{m=1}^{j}(g_{k+1,m+1} - g_{k,m+1} + g_{k,m} - g_{k+1,m}) \qquad (114)\end{aligned}$$

which, by noticing that in the sums over k each element deletes its follower, result in (82) where

$$h_k \triangleq \int_0^{T_{\text{a}}} H_{\text{all}}(kT_{\text{b}} - u)du \qquad (115a)$$

$$g_{k,m} \triangleq \int_0^{T_{\text{a}}}\int_0^{T_{\text{a}}} H^{(2)}_{\text{all}}(kT_{\text{b}} - u, mT_{\text{b}} - v)dudv\,. \qquad (115b)$$

For $t, t_1, t_z > 0$, it results

$$\begin{aligned}&\int_0^{T_{\text{a}}} H_{\text{all}}(t-\tau)d\tau\\ =&8\lambda_{\boldsymbol{\Psi}}R^2\sqrt{\pi D}\left\{\frac{2}{3}\left[\sqrt{t^3} - \sqrt{(t-T_{\text{a}})^3}\right] + \frac{\sqrt{\pi D}}{2R}\left(tT_{\text{a}} - \frac{T_{\text{a}}^2}{2}\right)\right\} \qquad (116)\end{aligned}$$

and

$$\int_0^{T_\mathrm{a}} H_\mathrm{all}^{(2)}(t_1-\tau,t_2-s)d\tau ds = 8R^2\lambda_{\boldsymbol{\Psi}}\sqrt{\pi D}$$
$$\times \int_0^{T_\mathrm{a}}\int_0^{T_\mathrm{a}} (\sqrt{t_1-\tau}+\sqrt{t_2-s}-\sqrt{t_1+t_2-\tau-s})d\tau ds$$
$$= 8R^2\lambda_{\boldsymbol{\Psi}}\sqrt{\pi D}\left\{\frac{2T_\mathrm{a}}{3}\right.$$
$$\times\left[\sqrt{t_1^3}-\sqrt{(t_1-T_\mathrm{a})^3}+\sqrt{t_2^3}-\sqrt{(t_2-T_\mathrm{a})^3}\right]$$
$$\left.+\frac{2}{3}\int_0^{T_\mathrm{a}}\left[\sqrt{(t_1+t_2-s)^3}-\sqrt{(t_1+t_2-s-T_\mathrm{a})^3}\right]ds\right\}$$
$$= 8R^2\lambda_{\boldsymbol{\Psi}}\sqrt{\pi D}\left\{\frac{2T_\mathrm{a}}{3}\left[\sqrt{t_1^3}-\sqrt{(t_1-T_\mathrm{a})^3}\right.\right.$$
$$\left.+\sqrt{t_2^3}-\sqrt{(t_2-T_\mathrm{a})^3}\right]-\frac{4}{15}\left[\sqrt{(t_1+t_2)^5}\right.$$
$$\left.\left.-2\sqrt{(t_1+t_2-T_\mathrm{a})^5}+\sqrt{(t_1+t_2-2T_\mathrm{a})^5}\right]\right\}. \quad (117)$$

Thus (115) become (83). □

ACKNOWLEDGMENT

I would like to thank the anonymous reviewers for useful comments which have greatly improved the quality of the paper. I am indebted with O. Andrisano and C. De Castro for useful discussions. Finally, I give special thanks to A. Conti and M. Pierobon for stimulating my interest on the field of molecular communications. I thank R. Verdone and all my colleagues at WiLab for their support.

REFERENCES

[1] I. F. Akyildiz, F. Brunetti, and C. Blázquez, "Nanonetworks: A new communication paradigm," *Comput. Netw.*, vol. 52, no. 12, pp. 2260–2279, Aug. 2008. [Online]. Available: http://dx.doi.org/10.1016/j.comnet.2008.04.001

[2] M. S. Kuran, H. B. Yilmaz, T. Tugcu, and B. Ozerman, "Energy model for communication via diffusion in nanonetworks," *Nano Communication Networks*, vol. 1, no. 2, pp. 86 – 95, 2010.

[3] T. Nakano, M. J. Moore, F. Wei, A. V. Vasilakos, and J. Shuai, "Molecular communication and networking: Opportunities and challenges," *IEEE Transactions on NanoBioscience*, vol. 11, no. 2, pp. 135–148, June 2012.

[4] M. Pierobon and I. F. Akyildiz, "Diffusion-based noise analysis for molecular communication in nanonetworks," *IEEE Transactions on Signal Processing*, vol. 59, no. 6, pp. 2532–2547, June 2011.

[5] M. Pierobon and I. F. Akyildiz, "Capacity of a diffusion-based molecular communication system with channel memory and molecular noise," *IEEE Transactions on Information Theory*, vol. 59, no. 2, pp. 942–954, Feb 2013.

[6] S. A. Salehi, H. Jiang, M. D. Riedel, and K. K. Parhi, "Molecular sensing and computing systems," *IEEE Transactions on Molecular, Biological and Multi-Scale Communications*, vol. 1, no. 3, pp. 249–264, Sept 2015.

[7] Y. Deng, A. Noel, W. Guo, A. Nallanathan, and M. Elkashlan, "Analyzing large-scale multiuser molecular communication via 3-D stochastic geometry," *IEEE Transactions on Molecular, Biological and Multi-Scale Communications*, vol. 3, no. 2, pp. 118–133, June 2017.

[8] F. Zabini, "Spatially distributed molecular communications: An asynchronous stochastic model," *IEEE Communications Letters*, vol. 22, no. 7, pp. 1326–1329, July 2018.

[9] F. Zabini, G. Pasolini, C. De Castro, and O. Andrisano, "On molecular communications via diffusion with multiple transmitters and multiple receivers," in *2018 IEEE Global Communications Conference (GLOBECOM)*, Dec 2018, pp. 206–212.

[10] M. Pierobon and I. F. Akyildiz, "A physical end-to-end model for molecular communication in nanonetworks," *IEEE Journal on Selected Areas in Communications*, vol. 28, no. 4, pp. 602–611, May 2010.

[11] A. Noel, K. C. Cheung, and R. Schober, "Improving receiver performance of diffusive molecular communication with enzymes," *IEEE Transactions on NanoBioscience*, vol. 13, no. 1, pp. 31–43, March 2014.

[12] M. B. Dissanayake, Y. Deng, A. Nallanathan, M. Elkashlan, and U. Mitra, "Interference mitigation in large-scale multiuser molecular communication," *IEEE Transactions on Communications*, vol. 67, no. 6, pp. 4088–4103, June 2019.

[13] N. R. Kim and C. B. Chae, "Novel modulation techniques using isomers as messenger molecules for nano communication networks via diffusion," *IEEE Journal on Selected Areas in Communications*, vol. 31, no. 12, pp. 847–856, December 2013.

[14] I. F. Akyildiz, J. M. Jornet, and M. Pierobon, "Nanonetworks: A new frontier in communications," *Commun. ACM*, vol. 54, no. 11, pp. 84–89, Nov. 2011.

[15] T. Nakano, T. Suda, Y. Okaie, M. J. Moore, and A. V. Vasilakos, "Molecular communication among biological nanomachines: A layered architecture and research issues," *IEEE Transactions on NanoBioscience*, vol. 13, no. 3, pp. 169–197, Sep. 2014.

[16] O. B. Akan, H. Ramezani, T. Khan, N. A. Abbasi, and M. Kuscu, "Fundamentals of molecular information and communication science," *Proceedings of the IEEE*, vol. 105, no. 2, pp. 306–318, Feb 2017.

[17] I. F. Akyildiz, M. Pierobon, S. Balasubramaniam, and Y. Koucheryavy, "The internet of bio-nano things," *IEEE Communications Magazine*, vol. 53, no. 3, pp. 32–40, March 2015.

[18] M. J. Moore, A. Enomoto, S. Watanabe, K. Oiwa, and T. Suda, "Simulating molecular motor uni-cast information rate for molecular communication," in *2009 43rd Annual Conference on Information Sciences and Systems*, March 2009, pp. 859–864.

[19] M. Gregori and I. F. Akyildiz, "A new nanonetwork architecture using flagellated bacteria and catalytic nanomotors," *IEEE Journal on Selected Areas in Communications*, vol. 28, no. 4, pp. 612–619, May 2010.

[20] M. Gregori, I. Llatser, A. Cabellos-Aparicio, and E. Alarcón, "Physical channel characterization for medium-range nanonetworks using flagellated bacteria," *Comput. Netw.*, vol. 55, no. 3, pp. 779–791, Feb. 2011.

[21] L. C. Cobo and I. F. Akyildiz, "Bacteria-based communication in nanonetworks," *Nano Communication Networks*, vol. 1, no. 4, pp. 244 – 256, 2010.

[22] I. Llatser, A. Cabellos-Aparicio, M. Pierobon, and E. Alarcon, "Detection techniques for diffusion-based molecular communication," *IEEE Journal on Selected Areas in Communications*, vol. 31, no. 12, pp. 726–734, December 2013.

[23] M. Pierobon and I. F. Akyildiz, "A statistical-physical model of interference in diffusion-based molecular nanonetworks," *IEEE Transactions on Communications*, vol. 62, no. 6, pp. 2085–2095, June 2014.

[24] A. O. Bicen and I. F. Akyildiz, "System-theoretic analysis and least-squares design of microfluidic channels for flow-induced molecular communication," *IEEE Transactions on Signal Processing*, vol. 61, no. 20, pp. 5000–5013, Oct 2013.

[25] M. Kuscu and O. B. Akan, "Modeling and analysis of sinw fet-based molecular communication receiver," *IEEE Transactions on Communications*, vol. 64, no. 9, pp. 3708–3721, Sep. 2016.

[26] N. Tavakkoli, P. Azmi, and N. Mokari, "Performance evaluation and optimal detection of relay-assisted diffusion-based molecular communication with drift," *IEEE Transactions on NanoBioscience*, vol. 16, no. 1, pp. 34–42, Jan 2017.

[27] A. Noel, K. C. Cheung, and R. Schober, "Using dimensional analysis to assess scalability and accuracy in molecular communication," in *2013 IEEE International Conference on Communications Workshops (ICC)*, June 2013, pp. 818–823.

[28] H. B. Yilmaz, A. C. Heren, T. Tugcu, and C. B. Chae, "Three-dimensional channel characteristics for molecular communications with an absorbing receiver," *IEEE Communications Letters*, vol. 18, no. 6, pp. 929–932, June 2014.

[29] D. T. Gillespie, "The chemical langevin equation," *The Journal of Chemical Physics*, vol. 113, no. 1, pp. 297–306, 2000. [Online]. Available: https://doi.org/10.1063/1.481811

[30] P. J. Thomas, D. J. Spencer, S. K. Hampton, P. Park, and J. P. Zurkus, "The diffusion-limited biochemical signal-relay channel," in *Advances in Neural Information Processing Systems 16*, S. Thrun, L. K. Saul, and B. Schölkopf, Eds. MIT Press, 2004, pp. 1263–1270. [Online]. Available: http://papers.nips.cc/paper/2522-the-diffusion-limited-biochemical-signal-relay-channel.pdf

[31] D. Arifler, "Connectivity properties of free diffusion-based molecular nanoscale communication networks," *IEEE Transactions on Communications*, vol. 65, no. 4, pp. 1686–1695, April 2017.

[32] D. T. Gillespie, "A diffusional bimolecular propensity function," *The Journal of Chemical Physics*, vol. 131, no. 16, p. 164109, 2009. [Online]. Available: https://doi.org/10.1063/1.3253798

[33] F. Zabini and A. Conti, "Inhomogeneous Poisson sampling of finite-energy signals with uncertainties in $\mathbb{R}^d$," *IEEE Transactions on Signal Processing*, vol. 64, no. 18, pp. 4679–4694, Sept 2016.

[34] F. Zabini, G. Pasolini, and A. Conti, "On remote source coding for signal estimation via poisson sampling," in *2016 9th International Symposium on Turbo Codes and Iterative Information Processing (ISTC)*, Sep. 2016, pp. 131–135.

[35] V. Jamali, A. Ahmadzadeh, and R. Schober, "On the design of matched filters for molecule counting receivers," *IEEE Communications Letters*, vol. 21, no. 8, pp. 1711–1714, Aug 2017.

[36] A. Gohari, M. Mirmohseni, and M. Nasiri-Kenari, "Information theory of molecular communication: Directions and challenges," *IEEE Transactions on Molecular, Biological and Multi-Scale Communications*, vol. 2, no. 2, pp. 120–142, Dec 2016.

[37] V. Jamali, A. Ahmadzadeh, W. Wicke, A. Noel, and R. Schober, "Channel modeling for diffusive molecular communication—a tutorial review," *Proceedings of the IEEE*, vol. 107, no. 7, pp. 1256–1301, July 2019.

[38] S. Chiu, D. Stoyan, W. Kendall, and J. Mecke, *Stochastic Geometry and Its Applications*, ser. in Probability and Statistics. Wiley, 2013.

[39] F. Lavancier, J. Møller, and E. Rubak, "Determinantal point process models and statistical inference : Extended version," *arXiv:1205.4818v5 [math.ST]*, 2012.

[40] N. Deng, W. Zhou, and M. Haenggi, "The ginibre point process as a model for wireless networks with repulsion," *IEEE Transactions on Wireless Communications*, vol. 14, no. 1, pp. 107–121, Jan 2015.

[41] F. Zabini and A. Conti, "Ginibre sampling and signal reconstruction," in *2016 IEEE International Symposium on Information Theory (ISIT)*, July 2016, pp. 865–869.

[42] J. F. Kingman, *Poisson Processes*, U. Oxford University Press, Ed., 1993.

[43] J. Møller and G. L. Torrisi, "Generalised shot noise Cox processes," *Advances in Applied Probability*, vol. 37, no. 1, pp. 48–74, 03 2005. [Online]. Available: http://dx.doi.org/10.1239/aap/1113402399

[44] A. Guo, Y. Zhong, W. Zhang, and M. Haenggi, "The gauss–poisson process for wireless networks and the benefits of cooperation," *IEEE Transactions on Communications*, vol. 64, no. 5, pp. 1916–1929, May 2016.

[45] F. Zabini, G. Pasolini, and A. Conti, "On random sampling with nodes attraction: The case of Gauss-Poisson process," in *2017 IEEE International Symposium on Information Theory (ISIT)*, June 2017, pp. 2278–2282.

[46] R. K. Ganti and M. Haenggi, "Interference and outage in clustered wireless ad hoc networks," *IEEE Transactions on Information Theory*, vol. 55, no. 9, pp. 4067–4086, Sep. 2009.

[47] F. Lavancier, J. Møller, and E. Rubak, "Determinantal point process models and statistical inference," *Journal of the Royal Statistical Society: Series B (Statistical Methodology)*, vol. 77, no. 4, pp. 853–877, 2015. [Online]. Available: http://dx.doi.org/10.1111/rssb.12096

[48] M. Haenggi, J. G. Andrews, F. Baccelli, O. Dousse, and M. Franceschetti, "Stochastic geometry and random graphs for the analysis and design of wireless networks," *IEEE Journal on Selected Areas in Communications*, vol. 27, no. 7, pp. 1029–1046, September 2009.

[49] J. Steinfeld, J. Francisco, and W. Hase, *Chemical Kinetics and Dynamics*. 2nd ed., Prentice-Hall, 1999.

[50] J. Moore and R. Pearson, *Kinetics and Mechanism*. John Wiley, 1981.

[51] B. Koo, C. Lee, H. B. Yilmaz, N. Farsad, A. Eckford, and C. Chae, "Molecular MIMO: From theory to prototype," *IEEE Journal on Selected Areas in Communications*, vol. 34, no. 3, pp. 600–614, March 2016.

[52] J. Philibert, "One and a half century of diffusion: Fick, Einstein, before and beyond," *Diffusion Fundam.*, vol. 4, pp. 6.1–6.19, 2006.

[53] Y. Deng, A. Noel, W. Guo, A. Nallanathan, and M. Elkashlan, "3D stochastic geometry model for large-scale molecular communication systems," in *2016 IEEE Global Communications Conference (GLOBECOM)*, Dec 2016, pp. 1–6.

[54] H. B. Yilmaz, G. Suk, and C. Chae, "Chemical propagation pattern for molecular communications," *IEEE Wireless Communications Letters*, vol. 6, no. 2, pp. 226–229, April 2017.

[55] F. Zabini, A. Calisti, D. Dardari, and A. Conti, "Random sampling via sensor networks: Estimation accuracy vs. energy consumption," in *2016 24th European Signal Processing Conference (EUSIPCO)*, Aug 2016, pp. 130–134.

Flavio Zabini (M'13) received the Laurea (*summa cum laude*) in telecommunications engineering and the Ph.D. in electronic engineering and computer science from the University of Bologna, Italy, in 2004 and 2010, respectively. In 2004, he developed his master's thesis at the University of California San Diego, La Jolla. In 2008, he was a Visiting Student with the DoCoMo Eurolabs of Munich, Germany. From 2013 to 2014, he was a Post-Doctoral Fellow with the German Aerospace Center, Cologne, Germany. He was with the IEIIT-Bo of CNR. He is currently a Researcher with the University of Bologna. His current research interests include random sampling techniques applied to sensor networks, performance-fairness tradeoff in communication systems, and molecular communications. He serves as an associate Editor for the IEEE Communication Letters and the KSII Transactions on Internet and Information Systems.